JOANA GREGÓRIO DA SILVA

In vitro protein thiol oxidation by endoplasmic reticulum enzymatic pathways

UNIVERSIDADE DO ALGARVE

Faculdade de Ciências e Tecnologia

2021

JOANA GREGÓRIO DA SILVA

In vitro protein thiol oxidation by endoplasmic reticulum enzymatic pathways

Integrated Master in Biological Engineering

Work developed under the supervision of:

Dr. Eduardo Pinho e Melo

UNIVERSIDADE DO ALGARVE

Faculdade de Ciências e Tecnologia

2021

In vitro protein thiol oxidation by endoplasmic reticulum enzymatic pathways

Declaration of Originality

I hereby declare to be the author of this original and unique work. Authors and references in use are properly cited in the text and are all listed in the included references section.

Declaro ser a autora deste trabalho, que é original e inédito. Autores e trabalhos consultados estão devidamente citados no texto e constam da listagem de referências incluída.

_____

(Joana Gregório da Silva)

To Iris and Benny, my fur babies.

To Mister Dudas, my favourite "little hooman".

To Grandma A., the brightest star.

The great thing about science is that you can get it
wrong over and over again because what you're after
–call it truth or understanding– waits patiently for you.
Ultimately, you'll find the answer because it doesn't change.
DUDLEY HERSCHBACH

Acknowledgements

I received an incredible amount of support and encouragement while planning and writing this dissertation.

First and foremost, I would like to acknowledge my supervisor, Professor Eduardo Melo, whose expertise was invaluable in developing the research questions and devising the methodology. His insightful feedback motivated me to sharpen my thinking, bringing my work to a higher level. I also want to thank him for all the opportunities he presented me to enrich my research.

I would like to acknowledge fellow researcher Carlos Lopes and laboratory technician Teresa Sancho for their invaluable guidance and assistance throughout my laboratory research.

I was extraordinarily fortunate to share the laboratory with Cátia Correia and Evandro Tavares. I want to thank them for their remarkable collaboration and, above all, their fantastic friendship. Cátia, Evandro, you are the best!

I would also like to thank my brother-in-law Paulo Moreira and Yasar Ahmed (developer of PyCORN) for their IT support. You provided me with some tools that were fundamental to complete my dissertation.

Marisa Santos, Jorge Carvalho, and Rita Sousa were also essential, with their stimulating discussions alongside some delightful distractions. You allowed me to relax here and then and ease my mind outside of my research. Thank you.

My parents and my brothers were always there for me and were crucial with all their love and wisdom. For this and much more, I am incredibly grateful. Finally, I could not have finished this dissertation without the unwavering support at all levels of my fiancé Filipe Moreira and my close friends, Cláudia Costa, Tânia Martins, Tânia Jordão and Márcio Rosa. Even scattered across the world, you are my People, my extended and so much cherished family.

Resumo

Os aminoácidos que compõem cada proteína estão covalentemente ligados por ligações peptídicas formando, coletivamente, as fundações que suportam as estruturas secundária e terciária da proteína. São as ligações covalentes mais prevalentes entre os aminoácidos das proteínas, seguidas pelas ligações dissulfureto. Estas últimas são ligações enxofre-enxofre (S-S) formadas dentro de uma proteína quando cada um dos grupos tiol (-SH) de dois resíduos de cisteína é oxidado, resultando na perda total de dois eletrões para um agente oxidante (Landgraf et al., 2017).

Landgraf e colegas (2017) sumariaram as funções das ligações dissulfureto nas proteínas em três vertentes principais: enquanto transmissores de sinal, como resíduos dos centros ativos na catálise enzimática e como suportes estruturais.

As ligações dissulfureto de sinalização atuam como sensores ambientais de oxirredução, participando na deteção de espécies de oxigénio reativas, na deteção de alterações nas condições de crescimento respiratórias, e na ativação da resposta ao stress oxidativo citoplasmático (Alvarez & Georgellis, 2010; Kang et al., 1999; Landgraf et al., 2017; Lee et al., 2004).

As ligações catalíticas de dissulfureto atuam como resíduos dos centros ativos em oxirredutases que catalisam a oxidação e isomerização de ligações de dissulfureto (Andersen et al., 1997; Gon et al., 2006; Jander et al., 1994; Landgraf et al., 2017).

Embora as funções de sinalização e catalíticas das ligações de dissulfureto sejam relevantes, esta tese debruça-se sobre as vias enzimáticas que existem no retículo endoplasmático e que catalisam a formação destas ligações com funções estruturais em proteínas.

As ligações dissulfureto formadas entre pares de cisteínas oxidadas têm um papel crítico na integridade estrutural, facilitando o correto enrolamento (*folding*) e estabilizando a estrutura terciária de muitas proteínas (Anfinsen, 1973; Zito et al., 2012). Por consequência, os sistemas biológicos desenvolveram, de forma evolutiva, inúmeros sistemas para a génese e manutenção de tais ligações. Os primeiros indícios científicos sobre a formação de pontes dissulfureto catalisadas por via enzimática surgiram com a descoberta da *protein disulfide isomerase* (PDI). Com este avanço seguiram-se anos de investigação centrada no esclarecimento da complexa rede de vias de

transporte de eletrões que suporta a formação das pontes dissulfureto (Ellgaard & Ruddock, 2005; Hatahet et al., 2009; Landgraf et al., 2017).

Nas células eucariotas a maturação de cerca de um terço das proteínas sintetizadas ocorre no retículo endoplasmático (RE). O *folding* proteico no RE envolve a formação de ligações dissulfureto com transferência de eletrões dos resíduos de cisteína na proteína para oxirredutases da família da PDI, a reoxidação desta pela *endoplasmic reticulum oxidoreductin-1* (ERO1) seguida pela redução do oxigénio molecular com formação de peróxido de hidrogénio (H_2O_2). Esta modificação pós-transducional é essencial para a estabilidade das proteínas, principalmente em proteínas secretadas para a membrana celular e para o meio extracelular.

Mais recentemente, foram identificadas várias vias alternativas para a síntese das pontes dissulfureto em eucariotas superiores. De entre estas, a via mais relevante tem a capacidade de reduzir o stress oxidativo no RE. A PDI interage com a *peroxiredoxin IV* (PRDX4), em vez de interagir com a ERO1, reduzindo-a e utilizando o H_2O_2 como aceitador final de eletrões (Tavender & Bulleid, 2010; Zito et al., 2010).

Esta dissertação visou essencialmente o estudo e avaliação da eficiência deste mecanismo alternativo, comparando-o com a principal via de *folding* oxidativo de proteínas no RE catalisada pela ERO1. Para tal, as proteínas envolvidas (PDI, ERO1 e PRDX4) foram utilizadas em experiências de oxidação *in vitro* da roGFP2, uma proteína fluorescente cujo espectro de excitação varia com a formação de pontes de dissulfureto. A roGFP2 atuou como proteína cliente ou substrato, sendo um modelo experimental ideal para avaliar o *folding* de proteínas e o seu estado redox, uma vez que a emissão de fluorescência depende da aquisição do estado nativo e do seu estado redox.

A metodologia aplicada incluiu a produção e purificação de proteínas recombinantes em *Escherichia coli* (*E. coli*) de todas as proteínas em estudo (PDI, ERO1, PRDX4 e roGFP2), bem como da *ubiquitin-like protease* (ULP). Foram usados géis de SDS-PAGE (eletroforese em gel de poliacrilamida na presença de dodecil sulfato de sódio) para avaliação da sobrexpressão e eficiência de purificação das mesmas.

As proteínas foram purificadas por cromatografia de afinidade, tendo por base a interação reversível entre a proteína de interesse e um ligando específico (níquel para proteínas com um His-tag ou glutationa para proteínas com tag de Glutationa S-Transferase, GST) ligado a uma matriz cromatográfica (Sepharose). Todas as proteínas com um tag de histidinas (PDI, roGFP2, PRDX4 e Ulp1) foram purificadas utilizando cromatografia de afinidade por iões metálicos imobilizados (IMAC). Por sua vez, a GST-ERO1 foi sujeita a cromatografia de afinidade por glutationa em *batch*, seguida de clivagem com Ulp1 do tag GST e subsequente remoção da Ulp1 por IMAC. A purificação da ERO1 é mais complexa, exigindo várias decisões estratégicas e a otimização de métodos e

condições para esta proteína específica. No entanto, as melhorias implementadas agilizaram o processo e promoveram um maior nível de pureza final da ERO1.

Para estudar a eficiência catalítica de cada via *in vitro*, nomeadamente os seus parâmetros cinéticos, fez-se variar a concentração de roGFP2 (de 0.1 a 10 μM) na presença de diferentes concentrações de PDI, ERO1 e/ou PRDX4 (1, 3 e 5 μM). Através da variação do rácio de fluorescência de excitação ao longo do tempo (492/400 nm [1]) para uma emissão de fluorescência a 530 nm, foi possível verificar a ocorrência de *folding* oxidativo da roGFP2 catalisado por ambas as vias. O substrato roGFP2 readquiriu a sua conformação nativa, restabelecendo as pontes dissulfureto intramoleculares (envolvendo a oxidação de grupos de tiol entre resíduos de cisteína) previamente quebradas por contacto com ditiotreitol (DTT, um forte agente redutor). Contudo, observou-se inibição por substrato para concentrações mais elevadas de roGFP2 (acima de 1 μM para a via primária da ERO1 e de 0.5 μM para a via alternativa da PRDX4).

Constatou-se igualmente que a oxidação foi substancialmente mais rápida na via principal (PDI/ERO1), e que a PDI atuou como limitante da velocidade de reação dessa mesma via. Para concentrações de substrato abaixo da inibição enzimática a velocidade de oxidação do substrato roGFP2 foi mais dependente da concentração de PDI do que de ERO1. Porém, na via secundária (PDI/PRDX4), a presença de inibição por substrato para concentrações relativamente baixas de roGFP2, não permitiu concluir qual dos catalisadores atua como limitante dessa via.

Testou-se ainda a conjunção das duas vias para avaliar uma possível sinergia entre elas, com a PRDX4 a utilizar H_2O_2 (produzido pela ERO1) como aceitador final de eletrões. Através destes ensaios verificou-se que as duas vias podem efetivamente atuar em sinergia, uma vez que a ERO1, na forma reduzida, é primeiramente oxidada pelo oxigénio residual presente no tampão, gerando H_2O_2, o qual pode oxidar a PRDX4. Uma vez oxidadas, tanto a ERO1 como a PRDX4 podem oxidar a PDI. Ao utilizar-se ERO1 reduzida num dos ensaios de sinergia das duas vias, verificou-se que ambas as vias se iniciaram suavemente, tornando-se cineticamente competitivas na oxidação da PDI. Estando oxidada, a PDI pôde então oxidar o substrato roGFP2.

Palavras-chave: produção e purificação de proteínas recombinantes, *folding* oxidativo de proteínas, *protein disulfide isomerase* (PDI), *endoplasmic reticulum oxidoreductin-1* (ERO1), *peroxiredoxin IV* (PRDX4), *oxidation sensitive Green Fluorescent Protein* (roGFP2).

[1] Este rácio reflete diretamente o grau de oxidação dos grupos tiol e a formação de ligações de dissulfureto na roGFP2.

Abstract

Around one-third of protein maturation in eukaryotic cells occurs in the endoplasmic reticulum (ER), where oxidative protein folding is a key step for the majority of proteins. This post-translational modification is essential for protein folding and stability and is mainly required for proteins that follow the secretory pathway towards the membrane. The main pathway involves the synthesis of intramolecular disulfide bonds with electron transfer from cysteine residues to oxidoreductases of the protein disulfide isomerase (PDI) family followed by re-oxidation of PDI by the endoplasmic reticulum oxidoreductin-1 (ERO1) and reduction of molecular oxygen, which generates hydrogen peroxide (H_2O_2).

More recently, an alternative pathway for the synthesis of these disulfide bonds was identified. In this pathway, PDI interacts with peroxiredoxin IV (PRDX4) instead of ERO1 and uses H_2O_2 as the final electron acceptor to reduce oxidative stress in the ER (Tavender et al., 2010; Zito et al., 2010).

This dissertation studied and evaluated the mentioned alternative pathway's efficiency and compared it with the main pathway catalysed by ERO1. The involved proteins (PDI, ERO1 and PRDX4) were expressed in *E. coli*, purified by affinity chromatography, and used *in vitro* to oxidise the client protein roGFP2, a fluorescent protein whose fluorescence excitation spectrum varies with the formation of a disulfide bridge.

To study the catalytic efficiency of each pathway, namely the kinetic parameters, roGFP2 concentration was varied in the presence of different concentrations of PDI, ERO1 and/or PRDX4. Oxidation of roGFP2 was observed in both pathways, although substrate inhibition was observed for higher substrate concentrations. It was clear that the PDI/ERO1 pathway's oxidation was substantially more efficient, with PDI acting as the rate-limiting step. It was also observed that the two pathways could act in synergy, with PRDX4 using the H_2O_2 produced by ERO1 to enhance oxidative folding capacity in the ER.

Keywords: recombinant protein expression and purification, oxidative protein folding, protein disulfide isomerase (PDI), endoplasmic reticulum oxidoreductin-1 (ERO1), peroxiredoxin IV (PRDX4), oxidation sensitive Green Fluorescent Protein (roGFP2).

List of Contents

List of Figures

List of Tables

List of Acronyms and abbreviations

A

A_{280}	absorbance at 280 nm
Amp	ampicillin
approx.	approximately
APS	ammonium persulfate
Asp	aspartic acid (or aspartate)

B

b	optical path length

C

c	protein concentration
$CaCl_2$	calcium chloride
CD	circular dichroism
Cys	Cysteine

D

ddH_2O	double-distilled water
dH_2O	distilled water
DNase	deoxyribonuclease
DTT	dithiothreitol

E

E	enzyme molecule
E. coli	*Escherichia coli*
e.g.	*exempli gratia*, for example, such as
ER	endoplasmic reticulum
ERAD	ER associated degradation
ERO1	endoplasmic reticulum oxidoreductin-1
ES	substrate molecule bound to an enzyme molecule catalytic site

F

FAD	flavin adenine dinucleotide
FT	flow-through
FTIR	fourier transform infrared spectroscopy

G

GFP	green fluorescent protein
Glu	glutamic acid
GOx	glucose oxidase
GPx7/8	Glutathione Peroxidase 7 and 8
GSH	reduced glutathione
GSSG	oxidised glutathione
GST	glutathione-S transferase tag

H

H_2O_2	hydrogen peroxide
His	poly-histidine tag
hPDI	human protein disulfide isomerase
HyPer	circularly permutated yellow fluorescent protein

I

i.e.	*id est*, that is
IMAC	immobilized metal ion affinity chromatography
IPTG	isopropyl β-D-1-thiogalactopyranoside

K

Kan	kanamycin
K_i	dissociation equilibrium constant
K_m	Michaelis-Menten constant

L

LB	Luria Bertani
Leu	leucine
Lys	lysine

M

M	protein marker/ladder
$MgCl_2$	magnesium chloride
MW	molecular weight
MWCO	molecular weight cut-off

N

n.d.	not defined
NaCl	sodium chloride
Ni	nickel
NMR	nuclear magnetic resonance

O

O/N	overnight
O_2	molecular oxygen
OD_{600}	optical density at 600 nm
OD_{280}	optical density at 280 nm
oxi	oxidised

P

P	product molecule
PDI	protein disulfide isomerase
PMSF	phenylmethylsulfonyl fluoride
PRDX4	peroxiredoxin IV
Prxs	Peroxyredoxins

Q

QSOX	quiescin-sulfhydryl oxidase

R

red	reduced
RNase	ribonuclease
roGFP2	redox-sensitive green fluorescent protein
RT	room temperature

S

S	substrate molecule
SD	standard deviation
SDS	sodium dodecyl sulphate
SDS-PAGE	sodium dodecyl sulphate polyacrylamide gel electrophoresis
SES	ternary complex of two substrate molecules bound to an enzyme molecule
SH	sulfhydryl group, thiol group
S-S	disulfide bonds

T

TBS	tris buffered saline
TEMED	tetramethylethylenediamine
Tris-HCl	tris hydrochloride

U

Ulp1	ubiquitin-like protease
UPR	unfolded protein response
UV	ultraviolet

V

v	velocity
VKOR	vitamin K epoxide reductase
V_{max}	maximum enzyme velocity
v/v	volume per volume

W

w/v	weight per volume

Symbols

δ	maximum dynamic range
ε	protein extinction coefficient

Chapter 1.
Introduction

1.1 Overview

Oxidative protein folding is a post-translational modification, essential for protein folding and stability and is mainly required for proteins that follow the secretory pathway towards the membrane. In eukaryotic cells, this key step for secretory protein maturation occurs in the endoplasmic reticulum (ER).

Because of its importance, oxidative protein folding in the mammalian ER is a redundant process, with complex and vast network pathways. The most prominent and canonical pathway involves the synthesis of intramolecular disulfide bonds promoted by the protein disulfide isomerase (PDI) family. PDI oxidises cysteines in nascent polypeptides to form disulfide bonds and can also reduce and isomerize disulfide bonds. Endoplasmic reticulum oxidoreductin-1 (ERO1) recycles reduced PDI family member PDIA1 using a Dinucleotide Adenine Flavin (FAD) cofactor to transfer electrons to oxygen, which generates hydrogen peroxide (H_2O_2) (A. G. Shergalis et al., 2020). Recently, parallel pathways have been identified. The most relevant so far has the ability to reduce the oxidative stress in the ER, in which PDI interacts with peroxiredoxin IV (PRDX4), reducing it and using H_2O_2 as the final electron acceptor (Tavender & Bulleid, 2010; Zito et al., 2010).

Accumulation of misfolded/unfolded proteins in the ER, caused by errors in the protein oxidative folding system, may lead to a disturbance in the normal functions of the ER. When the ER homeostasis is altered, it generates ER stress, which activates an unfolded protein response (UPR) (Mullick & Nayak, 2020). In turn, a failure of this response can trigger several disorders. UPR has been implicated in a variety of pathologies including metabolic, neurodegenerative and inflammatory diseases, and cancer (Galligan & Petersen, 2012).

Therefore, understanding protein folding mechanisms, particularly thiol-disulfide exchange and the functional interplay between ERO1, PDI and PRDX4 might lead to new biomedical approaches, including UPR targeting therapies (Galligan & Petersen, 2012).

1.2 Protein folding

In biological organisms, protein synthesis involves transcription, translation, and post-translational events. Most proteins only gain functionality when they fold, through a set of conformational changes, into unique three-dimensional structures. The ability to determine how an amino acid sequence folds to form a biologically active structure is one of the most important and challenging tasks in biology (Chang & Ventura, 2011).

Protein folding is complex and represents one of the most important processes at the protein function level (Malhotra & Kaufman, 2007b). In general, protein folding reactions are quite fast and their intermediates are transient and highly dynamic (Chang & Ventura, 2011). Moreover, the efficiency of these transitions depends strongly on environmental, genetic, and metabolic conditions, so conditions that disrupt or interfere with protein folding pose a threat to cell viability (Malhotra & Kaufman, 2007b).

The folding process was originally explained by Anfinsen (1972) which stated that a protein in the native, folded state is considered to be the thermodynamically most stable structure, and this structural set is determined by the amino acid sequence and environmental conditions (Powers et al., 2009). This fact implies that somehow the information required for a protein to acquire the native three-dimensional structure is imprinted in the primary sequence of the protein (Onuchic & Wolynes, 2004).

Although in evolution, a contemporary view of the protein folding is explained using an energy diagram (Figure 1.1). According to this principle, the unfolded state of a protein, represented by the highest energy state, can fold through several alternative pathways towards reaching the lowest energy and thermodynamically most stable folding state. Although there are several ways for a protein to reach the native state, there are also partially folded, misfolded, and even aggregated states that have lower energy than the unfolded state and where proteins can be trapped. However, imposed restrictions due to the chemistry and energy of the polypeptide chain itself limits the possible number of pathways that a polypeptide chain can follow under certain conditions. Despite this, the development of clusters with hydrophobic and electrostatic characteristics can be a barrier to the acquisition of the native state (Brodsky & Skach, 2011).

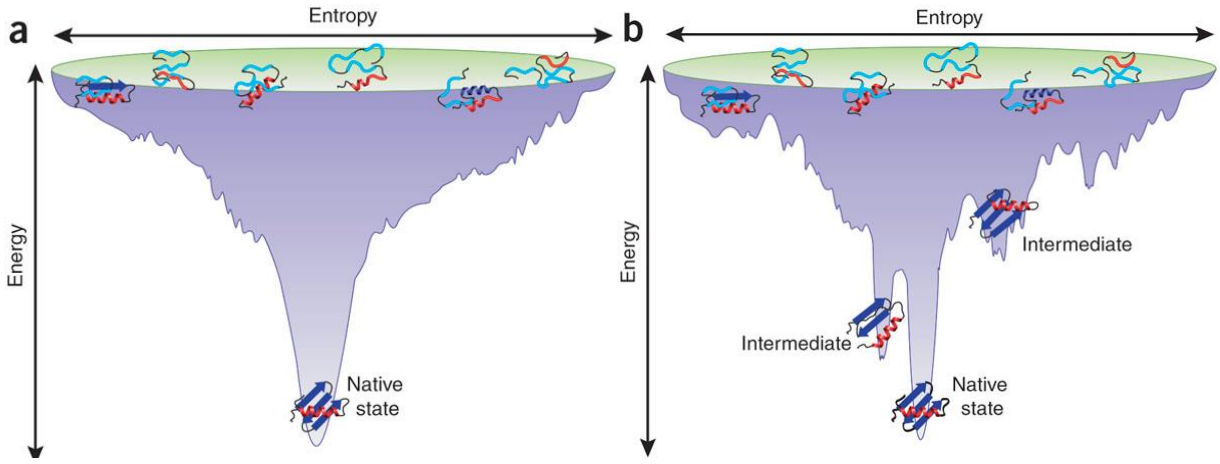

Figure 1.1. Schematic representation of folding funnels for hypothetical polypeptides.

Example of two energy landscapes, through which the polypeptide chain is funnelled to the native structure. **(a)** an ideal smooth and effective landscape for a small polypeptide. **(b)** a more rugged landscape, possibly via one or more populated intermediates. In both cases, the denatured state takes up a large number of structures possessing both native and non-native interactions elements (adapted from Bartlett & Radford, 2009).

In vivo, protein folding is assisted by a series of chaperone proteins, that bind to the transition states causing the protein folding to be conducted in the correct direction, and consequently avoiding the less favourable conformational states (Powers et al., 2009; Thomasson, 1997). Each protein involved in this process contributes differently and according to the properties and requirements of each client protein (Brodsky & Skach, 2011).

Besides conformational folding of the polypeptide chains driven towards the state with the lowest free energy, there are also several additional reactions that can influence the folding and the protein final structure, including glycosylation reactions, oligomerization and disulfide bond formation (Feige & Hendershot, 2011).

1.2.1 Protein stabilization through disulfide bonds

Disulfide bridges formation is one of the main factors for maintaining the three-dimensional structure of many proteins, assisting the folding process (Clark & Pazdernik, 2009). Intramolecular disulfide bridges formation involves the oxidation of the thiol groups (SH) of two cysteines (Cys)

towards the creation of *de novo* bonds between them, as well as the rearrangement of non-native disulfide bridges (Frand & Kaiser, 1999).

Under oxidizing conditions, and in the presence of two cysteine residues in a polypeptide chain, the covalent binding of these residues can occur, causing the polypeptide chain to bend, approaching the cysteine residues and thus helping the folding process (Clark & Pazdernik, 2009) (Figure 1.2).

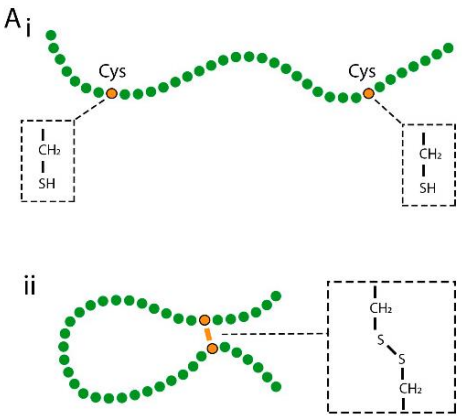

Figure 1.2. Disulfide bond formation.

It involves a reaction between the sulfhydryl (SH) side chains of two cysteine residues: an S^- anion from one sulfhydryl group acts as a nucleophile, attacking the side chain of a second cysteine to create a disulfide bond, and in the process releases electrons (reducing equivalents) for transfer (adapted from Robinson & Bulleid, 2020).

Due to its covalent nature, this post-translational modification is an essential step in protein maturation and stability. This type of bond has the potential to limit other energetically favourable modifications that might lead to non-native conformations, promoting the correct positioning to ensure the folding. They are also able to stabilize the proteins by reducing the entropy of the unfolded state (*i.e.* decreasing the entropy of the denatured state) and consequently, favouring the native state (Moroder & Buchner, 2009). It should be noted, however, that if the two cysteine residues are not properly aligned, these interactions might result in twisted conformations, culminating in less stable structures (Clark & Pazdernik, 2009). As a result, the effect of a disulfide bridge on a given protein is determined by its location in the protein structure (Moroder & Buchner, 2009).

Because disulfide bridges increase the stability of a protein conformation, their formation is very important, especially for proteins that go through the secretory pathway to the membrane (since the outside cell environment is harsher in terms of redox conditions and concentration of certain ions) (Feige & Hendershot, 2011; Moroder & Buchner, 2009). The creation of these bridges is critical for shielding proteins against damage caused by oxidizing and proteolytic enzymes, among others (Moroder & Buchner, 2009).

Previous *in vitro* studies in the protein folding field have shown that disulfide bridges can develop spontaneously, and that, the polypeptide chain may attain its natural shape, even when unassisted. The creation of these bridges, however, is slower than the other processes involved in folding since it is dependent on a redox reaction, which requires the presence of an electron acceptor element (Tu & Weissman, 2004). Due to the intricacy of this process, disulfide bond formation is considered to be a rate-limiting step in protein biosynthesis (Moroder & Buchner, 2009). Therefore, despite the extreme importance of these bonds in protein stability, their formation is in general difficult to achieve, particularly in proteins with a high number of possible bridges, as the probability of incorrect disulfide bridges factorially increases with a cumulative number of cysteines (Ren & Bardwell, 2011).

1.2.2 Protein quality control in health and disease

Eukaryotic cells have developed a complex and vast network of quality control mechanisms to prevent and lessen problems resulting from protein folding errors, present in all cellular organelles (Metzger, 2009).

In the endoplasmic reticulum, where the biosynthesis of secretory proteins occurs, there is a vast number of proteins that are part of the protein folding quality control mechanism, allowing the correct maturation of proteins before they transit to the Golgi apparatus. In the other cell organelles the evaluation of protein folding quality happens in a more limited way (Feige & Hendershot, 2011). This control system contributes to the correct folding of proteins, and also intervenes in cases where the proteins have folded into incorrect structures, forwarding them to the Unfolded Protein Response (UPR) system, or even destroying them through ER-associated degradation (ERAD), as shown in Figure 1.3 (Metzger, 2009).

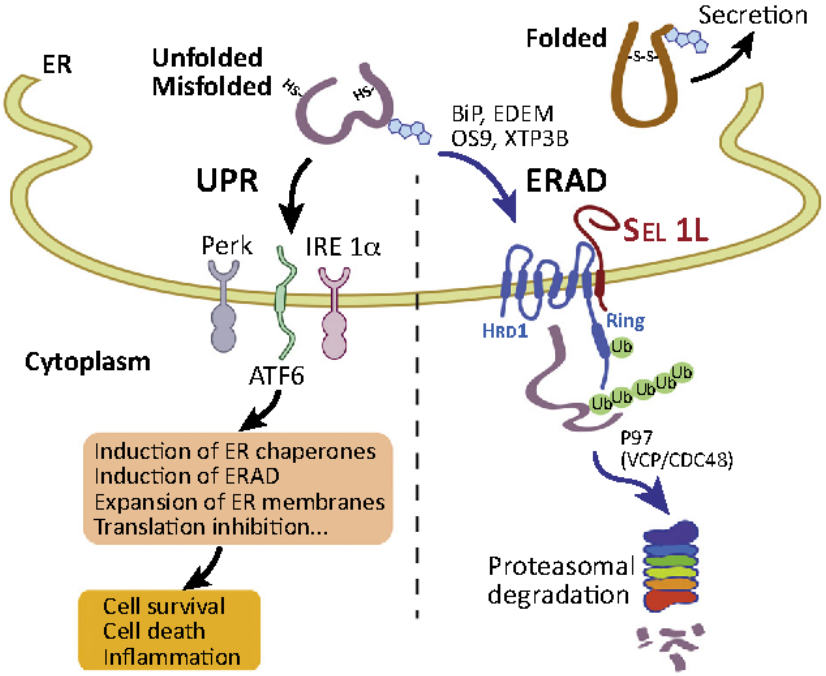

Figure 1.3. Overview of two crucial endoplasmic reticulum (ER) quality-control systems in mammals.

While folded proteins exit the ER, terminally unfolded or misfolded proteins in the ER activate unfolded protein response (UPR) via three sensors, IRE1α, PERK, and ATF6, which initiate multiple signalling pathways leading to the induction of ER chaperones and ER-associated degradation (ERAD), expansion of ER membranes, and translation inhibition. In addition, misfolded proteins can be recruited to the ERAD complex via the activity of various ER chaperones such as BiP, EDEM, OS9, and XTP3B for cytosolic degradation. Following retrotranslocation into the cytosol, substrates are ubiquitinated and, with the help of P97 (VCP/ CDC48) and degraded by the proteasome in the cytosol (adapted from Qi et al., 2017).

Accumulation of misfolded/unfolded proteins in the ER caused by errors in the protein oxidative folding system can lead to ER stress which triggers the UPR system. This essential adaptive intracellular signalling system, responds to metabolic, oxidative stress, and inflammatory response pathways (S. Wang & Kaufman, 2012), and is extremely important, especially in terms of diseases linked to improper protein folding (Metzger, 2009).

Although most of the secreted proteins are correctly folded, mutations, stress and random errors can decrease the yield or even the folding rate of the proteins, ultimately manifesting in a disease or pathology if the quality control mechanisms fail (Brodsky & Skach, 2011).

These diseases can be caused by genetic mutations resulting in inadequate or incorrect folded proteins, which leads to their premature degradation or their inability to perform their normal function. Others can be derived from the accumulation of proteins as toxic aggregates that should have been removed from the cell, interfering with the mechanism responsible for protein degradation. Similarly, some may directly affect the components of the quality control system, such as the ER and cytosol, leading to an overall incapacity of the cells to deal with poorly folded proteins (Brodsky & Skach, 2011; Metzger, 2009).

In humans, it was already established more than a hundred disorders (such as cystic fibrosis, liver disease, epilepsy, cardiac arrhythmias and Alzheimer) that share cellular pathologies resulting from incorrectly folded proteins that are prematurely degraded or accumulate as toxic aggregates in the ER (Brodsky & Skach, 2011). Researchers also believe that protein misfolding might be the cause of up to half of all human diseases (Chaudhuri & Paul, 2006).

UPR has been implicated in a variety of pathologies but has emerged, in the last decade, as a promising therapeutic target for a variety of diseases, including Alzheimer, Parkinson, alcoholic and non-alcoholic liver disease, and type 2 diabetes (Galligan & Petersen, 2012; Malhotra & Kaufman, 2007a).

It has also been reported that both PDI and ERO1 dysfunction critically impacts a variety of diseases states. Recent studies discovered that the triad PDI, ERO1 and PRDX4 are overexpressed in several cancers and linked to other disorders such as diabetes and neurodegenerative diseases (A. G. Shergalis et al., 2020).

While ERO1 seems to stimulate cell migration and invasion in ERO1-dependent cancers, PRDX4 has recently been shown to contribute to carcinogenesis, treatment resistance, metastasis, and tumour recurrence (Jia et al., 2019; A. G. Shergalis et al., 2020). The knockdown of ERO1α has been related to the suppression of cancer signalling proteins, supporting the search for new, selective ERO1 inhibitors for cancer therapy (A. G. Shergalis et al., 2020).

Understanding protein folding mechanisms, particularly thiol-disulfide exchange pathways and their interplay, might lead to new UPR targeting therapies that could aid in the treatment of a wide range of pathologies, and serve as a new approach for cancer therapy (Galligan & Petersen, 2012).

1.3 Oxidative folding in the Endoplasmic Reticulum (ER)

Protein folding plays a vital role in regulating biological activity and targeting proteins to different cellular locations (Dobson, 2003). This presents a challenge for the eukaryotic cell, especially regarding the proteins that follow the secretory path, as they must be able to operate correctly in the places they are requested. To overcome this problem, the eukaryotic cell has

developed a reticular organelle, the endoplasmic reticulum (ER), where the environment is oxidizing, and the conditions are similar to the conditions present outside the cell. Moreover, this organelle is equipped with chaperone proteins and enzymes that help in the folding process and their quality control (Feige & Hendershot, 2011).

The ER is organized in a kind of membrane labyrinth branched and interconnected, and its membrane forms a single plate covering a single internal space, the ER lumen (Figure 1.4). This compartmentalization of the ER allows the existence of the necessary redox conditions for disulfide bond formation.

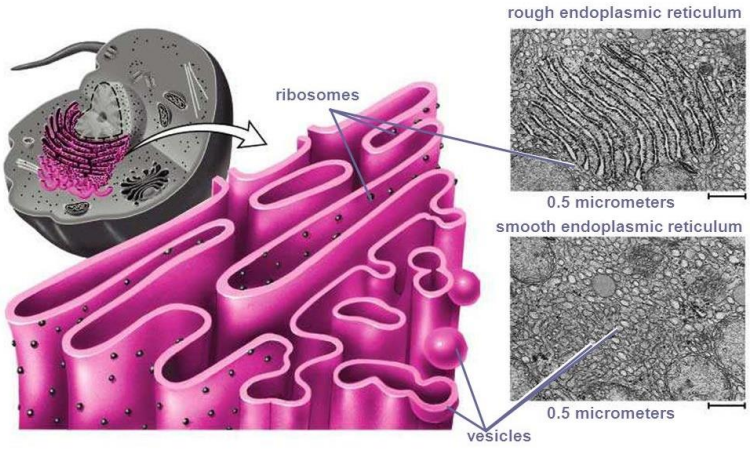

Figure 1.4. Representation of the endoplasmic reticulum (ER).

Left: an illustrative image of a eukaryotic cell (grey) and the ER (fuchsia). Right: electron microscopy of the rough endoplasmic reticulum containing aggregate ribosomes (top) and smooth ER (bottom) (adapted from Selvakumari, 2018).

While under strong reducing conditions disulfide bond formation is thermodynamically unfavourable, excessively oxidizing conditions can lead to protein misfolding (due to the formation of incorrect intra- and intermolecular bridges). As a result, the redox potential in the ER must be efficiently controlled (Moroder & Buchner, 2009).

This compartment presents millimolar concentrations of reduced glutathione (GSH) and oxidised glutathione (GSSG) ratios ranging from 1:1 to 3:1, respectively. Given the relative abundance of GSSG in the ER lumen, it was hypothesized that GSSG was the source of the oxidizing capacity required for the production of disulfide bridges. However, it seems that glutathione is not directly involved in the process of *in vivo* disulfide bond formation, indicating that another electron acceptor is implicated in the process (Frand & Kaiser, 1999).

Many proteins are constantly moving across the ER lumen to other destinations, including the plasma membrane and the extracellular space. In addition to these, there are other proteins that remain retained in the ER due to a four amino acid retention signal (Lys-Asp-Glu-Leu) at the C-

terminal end. These resident proteins function as catalysts for many reactions, some integrate the protein quality control system mentioned earlier and others are involved in disulfide bridge formation and contribute to the oxidative folding of proteins in the ER. An interplay between these functions is somewhat common (Moroder & Buchner, 2009).

The study of oxidative folding revealed that the unassisted natural occurrence of disulfide bond formation *in vitro* is a slow but spontaneous phenomenon (may take hours to days). Contrary, it was observed that, *in vivo*, this process is fast, indicating that in living cells, the formation and rearrangement of disulfide bridges must be catalysed by a set of proteins (Frand & Kaiser, 1999). Furthermore, oxidative folding revealed a high degree of diversity of folding mechanisms manifested mainly by the heterogeneity of intermediate structures (Chang & Ventura, 2011).

As it will be shown throughout this work, four components are involved in every redox electron flow system in disulfide bond formation: a client protein to be oxidised, a direct donor of disulfide bonds such as PDI, an enzyme that acts as a disulfide bridge generator capable of oxidizing the direct donor of disulfide bonds, and a final electron acceptor (Inaba, 2010).

1.3.1 Main pathway: PDI/ERO1

Both prokaryotes and eukaryotes cells have several proteins and cofactors that accelerate the formation of disulfide bridges towards the native state. In the ensemble of reactions involved in the oxidative folding of eukaryotic proteins, some proteins, intervening in the folded structure's acquisition and disulfide bridges formation, were identified, isolated, and characterized (Inaba, 2010).

Within this group, two proteins were implicated, a protein from the isomerase family called Protein Disulfide Isomerase (PDI), and a protein of the oxidoreductase family (dependent on the FAD) called Endoplasmic Reticulum Oxidoreductin-1 (ERO1). It has been reported that ERO1 is oxidised by molecular oxygen, and it acts as a PDI oxidiser, having the potential to oxidise cysteines into folded proteins.

A considerable part of this dissertation focused on the study and evaluation of the catalytic efficiency of the PDI/ERO1 pathway, following the *in vitro* oxidative folding of a substrate protein (roGFP2) and characterizing the kinetic parameters.

1.3.1.1 Protein Disulfide Isomerase (PDI)

PDI is one of the resident proteins in ER that has shown to be essential in the catalysis of the oxidation of SH groups in disulfide bonds (S-S) (Zinn & Leopold, 1973). This protein was one of the first to be identified and belongs to the protein superfamily of thioredoxins (Moroder & Buchner, 2009).

This enzyme is present in millimolar (mM) order concentrations in the ER lumen of both yeasts and mammalian cells (Walker & Gilbert, 1994). Structurally, mammalian PDI (Figure 1.5) is constituted by four main domains (**a**, **a'**, **b** and **b'**), a region of connection between the domains **b'** and **a'** (with about 19 amino acids), and also by an extension of residues at the end of C terminal (A. Shergalis & Neamati, 2016; C. Wang et al., 2010).

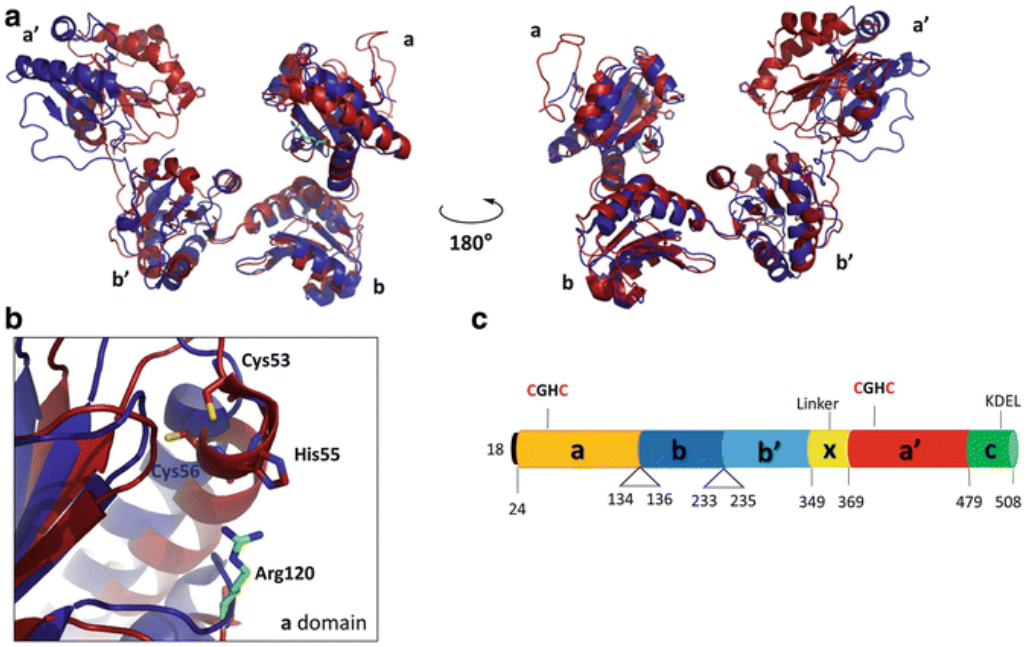

Figure 1.5. Model of the overall structure of PDIA1.

(a) Crystal structures of reduced (red) and oxidised (blue) PDIA1. (b) Close up of the CGHC active site of the **a** domain of reduced PDIA1 and associated arginine residue (green). (c) Domain structure of PDIA1.
Domain boundaries are numbered based on full-length PDI. The PDI active sites are located on the **a** and **a'** domains, which share 33.6% identity in PDIA1 and contain the four conserved amino acids Cys-Gly-His-Cys.
The structure of PDI reveals that the four domains are arranged in a "U" shape with the active centres facing each other at the ends of the "U". Therefore, the two inactive domains are inserted between the two active domains and the tail at the terminal "C". The interaction between the PDI and the unfolded proteins is facilitated by the presence of hydrophobic residues inside the U-shaped surface. (adapted from A. Shergalis & Neamati, 2016).

The **a** and **a'** domains are similar and contain two catalytically active cysteine residues each. Contrarily, domains **b** an **b'** have no active cysteine residues. The **a** and **a'** domains of this protein are capable of catalysing both oxidation and isomerization reactions (Moroder & Buchner, 2009). This capacity can be explained by the presence of Cys pairs in the catalytic centre of PDI. If the Cys

are in the oxidised form, PDI acts by giving these disulfides to the proteins in the substrate, thus promoting their oxidation. Conversely, if the Cys are in the reduced form, they can attack the disulfide bridges that have been incorrectly established (Dalbey & Heijne, 2002). Because of this dual functionality, PDI is regarded as a highly adaptable and versatile enzyme. The performance of both functions is influenced by the redox environment present in the ER lumen (Moroder & Buchner, 2009).

The formation of disulfide bridges between the thiol groups (SH) of two cysteine residues, assisted by PDI, entails the deprotonation of a free thiol to generate a thiolate anion. A transient covalent binding (called mixed disulfides) is then formed between the catalytic protein and the client protein. A second exchange takes place where the thiolate anion attacks and eliminates this transient binding. As a result, an oxidised and a reduced cysteine pair emerge, and the intramolecular bridge is effectively moved from one pair to another (Figure 1.6) (Moroder & Buchner, 2009).

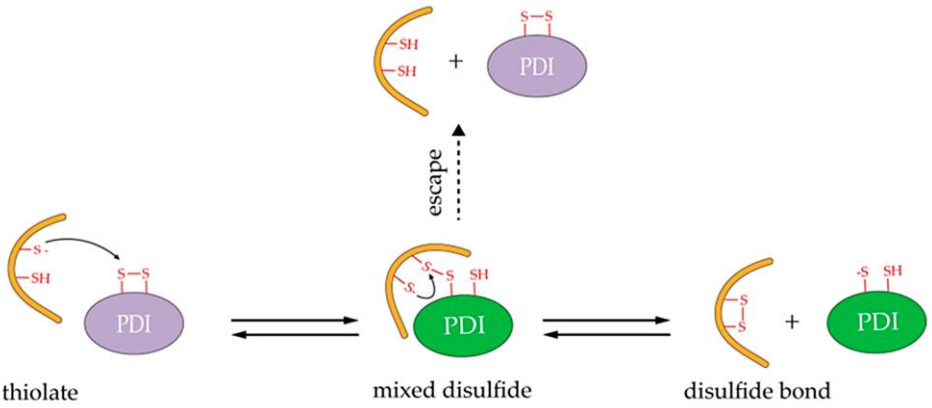

Figure 1.6. Schematic of the sulfhydryl groups (SH)/disulfides (S-S) reaction catalysed by PDI.

For simplicity, only one active site of PDI is shown. In the model are represented substrate proteins (yellow); free sulfhydryl, disulfide bond, or thiolate (red); oxidised PDI (purple) and reduced PDI (green) (adapted from Fu et al., 2021).

1.3.1.2 Endoplasmic Reticulum Oxidoreductin-1 (ERO1)

ERO1 is a membrane-associated ER-resident glycoprotein that uses FAD as a cofactor and is considered a key enzyme for disulfide bridge formation in eukaryotic cells, both in aerobic and anaerobic environments.

ERO1 is able to transfer electrons from its thiol groups to molecular oxygen in aerobic environments. However, the outcome of the electrons in anaerobic conditions remains unclear. It

has been described in the literature that free FAD in solution is sufficient to conduct the formation of disulfide bridges under anaerobic conditions. This factor provided insight into the mechanistic of oxidised ERO1 regeneration and disulfide bridge maintenance under such circumstances (Gross et al., 2006).

There is a solitary ERO1 protein in *Saccharomyces cerevisiae* (ERO1p) and two (ERO1α and ERO1β) in mammals. Both mammalian isoforms can oxidise PDI (Moroder & Buchner, 2009). A representation of human ERO1α is shown below in Figure 1.7.

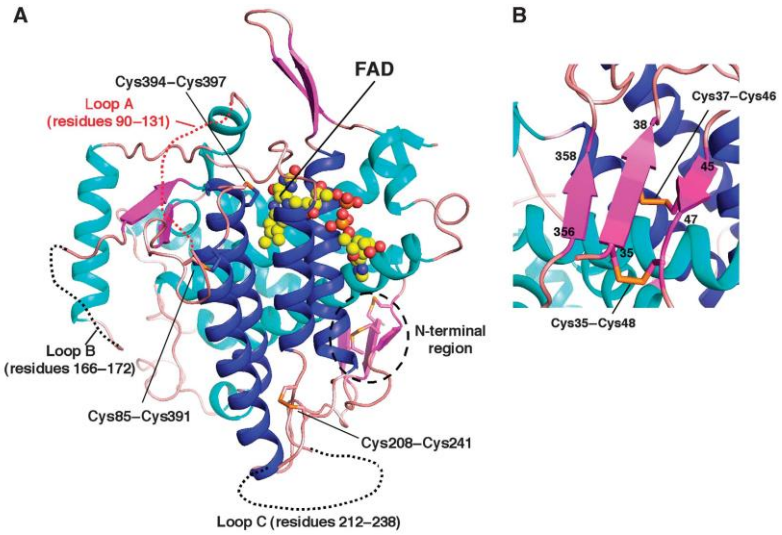

Figure 1.7. Model of the overall structure of human ERO1a.

Ribbon diagram of the hyperactive form of human ERO1a. Loop segments that could not be modelled due to the lack of electron density are shown by dotted lines. The regulatory loop including Cys94, Cys99, Cys104 and Cys131 is illustrated by a red dotted line. Structural and active-site disulfides characterized in this study are represented by sticks. The four-helix bundle constituting the catalytic core region of ERO1a is shown in dark blue. The FAD molecule is represented by balls, in which carbon, nitrogen, oxygen and phosphorus atoms are in yellow, blue, red and orange, respectively. (B) Close-up view of the N-terminal region of human ERO1a. Disulfide bridges formed in this region are represented by sticks. Numbers indicate the residue number from the N-terminus (adapted from Inaba et al., 2010).

1.3.1.3 Reaction mechanism

The transfer of a disulfide bridge between ERO1 and PDI involves the exchange between thiol groups and disulfides between one enzyme in the reduced form and the other enzyme in the oxidised form. In this reaction, an intermediate with an intermolecular disulfide bond (mixed disulfide) is formed due to the nucleophilic attack of the disulfide bridge in the oxidised species (ERO1) by the thiolate anion derived from reactive cysteine in the reduced species (PDI). This

intermediate is resolved by intramolecular attack by a second thiolate anion derived from the same enzyme (Frand & Kaiser, 1999).

Figure 1.8 schematically summarizes PDI/ERO mediated pathway for oxidative folding.

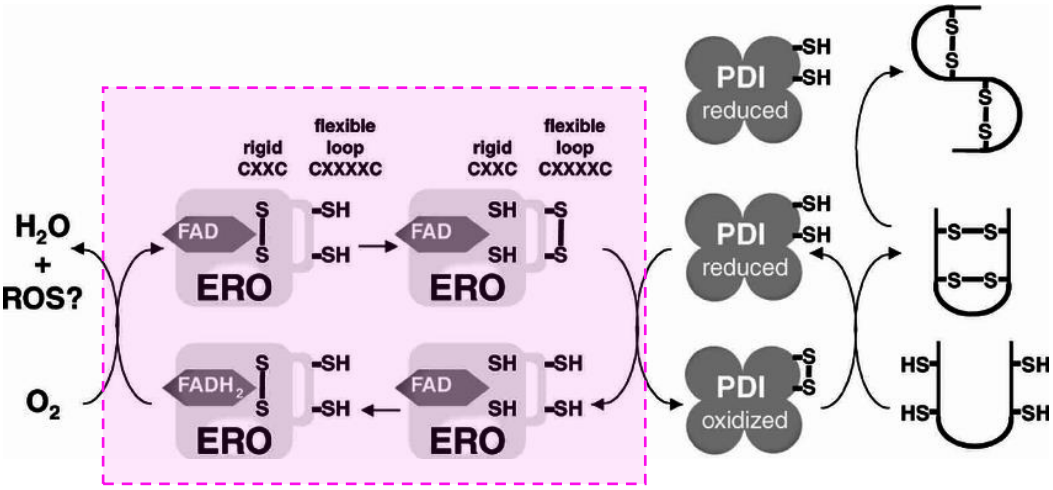

Figure 1.8. Proposed model for PDI/ERO1 mediated oxidative protein folding in the ER.

Oxidised PDI functions as disulfide donor for the oxidative folding of ER client proteins (thiol-oxidation), while reduced PDI can shuffle their disulfide bonds (disulfide isomerization, top right). For simplicity, only one of the two redox-active sites of PDI is shown. PDI is recharged by a cascade that consists of ERO1, its cofactor FAD and O_2. Electrons flow from the ER client to the active site of PDI. Next, the electrons from PDI flow to ERO1 (to the flexible CXXXXC motif and from there to a "rigid" CXXC motif present in the interior of ERO1). Finally, electrons flow from ERO1 to FAD, with O_2 as terminal electron acceptor and H_2O_2 generation (adapted from Van Anken & Braakman, 2005).

ERO1 protein has two pairs of catalytic cysteines, capable of oxidizing PDI, the active centre cysteines, and the shuttle cysteines. Direct oxidation of PDI occurs by the shuttle cysteine pair, which in turn is reoxidised by the active centre cysteines. The active centre cysteines are then reoxidised by electron transfer to the FAD cofactor and molecular oxygen, producing hydrogen peroxide. This mechanism is highlighted in Figure 1.8 (pink square).

Because each synthesis of a disulfide bond by ERO1 is connected with the generation of a hydrogen peroxide molecule, which accumulates and causes oxidative stress, ERO1's enzymatic activity has to be controlled. Therefore, to maintain the redox equilibrium in the ER, ERO1 is under the action of a regulatory mechanism in which two pairs of non-reactive cysteines operate as redox environment sensors (Inaba, 2010). Under oxidizing conditions, the formation of disulfide bridges on the regulatory cysteines limits the ability of the "shuttle" cysteines to oxidise PDI. Under reducing conditions, regulatory cysteines reduction enables the movement of the loop containing the shuttle cysteines, allowing the oxidizing activity of ERO1 (Sevier & Kaiser, 2008).

1.3.2 Alternative pathway: PDI/PRDX4

Great efforts have been made to identify different pathways besides PDI/ERO1 and clarify the intricate system behind disulfide bond formation in the ER. Zito and colleagues (2010) searched for possible alternatives through the isolation of probable PDI oxidizing proteins *in situ*, where PRDX4 was identified as the most prominent candidate. In the presence of hydroperoxides, this protein is capable of oxidizing PDI, and the oxidation of the substrate proteins is subsequently achieved (Zito et al., 2010).

Mouse knock-out experiments show that PRDX4 is not essential, probably due to the redundancy of disulfide bond formation in the mammalian ER, as there is a multiplicity of pathways for this purpose and a PDI/ERO1 predominance. Nevertheless, PRDX4 plays a vital role in the formation of disulfide bonds in ERO1 deficient cells (Zito et al., 2010).

Another considerable part of this dissertation focused on the study and evaluation of the catalytic efficiency of this alternative pathway, following the *in vitro* oxidative folding of roGFP2 and comparing it with the main pathway.

1.3.2.1 Peroxiredoxin IV (PRDX4)

Peroxyredoxins (Prxs) comprise a family of peroxidases found in prokaryotes, archaeobacteria and eukaryotes. These enzymes reduce hydrogen peroxide and alkyl hydroperoxides to water and alcohol respectively (Figure 1.9) with the use of reducing equivalents derived from donor molecules containing thiol groups (NCBI, 2019).

$$AH_2 + H_2O_2 \xrightarrow{\text{Peroxidase}} A + 2H_2O$$

$$AH_2 + ROOH \xrightarrow{\text{Peroxidase}} A + ROH + H_2O$$

Figure 1.9. Representative reactions catalysed by peroxidase activity.

Peroxidases or a group of oxidoreductases typically catalysed biological reactions, in which peroxides such as hydrogen peroxide (H_2O_2) and alkyl hydroperoxide (ROOH) are reduced, while a redox substrate (AH_2) acting as an electron donor is oxidised (adapted from Garg et al., 2015).

In eukaryotes, there is a high number of genes encoding for peroxiredoxins due to the existence of many isoforms destined for different subcellular compartments.

Each of the isoforms is unique in the sense that it is submitted to different reaction intermediates during catalysis, has a different distribution in organelles and presents distinct patterns of expression during development. Some of these isoforms appear to participate in intracellular signal transduction by controlling the concentration of hydrogen peroxide, while others provide defence against oxidative damage, playing a critical role in the cellular response to oxidative stress (Rhee et al., 2001).

This class of enzymes can be categorised into five subfamilies: Prx1 (or Prx1/AhpC), Prx6, Prx5, Tpx, and PrxQ (or PrxQ/BCP), as well as a sixth possible subfamily AhpE (which is not well represented and thus cannot be reliably classified). Within each subfamily, the sequence-level homology tends to be higher than 30% and between subfamilies from 15% to 30% (Karplus, 2015).

Mammal peroxiredoxin IV (PRDX4, sometimes also referred as PRDX IV or Prx IV), along with peroxiredoxin I, II and III, belong to the peroxiredoxin subfamily Prx1 that have cysteine residues preserved in the NH_2- and COOH- terminal chains separated by 121 amino acid residues (Rhee et al., 2001). The overall sequence homology of PRDX4 with the others is at least 56% or higher. The sequences surrounding both cysteine residues are highly conserved which may indicate the importance of those motifs for the activity of Prx 1 protein family (Rhee et al., 2001).

Just like the other peroxiredoxins within the subfamily (Prx1), the structure of human PRDX4 (Figure 1.10) reveals that the enzyme forms a decamer ring by compressing a pentamer of dimers. However, PRDX4 is the only one that maintains a stable decameric structure, regardless of the redox state (Sato & Inaba, 2012).

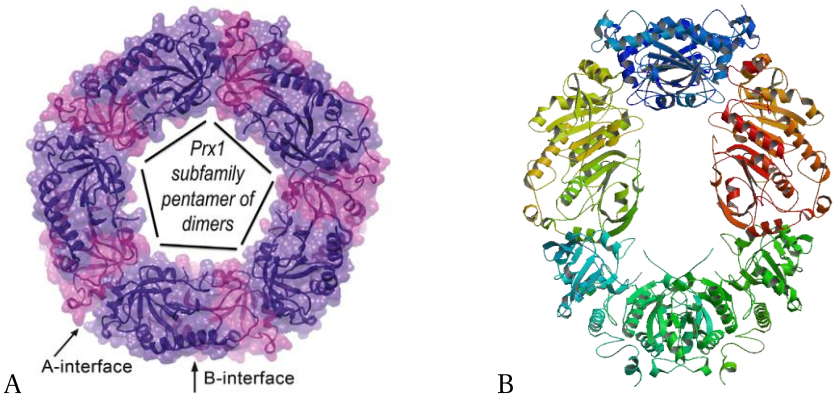

Figure 1.10. Prx1 subfamily decamer and crystal structure of PRDX4 (PDB 2PN8).

A) Decamer commonly seen for Prx1 subfamily such as mammalian PRDX4. The decamer is formed of a pentamer of B-type dimers associated through the A-type interfaces. B) The crystal structure of the decameric PRDX4. In biological systems, PRDX4 can exhibit dimeric and decameric states. The presence of either may be redox-regulated. PRDX4 protein can form heterodimer or multimer with other Prx isoforms (adapted from Abbasi et al., 2012; Karplus, 2015).

PRDX4 can be present in biological systems as both dimers and decamers, the presence of either states may be redox-regulated. This enzyme can also form heterodimers or multimers with other Prx isoforms (Mishra et al., 2013). PRDX4 is abundantly expressed in pancreas, liver and heart and with less extension, in blood, leukocyte and brain (Schulte, 2011). It is mainly localized in the endoplasmic reticulum (ER), but can be present in the cytosol, lysosome, nucleus, or secreted (Fujii & Ikeda, 2002; Leyens et al., 2003).

PRDX4 antioxidant properties may play a fundamental role in the redox balance in the ER. However, under strong oxidative stress conditions, PRDX4 can undergo further oxidation to sulfinic/sulfonic acid forms which can only be reduced by sulfiredoxin (Jeong et al., 2012). This overoxidised/hyperoxidised form of PRDX4 has no antioxidant properties, but may still function as molecular chaperone and assist in protein folding (Rhee & Woo, 2011; Zito et al., 2010). It has also been demonstrated that PRDX4 can mediate multiple cell signalling pathways (Mishra et al., 2013).

1.3.2.2 Reaction mechanism

As described earlier, the literature supports the conclusion that PRDX4 is, in fact, capable of promoting the formation of disulfide bridges in the presence of PDI. Since ERO1 accepts electrons directly from the reduced active centre of the PDI, it seems plausible that this alternative pathway could use a similar process in the transfer of its electrons.

Figure 1.11 schematically summarizes this PRDX4 mediated pathway for oxidative folding.

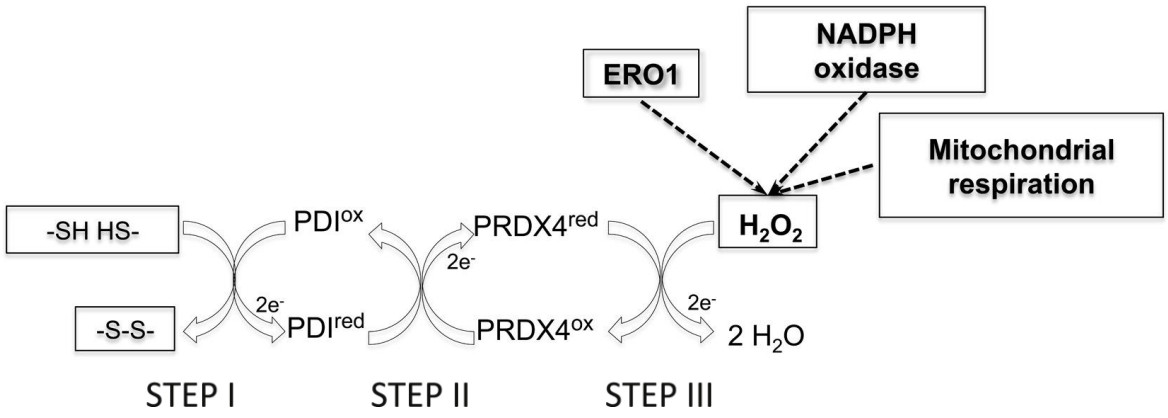

Figure 1.11. Model for PRDX4-Mediated Oxidative Protein Folding in the ER.

Disulfide bond formation in the substrate protein (step I) leaves PDI in a reduced state. PDI is reoxidised by reducing the active-site disulfide (formed between two PRDX4 protomers) in step II. PRDX4 is reoxidised by interaction of its peroxidic cysteine (C127) with H_2O_2, releasing one molecule of water. The sulfenic acid is resolved by C287, regenerating the disulfide and releasing the second molecule of water (step III). PRDX4 may utilize H_2O_2 produced by different sources, including ERO1 (adapted from Zito et al., 2010).

1.3.3 Synergy between pathways: PDI/ERO1/PRDX4

Konno, Zito and colleagues (2015; 2010) observations were consistent with the existence of an ER-localized PRDX4 mechanism for disulfide bond formation, parallel and ERO1-independent, fuelled by an alternative and unknown lumenal source of H_2O_2 in mammalian cells. Nevertheless, in their studies, the authors were unable to verify whether a synergy between these pathways could actually occur *in vivo*. Conversely, Tavender and co-workers showed that mammalian PRDX4 metabolises hydrogen peroxide produced by ERO1 (Tavender et al., 2010; Tavender & Bulleid, 2010).

In this dissertation, two specific assays were conducted combining the catalysts from PDI/ERO1 and PDI/PRDX4 pathways to characterize the potential synergy between them. The proposal interaction mechanism is exemplified above in Figure 1.12 and Figure 1.13.

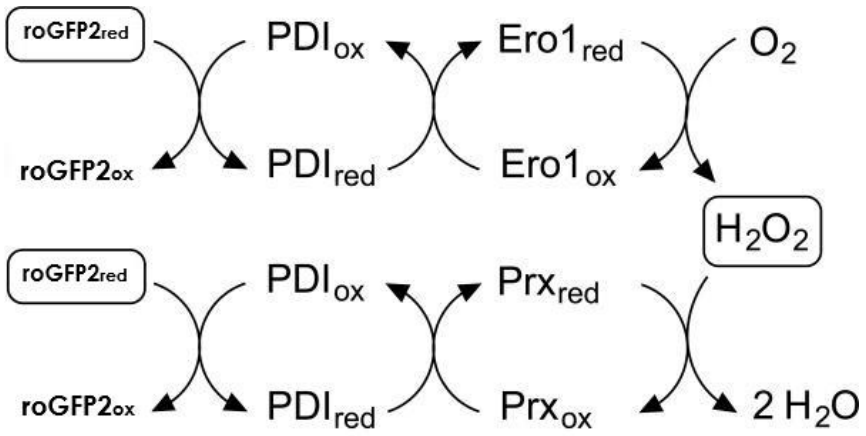

Figure 1.12. Proposed mechanism for redox cycling in the ER.

This mechanism proposes an interaction between PDI, ERO1 and PRDX4 (referred to in the scheme as Prx). The client protein is represented by roGFP2 (adapted from Hudson et al., 2015).

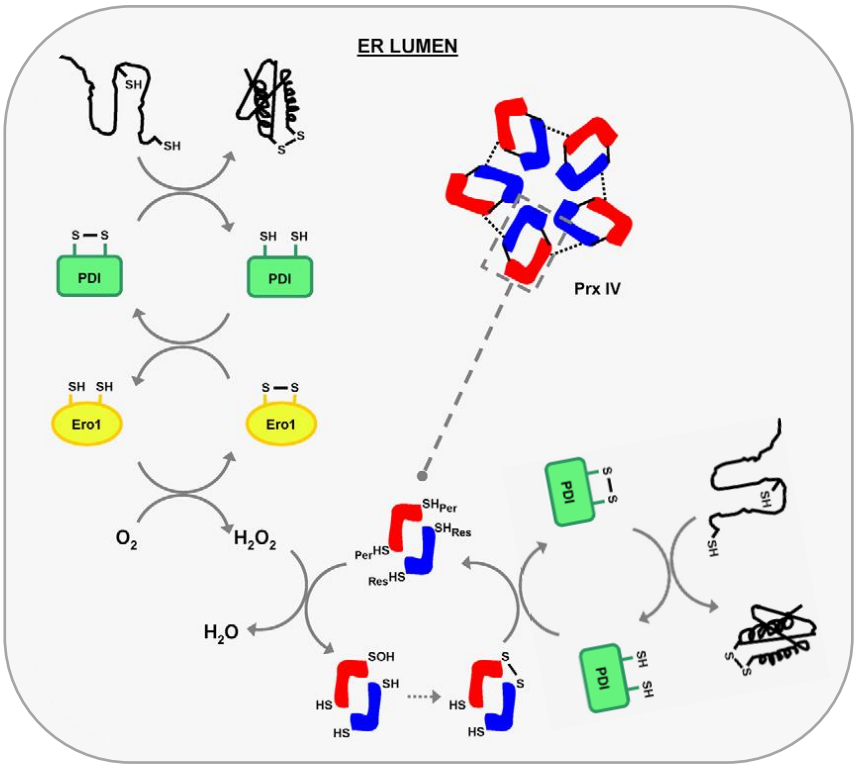

Figure 1.13. Schematic illustrating the role of PRDX4 in peroxide elimination and a possible synergy between PDI, ERO1 and PRDX4 during formation of disulfide bonds in the mammal ER.

Oxidation of PDI facilitates the introduction of a disulfide into a client protein during PDI-catalysed oxidative folding (represented on the top left and at the bottom right). As ERO1 is re-oxidised by molecular oxygen the hydrogen peroxide produced is catabolised by PRDX4 (referred in the scheme as Prx IV), resulting in changes in PRDX4 redox state (SHPer, peroxidatic cysteine; SHRes, resolving cysteine). Continued peroxidase activity requires a thiol-dependent recycling pathway, provided by PDI (adapted from Tavender & Bulleid, 2010).

In the reaction mediated by ERO1, the oxidised PDI is reduced by establishing the disulfide bridge in the substrate protein and sequentially, oxidised ERO1 acts on the reduced PDI, re-oxidizing it again. The re-oxidation of ERO1 involves the reduction of molecular oxygen (O_2) generating hydrogen peroxide (H_2O_2). Concomitantly, in the PRDX4 mediated reaction, the oxidised PDI is also reduced by establishing disulfide bridges in the substrate protein (roGFP2) and then re-oxidised by the oxidised PRDX4. Lastly, the now reduced PRDX4 is re-oxidised by transferring electrons to H_2O_2 and forming two molecules of water during the process.

1.3.4 Other pathways

Although their physiological roles are still poorly understood, other pathways have gained some late attention – *e.g.* PDI oxidases glutathione peroxidase7 (GPx7), glutathione peroxidase 8 (GPx8) and vitamin K epoxide reductase (VKOR); and a PDI-second pathway using quiescin-sulfhydryl oxidase (QSOX).

In the last years, new alternatives to PDI/ERO1 mediated oxidative protein folding in the ER have been investigated and pursued. PDI/PRDX4 mediated pathway has a growing relevance, but other enzymatic pathways have gained some late attention. In these routes, different enzymes (GPx7/8, VKOR) can serve as oxidants for reduced PDI (PDI-first pathways, Figure 1.14) or directly oxidise the substrate (QSOX) in which case PDI's role is confined to the isomerization phase of oxidative folding (PDI-second pathways). Nevertheless, their physiological roles are still poorly understood (Hudson et al., 2015). A brief overview is shown in this section.

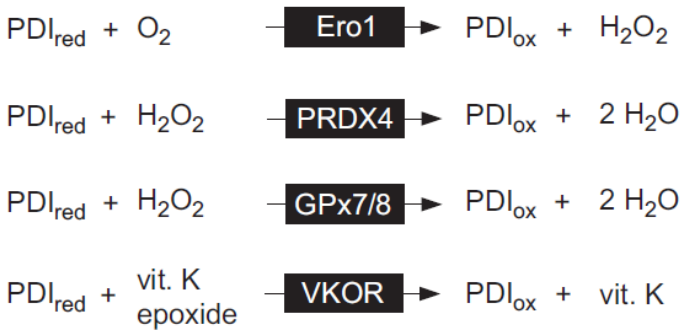

Figure 1.14. Some enzymatic oxidants for reduced PDI in PDI-first pathways mediated oxidative protein folding in the ER (adapted from Hudson et al., 2015)**.**

1.3.4.1 Glutathione Peroxidase 7 and 8 (GPx7/8)

GPx7 and GPx8 are two ER-resident PDI peroxidases, most closely related to the thioredoxin peroxidase family. In the presence of hydrogen peroxide, they can accelerate the folding of reduced proteins through re-oxidization of PDI (Slosky et al., 2016).

1.3.4.2 Vitamin K Epoxide Reductase (VKOR)

VKOR is a transmembrane ER-resident protein that uses a series of disulfide exchange steps to transmit reducing equivalents from reduced PDI to vitamin K1, K2 and their respective epoxide derivatives. Vitamin K dependent carboxylases can then use the corresponding hydroquinones for γ -carboxylation of glutamate residues in blood clotting factors, (*e.g.*, blood factors VII, IX and X).

1.3.4.3 Quiescin-Sulfhydryl Oxidase (QSOX)

In recent times, QSOX has been reported as a possible catalyser in disulfide bridges formation, along with the PDI/ERO1 pathway. Although its functions and physiological substrates remain under examination, it is known that this enzyme is found mainly on the Golgi apparatus. Studies indicate that QSOX primary role may be related to the promotion of a better and more orderly protein maturation or the connection of secreted proteins, instead of the introduction of disulfide bridges in individual proteins. Either way, PDI does not represent the direct oxidiser in this oxidative folding pathway, as QSOX can be the direct oxidiser of some substrate proteins, introducing *de novo* disulfide bridges (Betz, 1993). In the other mentioned pathways PDI serves as both an oxidant and an isomerase. Here, the initial oxidation is performed directly by a QSOX, while PDI functions in the second phase by shuffling mispaired disulfide bonds as shown below (Figure 1.15).

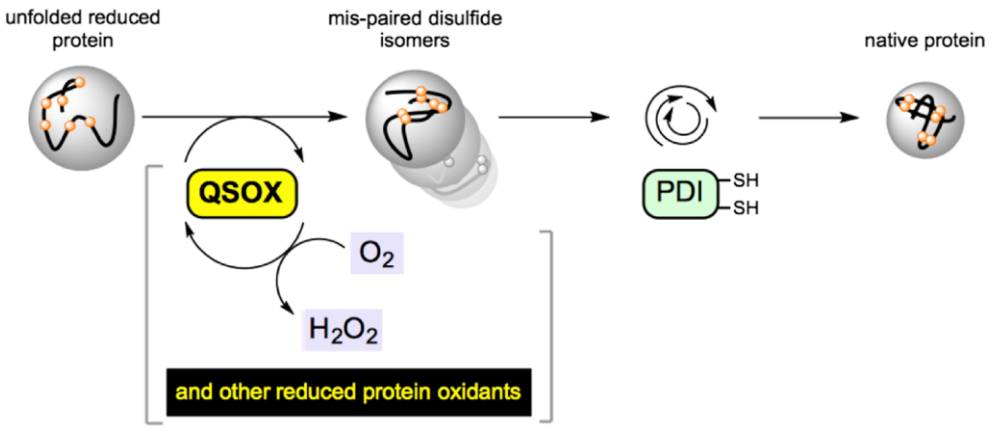

Figure 1.15. QSOX pathway, a PDI-second pathway of protein oxidative folding.

The initial oxidation of reduced proteins is PDI-independent therefore, PDI only engages in the second phase of oxidative protein folding (adapted from Hudson et al., 2015)

1.4 *In vitro* oxidative folding

1.4.1 Fluorescence spectroscopy as a logical approach

Protein folding is considered to play a fundamental role in cellular processes ranging from signalling to cell fate decisions. Being able to measure these processes dynamically and quantitatively, both *in vitro* and *in vivo*, has become crucial (Aller et al., 2013). Thus, a growing repertory of methodologies has been applied to thiol redox biochemistry to understand the underlying principles and the cooperation between the redox processes, especially spectroscopic approaches – varying from fluorescence to circular dichroism (CD), nuclear magnetic resonance (NMR) or fourier transform infrared spectroscopy (FTIR) (Gomes & Faísca, 2019). These techniques enable researchers to track structural and conformational changes in proteins from a variety of perspectives, including as a function of time in folding/unfolding kinetic assays, chemical and thermal denaturation, or the effect of the chemical environment (solution pH, metal ion, ligand/inhibitor) (Gomes & Faísca, 2019).

Tompa (2009) describes fluorescence as the emission of a photon from an electronically excited state of the fluorophore (in which excitation occurs by the absorption of an incoming photon) and is normally recorded in the form of excitation (absorption) and emission spectra (which are intensities of light against wavelength). Fluorescence is easy to detect and very sensitive, providing real-time measurements (Lakowicz, 2006).

In this thesis, the experimental approach to monitor the *in vitro* oxidative folding was through fluorescence spectroscopy of roGFP2, a fluorescent protein whose fluorescence excitation spectrum varies with the formation of native disulfide bridges. The catalytic efficiency of endoplasmic reticulum enzymatic pathways PDI/ERO1 and PDI/PRDX4 was characterized by varying roGFP2 concentration in the presence of different concentrations of the other involved enzymes. In the PDI/PRDX4 pathway assays, it was also added glucose and glucose oxidase as a source of H_2O_2, for PRDX4 activity.

The following section focuses on roGFP2 and its optical characteristics.

1.4.2 RoGFP2 as a model system

Redox-sensitive GFPs (roGFPs) are genetically modified proteins, product of the replacement of exposed residues in the β barrel structure of jellyfish *Aequorea victoria* green fluorescent protein (GFP) by cysteines in appropriate positions to form disulfide bridges. RoGFPs show two excitation peaks around 400 and 475–490 nm, corresponding to the neutral and anionic chromophore forms, respectively (Hanson et al., 2004). Excitation of either chromophore form leads to similar emission at about 510 nm (Hanson et al., 2004; Wierer et al., 2011).

Given the newly introduced disulfide bond near the roGFP chromophore, the relative amplitudes of the excitation maxima, is highly dependent on the redox-potential of the surrounding medium established by the native state acquisition and protein redox state (Wierer et al., 2011). Because their fluorescence is remarkably stable, these proteins can be used as highly-sensitive and non-invasive ratiometric local probes for the redox-potential both *in vitro* and *in vivo* (Østergaard et al., 2001; Wierer et al., 2011).

RoGFPs have been widely used in a multitude of cellular systems (Bizzarri et al., 2009; Morris, 2010), varying from plants (Meyer and Dick, 2010), to yeasts, to several different mammalian animal cellular systems (including Drosophila and disease models), but most importantly for the context of this work, in many *in vitro* studies (Esposito et al., 2017).

RoGFP2 is based on GFP with mutations C48S, S147C, Q204C and S65T, which enhances GFP chromophore (Figure 1.16). Exhibits two excitation peaks at around 490 and 400 nm (emission at 530 nm) and is insensitive to pH changes within the physiological range (Schwarzländer et al., 2008). RoGFP2 redox-dependent fluorescence ratio is insensitive to H_2O_2 changes (Esposito et al., 2017) and, like with other roGFPs, directly reflects the extent of thiol oxidation and disulfide bond formation. Therefore, roGFP2 is an ideal experimental model to evaluate protein folding and redox state.

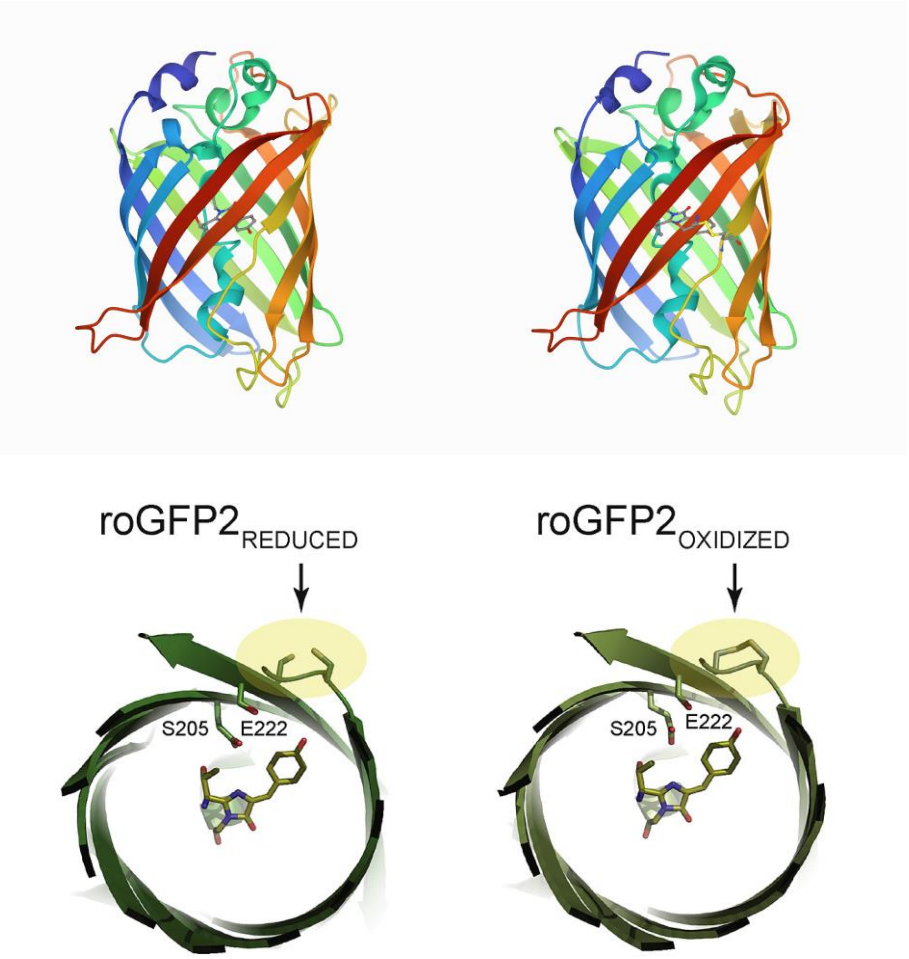

Figure 1.16. Models of roGFP2 in reduced and oxidised forms.

Left column: Reduced roGFP2 (PDB 1JC0). Right column: oxidised roGFP2 (PDB 1JC1). The engineered cysteines S147C and Q204C are highlighted in yellow. The thiol formation affects the interaction of the residues S205 and E222 with the chromophore (adapted from Hanson et al., 2004; Reuter et al., 2019).

Plenty of other biosensors based on engineered fluorescent proteins have been developed and characterized. Among them, HyPer[2] was also a potential model for the fluorescence assays developed in this thesis. However, previous testing revealed that in our experimental setting HyPer

[2] HyPer is a circularly permutated yellow fluorescent protein (YFP) designed to include the regulatory domain of the H_2O_2-sensing protein OxyR (Belousov et al., 2006). Therefore is a fluorescent ratiometric sensor that responds to H_2O_2 in a concentration-dependent way (Melo et al., 2017). This response is based in the oxidation and simultaneous creation of disulfide bonds between cysteines C199 and C208 from the OxyR domain. The degree of thiol oxidation and disulfide bond formation is closely related to the fluorescence intensity ratio of HyPer when stimulated at 488 and 405 nm (emission at 530 nm) (Correia et al., 2020).

could potentially be an unreliable probe [3]. Thus, the obvious approach was to use roGFP2 as the substrate.

In vitro assays with fluorescent proteins such as roGFP2 may help determine factors affecting the generation of native disulfide bridges *in vivo*. A comprehensive analysis of PDI, ERO1 and PRDX4 kinetic activity through *in vitro* fluorescence studies with this probe, can contribute to a better understanding of their role in the *in vivo* protein oxidative folding context.

1.4.3 Enzyme kinetics and substrate inhibition

For many enzymes, the speed of catalysis, defined by the number of moles of product formed per second, varies with the substrate concentration. The catalysis speed increases with substrate concentration in an approximately linear fashion for low substrate concentrations, and starts to plateau as the enzyme approaches saturation and maximum reaction speed (Berg et al., 2002). This behaviour is described by a Michaelis–Menten kinetics (Figure 1.17). As it will be demonstrated later on, this may not apply to the proteins studied throughout this thesis, since our observations are consistent with the presence of substrate inhibition in both pathways (PDI/ERO1 and PDI/PRDX4).

Substrate inhibition is one of the most common deviations from Michaelis–Menten kinetics, occurring in approximately 20% of known enzymes (Chaplin & Bucke, 1990; Kokkonen et al., 2021; Reed et al., 2010; Yoshino & Murakami, 2015). It is generally attributed to the formation of an unproductive enzyme-substrate complex after the simultaneous binding of two or more substrate molecules. Instead of approaching the maximum reaction speed at the saturation phase, the velocity of catalysis starts to decrease as excess substrate inhibits the enzyme (Kokkonen et al., 2021). This means that the velocity curve of a reaction rises to a maximum as substrate concentration increases and then descends either to zero (complete inhibition) or to a non-zero asymptote (partial inhibition) as shown in Figure 1.17 (Yoshino & Murakami, 2015).

[3] Observations inferred that HyPer was sensitive, not only but also to the H_2O_2 produced directly by glucose oxidase in the PRDX4/PDI pathway, providing unreliable read-outs.

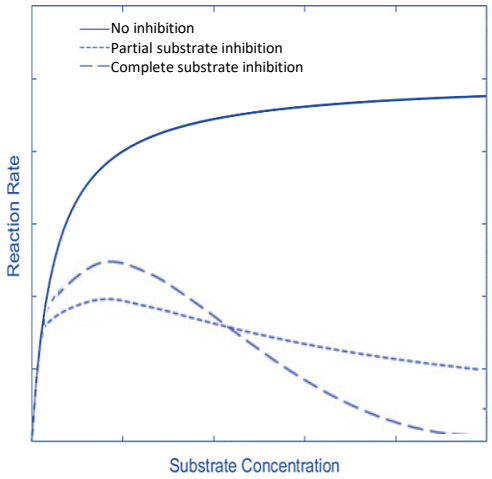

Figure 1.17. Enzyme kinetics graph showing the reaction rate as a function of substrate concentration for a hypothetical enzyme.

This plot demonstrates the effects of substrate inhibition on the reaction rate of enzymatic reactions. The Michaelis-Menten model is represented by the solid line and the Haldane model (for substrate inhibition) is represented by the dotted lines. The substrate inhibition models show a peak reaction rate before it declines as substrate concentration increases (adapted from Chezeau & Vial, 2019).

The model of substrate inhibition developed by Haldane is the most extensively used, in which there are two substrate-binding sites, but only one is catalytic. The binding of the substrate to the allosteric binding site in both the empty enzyme or the enzyme-substrate complex, creates an inhibitory complex and the catalysed reaction becomes very slow or even totally stalled (Kokkonen et al., 2021).

Recently, Kokkonen and colleagues (2021) brought a new perspective to this topic, suggesting that substrate inhibition can be caused by a substrate molecule blocking the exit of the product from the enzyme–product complex.

1.5 Objectives, challenges and research strategy

The global aim of this study was to characterise, in an *in vitro* context, the protein thiol oxidation by the endoplasmic reticulum enzymatic pathways PDI/ERO1 and PDI/PRDX4 applying real-time fluorescence spectroscopy. Another major goal of this work was to implement the recombinant protein expression and purification process for all the proteins under study, including *ubiquitin-like protease* (Ulp1, used during ERO1 purification) and roGFP2. This

fluorescent protein, whose fluorescence excitation spectrum varies with the formation of a disulfide bridge, was selected as the client protein/ substrate to undergo the oxidation process in the *in vitro* assays.

The specific objectives included:

- To obtain high levels of protein expression in each batch culture;
- To develop tools and strategies to optimize ERO1 purification, improving the efficiency and consistency of such process, as ERO1 purification proved to be challenging;
- To study the catalytic efficiency of each pathway, namely the kinetic parameters, varying the concentration of the involved enzymes;
- To identify, for each pathway, the enzyme that acts as the reaction's rate-limiting step;
- To confirm the presence or absence of inhibition by the substrate for higher concentrations of the client protein, as there was preliminary evidence of this type of inhibition in these pathways (unpublished studies);
- To test the conjunction of both pathways to assess a possible interaction between them, with PRDX4 using H_2O_2 (produced by ERO1) as the final electron acceptor.

In the current thesis, several approaches were employed to achieve the objectives and address the research challenges.

To obtain the necessary proteins for the subsequent *in vitro* assays the strategies included:

- Applying a previously and well-established production system (Avezov et al., 2013; Blais et al., 2010) for the recombinant protein expression in *E. coli* batch cultures, using BL21(DE3) (roGFP2, PDI, PRDX4 and Ulp1 expression) and Rosetta(DE3) cells (ERO1 expression).
- Purifying all proteins by affinity chromatography, based on the reversible interaction between the protein of interest and a specific ligand (nickel for proteins with a His-tag or glutathione for proteins with a GST tag) attached to a chromatographic matrix (Sepharose). Applying immobilized metal ion affinity chromatography (IMAC) to all histidine tag proteins (PDI, roGFP2, PRDX4 and Ulp1);
- Improving ERO1 purification by rearranging the process steps, shortening their length when possible, avoiding unnecessary intermediate steps and using a new or fully regenerated glutathione-sepharose matrix. In turn, subjecting GST-ERO1 to batch glutathione affinity chromatography followed by cleavage with Ulp1 of the GST tag and subsequent removal of Ulp1 by IMAC;

- Using SDS-PAGE (Sodium Dodecyl Sulfate–PolyAcrylamide Gel Electrophoresis) to evaluate protein overexpression and purification efficiency.

The approaches for the fluorescence *in vitro* experiments comprised:

- Applying a good experimental model to evaluate protein folding and its redox state. RoGFP2 proved to be an ideal probe for such studies;
- Running triplicates for each *in vitro* assay for statistical significance, when possible. All experiments, except for the PDI/ERO1 pathway were run in triplicate. This experimental decision was based on logistic limitations since ERO1 purification presented its challenges, being more difficult to obtain in large quantities compared to other proteins;
- Maintaining similar conditions for all assays, such as setting a fixed temperature (25 °C), adding components with celerity and always in a specific sequence, applying the same excitation and emission settings. Nevertheless, three different slit profiles were created for increased protein concentrations, as for high emission intensity, linearity of the detection was compromised;
- Adding a source of hydrogen peroxide (H_2O_2), in the PDI/PRDX4 pathway that could generate gradually H_2O_2 (which would then be consumed by PRDX4 activity). This was accomplished through the presence of glucose and glucose oxidase (Panayiotidis et al., 1999). It was an important strategy, as introducing a large amount of H_2O_2 at the beginning of the reaction could oxidise sensitive amino acids in the enzymes (Halliwell & Gutteridge, 1984), compromising their activity and consequently our findings.

Chapter 2.
Material and methods

2.1 Recombinant protein expression and purification

2.1.1 Plasmids and microorganisms

In the present study, all expression constructs (plasmids, Table 2.1) were provided by Professor David Ron from the Cambridge Institute for Medical Research (CIMR), Cambridge, United Kingdom. The restriction map of most plasmids is shown in **Appendix II**. All *Escherichia coli* strains (BL21(DE3), Rosetta and TOP 10) were maintained at -80ºC and plasmids ready for use at -20ºC.

Plasmid stocks were maintained in Top10 strains at -80ºC and, when necessary, were extracted using a standard protocol and Zymo Research's kits (ZR Plasmid Miniprep – Classic).

Table 2.1. Plasmids used for protein expression of roGFP2, PDI, ERO1, PRDX4 and Ulp1.

Insert description, antibiotic resistance (Ampicillin - Amp, Kanamycin - Kan), insert cloning sites, expression *E. coli* strains and affinity tag (Histidine – His, Glutathione S-transferase – GST). All these plasmids incorporate the T7 promoter (used to regulate gene expression of recombinant proteins).

Protein	Plasmid	Insert description	Resistance	Cloning Sites	Expression	Affinity Tag
roGFP2-H6	pET-15b	NA[1]	Amp	NcoI/Bam HI	BL21(DE3)	His
hPDI A1	pTrcHis-A	hPDIwt (18-508)	Amp	NcoI_NheI/ Bam HI	BL21(DE3)	His
ERO1	pGex	GST-Smt3-mERO1α (23-464)	Amp	Bam HI/SacI	Rosetta(DE3)	GST
PRDX4	pRSET-A	PRDX4 (37-274)	Amp	Bam HI/ Hind III	BL21(DE3)	His
Ulp1	pET-28b	ULP 1 Sumo protease (403-621)	Kan	XbaI /EcoRI	BL21(DE3)	His

[1] *Not available*

2.1.2 Media and cultivation conditions

Unless otherwise stated, Luria-Bertani medium as described by Miller (NZYTech, LB broth powder) at a final concentration of 25 $g.L^{-1}$ (final pH 7.0 ± 0.2 at 25ºC) was used for all cultivation processes and LB-agar plates (with added 15 $g.L^{-1}$ agar), containing 10 $g.L^{-1}$ Tryptone, 10 $g.L^{-1}$ NaCl, 5 $g.L^{-1}$ yeast extract.

All media were sterilized in an autoclave (Raypa, Stericlav-S AES-75) at 121ºC and 1 bar for 20 min.

LB-agar plates were preserved at 4ºC and incubated at 37ºC (Nüve, EN400) overnight (O/N).

All bacteria in liquid culture were grown at 37ºC with vigorous shaking (200–220 rpm, Infors-HT, Multitron Standard) or at 37ºC and 400 rpm in the case of Eppendorf tubes (Biosan, Thermo–Shaker TS-100).

Most bacterial growth was made in the presence of antibiotics from NZYtech, ampicillin 100 $\mu g.mL^{-1}$ (Amp) or kanamycin 50 $\mu g.mL^{-1}$ (Kan), according to transformants acquired resistance (Table 2.1). Antibiotics were not employed for the preparation of chemically competent *E. coli* cells.

Inocula were prepared in Erlenmeyer flasks containing 50 mL of medium (headspace to volume ratio of 5:1) and incubated O/N or during the day in case of Rosetta strain (used for ERO1 expression).

Fermentations were performed in Erlenmeyer flasks containing 500 mL of medium (headspace to volume ratio of 5:1) and incubated during the day at 37ºC. Exception made for Rosetta strain incubated at 37ºC until Isopropyl β-D-1-thiogalactopyranoside (IPTG, NZYtech, 1mM final concentration) induction and then at 16ºC O/N, always at 180 rpm. Each batch had a total volume of 2 L (Blais et al., 2010).

In some situations, all fermentations were executed using the same conditions as the Rossetta strain to facilitate the laboratory workflow.

When required, cell growth was monitored by optical density at 600 nm (OD_{600}) measured in a Shimadzu UV-1700 Spectrophotometer.

2.1.3 Preparation and transformation of chemically competent *E. coli* cells

A standard method of rendering chemically competent cells (BL21(DE3), Rosetta) was used for uptake of DNA involving chilled sterilized 0.1 M calcium chloride solution ($CaCl_2$).

Firstly an *E. coli* loop was incubated O/N in 5 mL of LB broth (40 $g.L^{-1}$). A 40 mL culture was then inoculated with 100 µL of the previous and grown in LB medium until OD_{600} reached 0.5 (mid-exponential phase, approximately 3 h).

The cells were swirled on ice for 3 to 5 min, then centrifuged at 4°C and 6000 rpm for 8 min in a Thermo Scientific's Sorvall Legend X1 high-performance benchtop centrifuge. The supernatant was discarded, and cells were carefully resuspended in 10 mL of chilled $CaCl_2$ for 5 to 10 min. The centrifugation and pellet resuspension were repeated, cells were kept on ice for 20 min and centrifuged once more. The supernatant was discarded, and the pellet resuspended in 1800 µL of $CaCl_2$ and 300 µL of sterilized 80% glycerol in water.

The competent cells were divided into aliquots of 100 µL each in sterile Eppendorf tubes and stored at -80°C until use.

For transformation, frozen competent cells (100 µL) were thawed on ice, mixed with 1 µL of the target plasmid and kept on ice for 30 min. The cells were then subjected to a heat pulse at 42°C for 50 sec (Biosan, Thermo–Shaker TS-100), chilled on ice for 5 min, diluted into 250 µL of LB-broth with no antibiotic and left to incubate for 45 min (to recover from heat shock). Samples were then plated (50 µL/plate) on LB-agar plates containing the antibiotic to which the transformants have acquired resistance and were incubated. Afterwards, plates were examined, and single colonies were selected for further expansion.

2.1.4 Inocula and batch fermentations

Each inoculum was prepared by incubation of a single transformant colony in LB medium with Amp or Kan.

Batch fermentations started by transferring inocula cultures to fresh media (containing the appropriate antibiotic) to obtain an initial OD_{600} of 0.1 (corresponding approx. to 20 mL) and incubated under conditions described in section 2.1.2. Bacterial growth was monitored, and

protein expression was induced by supplementing IPTG when OD_{600} reached between 0.7 and 0.9 (approx. 2 h). From this point on, cells used most of their resources to produce intracellular targeted protein and did not grow much further.

Bacteria cultures were concluded when OD_{600} stabilization was verified (mid stationary phase, approx. 4 h), and downstream processing began by harvesting and centrifuging cell cultures in a Beckman Coulter's Avanti JXN-30 high-performance centrifuge (15 min at 11300 x g and 4ºC). Supernatants were discarded and pellets stored in 50 mL falcon tubes at -20ºC pending further purification steps.

Samples were collected (1 mL) before and after IPTG induction, centrifuged (5 min at 5000 rpm, VWR, Micro2416), and pellets stored at -20ºC until assessment by Sodium Dodecyl Sulfate-Polyacrylamide Gel Electrophoresis (SDS-PAGE, section 2.1.8) to verify protein expression.

2.1.5 Cell disruption

Frozen pellets were thawed at room temperature (RT), resuspended in lysis buffer (see composition below, and sonicated for a total time of 4 min (On 10", Off 10" cycle, 70% amplitude) in a high-intensity ultrasonic processor (Sonics, VibraCell VCX 130). The lysates were centrifuged twice (45000 x g for 30 min at 4ºC, Beckman Coulter) to remove cell debris. Pellets were discarded, and final supernatants were filtrated through a 0.22 µm syringe filter) (Blais et al., 2010).

Lysis buffer contained TBS 1x (50 mM Tris-HCl, 150 mM NaCl, pH 7.4) supplemented with final concentrations of serine protease inhibitor phenylmethylsulphonyl fluoride (PMSF, 1 mM, Fluka), aspartyl peptidases inhibitor pepstatin A (10 µg.mL^{-1}), deoxyribonuclease (DNase, 10 µg.mL^{-1}, Sigma-Aldrich), ribonuclease (RNase, 10 µg.mL^{-1}, Sigma-Aldrich) and magnesium chloride ($MgCl_2$, 0.1 M) as cofactor of DNase. In some productions, such as ERO1, were also used cOmplete Protease Inhibitor Cocktail tablets from Roche.

2.1.6 Affinity chromatography

Recombinant human PDIA1, roGFP2, PRDX4 and Ulp1 were purified by immobilized metal ion affinity chromatography (IMAC) with pre-packed Ni-Sepharose High-Performance columns (Avezov et al., 2013; Correia et al., 2020).

ERO1 (GST-Smt3-mERO1a (23-464)) was subjected to batch Glutathione affinity chromatography followed by removal of GST tag by enzymatic cleavage with Ulp1 (a recombinant fragment of Ubiquitin-like-specific protease 1 that cleaves at the C-terminal end of the propeptide Smt3, plasmid Ulp1_pET-28b) and subsequent Ulp1 removal by IMAC (Blais et al., 2010).

Column chromatography was performed using an AKTA FPLC System (Amersham Biosciences) controlled through UNICORN software on a PC platform.

Target proteins were maintained on ice, and 100 µL samples were collected throughout these processes and stored at -20ºC until assessment by SDS-PAGE (section 2.1.8) to verify its purity.

2.1.6.1 Purification of His-tagged recombinant proteins: PDI, roGFP2, PRDX4 and Ulp1

His-trap HP columns (GE Healthcare) were equilibrated with approx. 5 column volumes of binding buffer (50 mM Tris-HCl, 150 mM NaCl, 20 mM Imidazole, pH 7.4) before loading the filtrated cell lysate into the matrix (resorting to a superloop) and followed by a column wash with 5 to 10 column volumes of the same buffer – or until optical density at 280 nm (OD_{280}) and conductivity stabilization. Then His-tagged proteins were eluted with a 30 min linear gradient of elution buffer (50 mM Tris-HCl, 150 mM NaCl, 500 mM imidazole, pH 7.4) confirmed by OD_{280} and conductivity stabilization, and 2 mL fractions of the purified proteins were collected.

Columns were re-equilibrated with binding buffer (approx. 5 column volumes) and stored in ethanol 20% (v/v) at 4ºC.

According to the column's specifications, chromatography's flow rate ranged from 0.5 to 2 mL/min, depending on system pressure, not surpassing a max of 0.3 MPa.

2.1.6.2 Purification of GST-tagged recombinant protein: ERO1

Successful purification of GST fusion protein ERO1 required several strategic decisions and optimization of methods and conditions for this specific protein. The presented protocol achieved the best performance.

Batch purification started with Glutathione Sepharose 4B (GE Healthcare 2.5 mL for a 35 mL sample) being pre-washed threefold with 5-bed volumes of binding buffer (50 mM Tris-HCl, 150 mM NaCl, 5 mM DTT, pH 7.4) and sedimented by centrifugation at 500 g for 5 min (Thermo Scientific). The supernatant was carefully decanted.

Filtrated cell lysate was added and incubated O/N at 4ºC in a 50 mL falcon with gentle end-over-end mixing and sedimented in the end. Over time, white beads became lightly yellow toned as GST-ERO1 bound to the matrix (this pale colouration comes from ERO1 itself).

The slurry was washed and sedimented fourfold with 10-bed volumes of TBS 1x. Wash fractions were kept until SDS-PAGE confirmation that no ERO1 elution occurred during these washes.

Recombinant GST-ERO1 adsorbed into the matrix was detached from its GST tag by 4 h incubation with Ulp1 (diluted 1:500) in TBS 1x at 4ºC. As the specific enzymatic cleavage took place, beads regain their white colour, and the supernatant became lightly yellow.

The slurry was sedimented and washed twice with 3-bed volumes of TBS 1x. The supernatant containing ERO1 and Ulp1 was filtered through a 0.22 µm syringe filter and proceeded to Ulp1 removal through IMAC purification.

His-trap HP column was equilibrated, and sample loaded as described before (section 2.1.6.1), followed by ERO1 recover in the flow-through during wash with 5 column volumes of the same buffer (or until OD_{280} and conductivity stabilization). Fractions of the purified protein were collected. Chromatography's flow rate was lower than used for other His-tagged proteins (ranged from 0.5 to 1 mL/min), allowing a better binding of Ulp1.

Ulp1 was eluted with 3 to 4 column volumes of elution buffer (50 mM Tris-HCl, 150 mM NaCl, 500 mM imidazole, pH 7.4), and the column was re-equilibrated and stored in ethanol 20% (v/v) at 4ºC.

Glutathione Sepharose 4B beads were regenerated by eluting the GST tag twice with 5-bed volumes of elution buffer (50 mM Tris-HCl, 150 mM NaCl, 40 mM reduced glutathione, pH 7.4), washed with TBS 1x and stored in ethanol 20% (v/v) at 4ºC.

It was clear that the purification worked better when using new Glutathione Sepharose 4B or when the matrix was fully regenerated – to remove precipitated or denatured substances and hydrophobically bond substances – besides being previously eluted. This regeneration process was done according to GE Healthcare's protocol.

2.1.7 Protein dialysis, concentration, and quantification

After validation of protein purity by SDS-PAGE, the final steps of protein purification were performed.

Eluted target proteins were dialysed against TBS (1x) to remove imidazole, using Thermo Scientific dialysis membranes (SnakeSkin Dialysis Tubing, 7K MWCO, 22 mm circular internal diameter) pre-soaked in ultrapure water. Once loaded and sealed in both ends with clamps, membranes were immersed in 5 L of dialysis buffer for a minimum of 24 h with at least one buffer exchange and maintained at 4ºC with gentle stirring.

Dialysed proteins were concentrated using Amicon Ultra-15 10K centrifugal filter devices, which provided fast ultrafiltration. With a molecular weight cut-off (MWCO) of 10 kDa, the high recovery Ultracel regenerated cellulose membranes retained >90% of molecules above this molecular weight. Samples were subjected to consecutive 5 min centrifuge cycles at 4500 x g (fixed-angle rotor, Thermo Scientific) for maximum volumes of 12 mL per cycle and were carefully resuspended in between cycles.

Purified proteins (2 µL samples) were analysed in a NanoDrop 2000c spectrophotometer (Thermo Scientific) for quantification and quality control. A 260/280 ratio should be around 0.6; higher ratios may indicate DNA contamination of target proteins.

Using absorbance at 280 nm (A_{280}), protein concentration (c) was calculated by application of Lambert-Beer equation, considering each protein's unique extinction coefficient ε (Table 2.2) and the optical path length b.

$$A_{280} = c \times \varepsilon \times b \quad (1)$$

Table 2.2. Molecular weights (MW) and protein extinction coefficient (ε) at 280 nm for oxidised (oxi) and reduced (red) states of roGFP2, PDI, ERO1, PRDX4 and Ulp1.

Protein	roGFP2-H6	ERO1		hPDI A1	PRDX4	Ulp1
		w/ GST	w/o GST			
MW (kDa)	29	90	51.6	56.8	30.9	25.5
ε_{oxi} ($M^{-1}cm^{-1}$)	23505	NA[1]	70205	45755	38640	30035
ε_{red} ($M^{-1}cm^{-1}$)	23380	NA[1]	69330	45380	38390	29910

[1] *Not available*

Purified, concentrated, and quantified proteins were divided into 500 µL aliquots and stored at -80°C until use.

2.1.8 Protein analysis: SDS-PAGE

Samples were subjected to SDS-PAGE technique (Sodium dodecyl sulphate polyacrylamide gel electrophoresis) on a Bio-Rad's Mini-PROTEAN Tetra hand-cast system to assess protein expression and purification.

Two protein ladders, Precision Plus Protein Unstained Standards (Bio-Rad) and NZYBlue Protein Marker (NZYTech), were used to monitor proteins running during SDS-PAGE and estimate their molecular weight.

Samples were treated as described below, before being loaded (20 µL each) into the gels, alongside 2.5 µL of the protein marker.

Pellet samples from bacterial growths were resuspended in ddH_2O according to their OD_{600} at the time they were collected (100 µL before and 250 µL after induction with IPTG), enabling them to be compared later in gels. Samples from purification processes were also normalized proportionally to their expected concentration range. In order to denature proteins and make them negatively charged, 30 µL of diluted samples were mixed with 10 µL of loading buffer 4x (62.5 mM Tris-HCl pH 6.8, 2% (v/v) SDS, 10% (v/v) glycerol, 2% (w/v) Orange G, 10% β-mercaptoethanol freshly added) and exposed to heat at 100ºC for 5 min.

Two-part gels (composed of stacking and resolving gels) were hand cast and prepared according to standard recipe and protocol, using a premixed 40% acrylamide/bis-acrylamide solution from Bio-Rad (Table 2.3), 1 mm spacer glass plates and 10 well combs. Each gel part took 30 min to polymerize, and a layer of dH_2O was used to smooth the surface of the resolving gel and prevent air bubble formation.

Table 2.3. Composition of each part of a 12% acrylamide SDS-PAGE gel.

Stacking gel has a lower percentage of acrylamide (5%), a lower pH, and a different ionic composition that helps to compress proteins. Resolving gel has a higher concentration of acrylamide (12%), capable of retarding the movement of the proteins.

	Revolving Gel 12% acrylamide	Stacking Gel 5% acrylamide
ddH_2O	2.5 mL	1.45 mL
1 M Tris-HCl pH 6.8	NA[1]	0.25 mL
1.5 M Tris-HCl pH 8.8	1.25 mL	NA[1]
Acrylamide/Bisacryilamide 40%	1.5 mL	0.25 mL
10% SDS	50 µL	20 µL
10% APS (freshly added)	50 µL	20 µL
TEMED (freshly added)	5 µL	2 µL

[1] *Not applied*

Mini-PROTEAN Tetra Cell was wired to PowerPac Basic power supply (Bio-Rad), and preloaded gels were typically run at 90 V for 15 min (or until samples reached the bottom of the stacking gel) and then at 150 V, using running buffer 1x (diluted from stock solution 10x: 250 mM Tris, 192 mM glycine, 1% (v/v) SDS, pH 8.3). The runs were finished once the samples reached the lower part of the resolving gel without leaving it.

Gels were visualized by staining O/N at RT with a Coomassie staining solution (0.25% (w/v) Brilliant Blue R, 50% (v/v) methanol, 7.5% (v/v) acetic acid) and de-staining with 20% ethanol/10% acetic acid solution, before being digitalized in a gel imaging system (AlphaImager HP, Cell Biosciences).

2.2 Fluorescence assays: *in vitro* oxidative folding of roGFP2

In vitro experiments were performed to characterize two possible oxidative folding pathways and the potential interaction between them (PDI/ERO1 and PDI/PRDX4). For each pathway, the substrate concentration was varied (from 0.1 to 10 μM) in the presence of different concentrations of PDI (reduced), ERO1 or PRDX4 (1, 3 and 5 μM).

Reduced roGFP2 was used as the sensor protein, and the variation of its excitation spectrum as disulfide bonds are formed was assessed by fluorescence spectroscopy.

The intensity of fluorescence emission at 530 nm after sequential excitation at 380 and 520 nm was measured using FluoroMax-4 (Horiba Scientific) controlled through FluorEssence software and paired with OriginPro for data management (Correia et al., 2020).

Three slit profiles were created for increasing protein concentrations, as for high emission intensity (over 12,000,000 CPS), linearity of the detection was compromised. The first profile for lower protein concentrations was set for 4 nm slits, intermediate for 2 nm and the last for 1 and 2 nm (excitation and emission slits, respectively).

All essays were performed with vacuum degassed buffer (TBS 1x) in a closed quartz cuvette (10 mm pathlength, Hellma Analytics) – to reduce possible protein oxidation by air exposure – gentle magnetic stirring, 25ºC pre-set temperature and 1500 μL working volume. Reactions were monitored in real-time over 100 scan cycles, 14 s each with no delay between them.

The apparent rate constants for roGFP2 oxidation were calculated from linear fits of fluorescence excitation ratio 492/400 nm.

2.2.1 Protein reduction

PDI and roGFP2 were reduced by incubation with 20 mM of dithiothreitol (DTT) for 1 h at RT with gentle end-over-end mixing, and then DTT removal on PD MiniTrap G-25 gel filtration column (GE Healthcare) (Avezov et al., 2013; Correia et al., 2020). Columns were first equilibrated with 3-column volumes of degassed TBS 1x (approx. 8 mL), allowing the buffer to enter the packed bed entirely before loading the samples. Reduced proteins (0.5 mL) were slowly added to the packed bed, fully infiltrating in it, and eluted with 1.0 mL of the same buffer. Eluates were then

collected in Eppendorf tubes (0.8-0.9 mL), divided into 3 chilled PCR tubes (to lessen air exposition and consequent protein re-oxidation) and stored at -80°C or preferably kept on ice and promptly used. Columns were again equilibrated with degassed 1x TBS buffer (approx. 3 column volumes) and stored in ethanol 20% (v/v) at RT. Eluted proteins were additionally quantified by NanoDrop, as the gel filtration step to remove DTT slightly dilutes them.

For one of the synergy assays, this procedure was also applied to PRDX4 and ERO1 samples.

2.2.2 Main pathway: PDI / ERO1

This pathway was characterized throughout 35 experiments performed as described in Figure 2.1. Each comprised 1 complete reaction and 5 controls.

Components were added with celerity and in a specific sequence (degassed buffer, reduced sensor (roGFP2), reduced PDI and lastly, ERO1 to initiate the reaction) since roGFP2 oxidation by PDI/ERO1 (or PDI/PRDX4) develops relatively fast and early data points were vital for subsequent analysis.

Controls with just buffer, sensor and DTT (20 mM final concentration) or H_2O_2 (20 µM final concentration) were considered standards and were analysed 20 min after components addition (10 cycles).

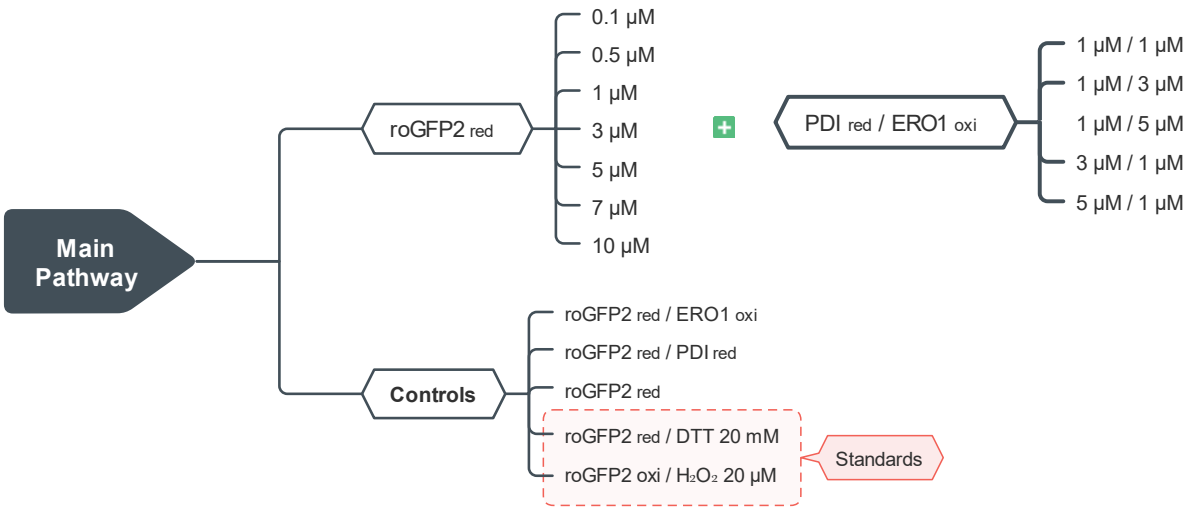

Figure 2.1. Main pathway fluorescence assays layout.

2.2.3 Alternative pathway: PDI / PRDX4

The *in vitro* study of this oxidation pathway required using hydrogen peroxide (H_2O_2) as a terminal electron acceptor (Zito et al., 2010), generated by the presence of glucose (2.5 mM) and glucose oxidase type II from *Aspergillus niger* (GOx, Sigma, 10 mU/mL) as described in Figure 2.2.

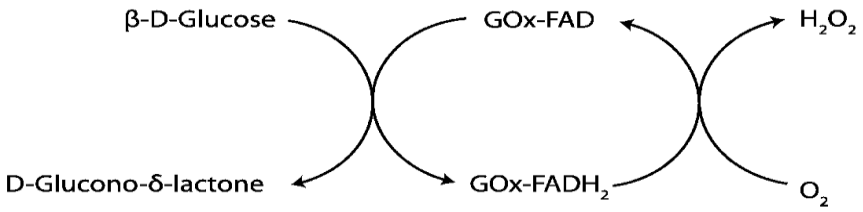

Figure 2.2. The reduction of oxygen and oxidation of glucose into hydrogen peroxide and gluconolactone, catalysed by glucose oxidase (adapted from Zavada et al., 2016).

Experiments were conducted as shown in Figure 2.3. Each included the complete reaction performed in triplicate, 3 negative controls also in triplicate and 2 standards.

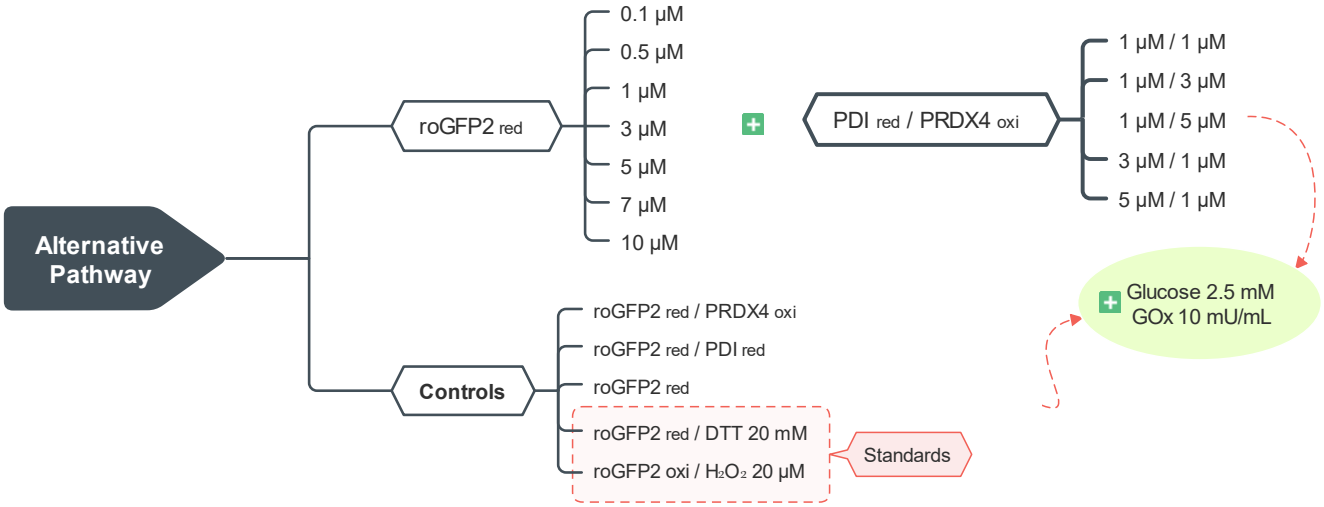

Figure 2.3. Alternative pathway fluorescence assays layout.

Components were also added with celerity and in a specific sequence (degassed buffer, glucose, reduced sensor, reduced PDI, PRDX4 and lastly, GOx to initiate the reaction). Standards were executed as above (section 2.2.2).

2.2.4 Synergy between pathways: PDI / ERO1 / PRDX4

The potential synergy between both pathways was characterized by 2 additional experiments performed as described in Figure 2.4. Each included a complete reaction assay in triplicate and triplicate controls. In the complete reaction mixture, PRDX4 and ERO1 were added simultaneously to the samples. As before, components were combined with celerity and in a particular order (degassed buffer, reduced sensor, reduced PDI and lastly, reduced PRDX4/ERO1 combo to initiate the reaction). Standards were executed as in section 2.2.2.

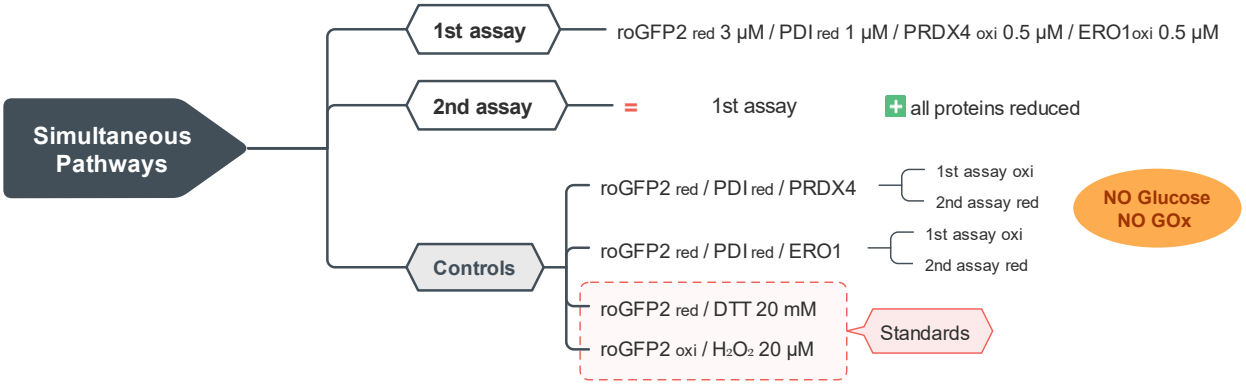

Figure 2.4. Sinergy between pathways fluorescence assays layout.

Chapter 3.
Results and discussion

3.1 Recombinant protein expression and purification

The recombinant proteins were expressed applying a previously established production protocol (Avezov et al., 2013; Blais et al., 2010), optimized when necessary.

While purified recombinant roGFP2, ERO1, PDI and PRDX4 were further used in the fluorescent assays (*in vitro* oxidative folding of roGFP2), Ulp1 was used during ERO1 purification to cleave the GST tag.

3.1.1 Batch fermentation and protein expression analysis by SDS-PAGE

All proteins were produced as described in the methodology (section 2.1), using BL21(DE3) (roGFP2, PDI, PRDX4 and Ulp1 expression) and Rosetta(DE3) cells (ERO1 expression). In this study, we show a representative batch fermentation for each protein (Figure 3.1). However, more than one batch was carried out to obtain enough protein for all the subsequent fluorescence assays.

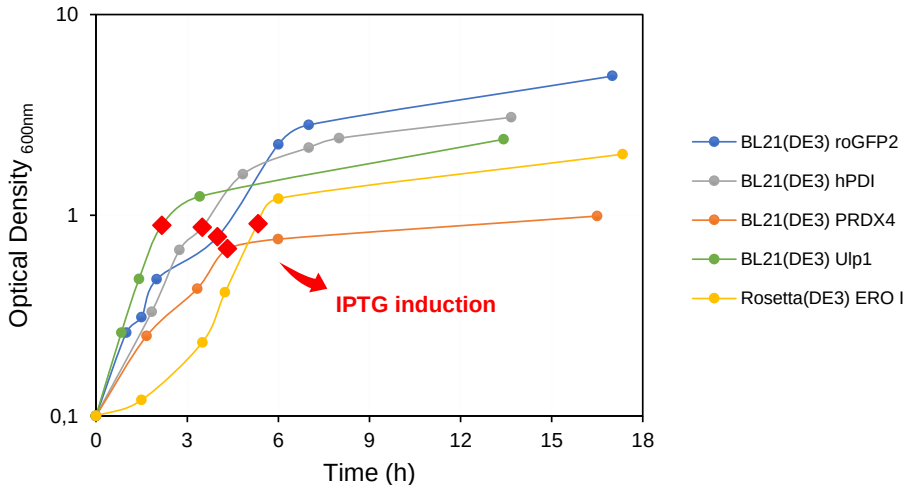

Figure 3.1. ***E. coli BL21(DE3)*** **and** ***Rosetta(DE3)*** **batch cultures used to express roGFP2, PDI, PRDX4, Ulp1 and ERO1.**
Over time, growth was monitored by OD at 600 nm at selected intervals and plotted on a semi-logarithmic scale. IPTG induction occurred between OD 0.7 and 0.9 (♦).

Bacterial growth was monitored through optical density measurements at 600 nm, and protein expression was induced with IPTG supplementation into the medium when OD_{600} reached between 0.7 and 0.9 (approx. 2 to 5 h). From this point on, cells used most of their resources to produce the target proteins intracellularly and, in most cases, did not grow much further (Figure 3.1).

For all cultures presented in Figure 3.1, protein expression was done at 16ºC O/N, and fermentations were ended at a late stationary phase (approx. 10 h to 13 h). Protein expression could be carried out during the day at 37ºC, exception made for ERO1, which has a higher probability of forming inclusion bodies, so induction at lower temperatures is always preferable. In this situation, cells would be harvested in mid stationary phase as soon as OD_{600} stabilization was verified (approx. 5 h).

To verify protein expression, samples were collected before and after IPTG induction (at the end of each batch) and analysed by SDS-Page (Figure 3.2), which provided a size-dependent separation of proteins, allowing a reliable estimation of the molecular weight. The underlying principles of SDS-PAGE are further detailed in **Appendix I**.

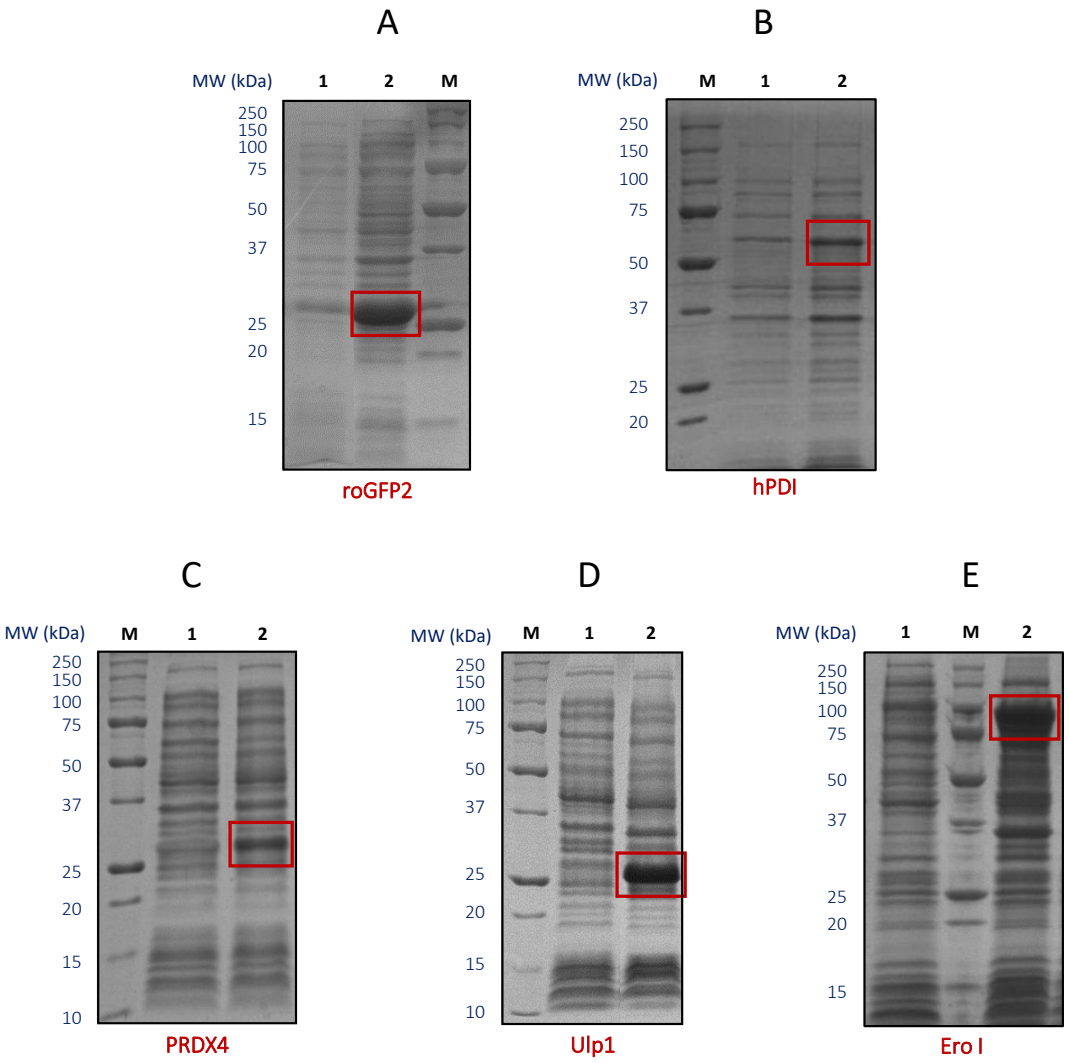

Figure 3.2. 12% SDS-Page gels used to verify recombinant protein expression in *E. coli* cultures.

Proteins under analysis were roGFP2 (MW 29 kDa, panel A), hPDI (MW 56.8 kDa, panel B), PRDX4 (MW 30.9 kDa, panel C), Ulp1 (MW 25.5 kDa, panel D) and GST-ERO I (MW 90 kDa, panel E). All panels show the protein extract from cell lysate before IPTG induction (lane 1) and after IPTG induction (lane 2) and the applied protein marker/ladder (Precision Plus Protein Unstained Standard from, Bio-Rad, lane M).

For all cultures, a thicker and more prominent band was visible after IPTG induction (Figure 3.2, lane 2) compared to the sample before IPTG (Figure 3.2, lane 1) at the expected molecular weight for the target recombinant protein.

In PDI's case, the SDS-PAGE gel showed in Figure 3.2 (panel B) is not the best example among the ones carried out during this work, as after IPTG induction (lane 2), we can see just a slightly thicker band around 57 kDa, instead of a pronounced denser band. Overexpression was more evident in other PDI fermentations; however, those gels were not digitalized.

The notorious protein overexpression indicates that roGFP2, PDI, Ulp1, PRDX4 and ERO1 were present in the bacterial extracts at the end of each batch fermentation.

Once the efficiency in protein expression was confirmed, we were able to proceed with downstream processing. Centrifuged bacterial pellets were resuspended and disrupted by sonication, and the resulting soluble protein fraction was prepared to be purified through affinity chromatography methods (cell debris and insoluble protein fraction were no longer needed and therefore discarded).

3.1.2 Affinity chromatography and protein purification analysis by SDS-PAGE

The soluble protein mixture was purified by affinity chromatography based on the reversible interaction between the protein of interest (His or GST-tagged proteins) and a specific ligand (nickel or glutathione, respectively) attached to a chromatography base matrix (Sepharose) as portrayed in Figure 3.3.

While all His-tagged proteins (PDI, roGFP2, PRDX4 and Ulp1) were purified using immobilized metal ion affinity chromatography (IMAC), GST-tagged ERO1 was subjected to batch Glutathione affinity chromatography followed by GST tag cleavage with Ulp1 and subsequent Ulp1 removal through IMAC.

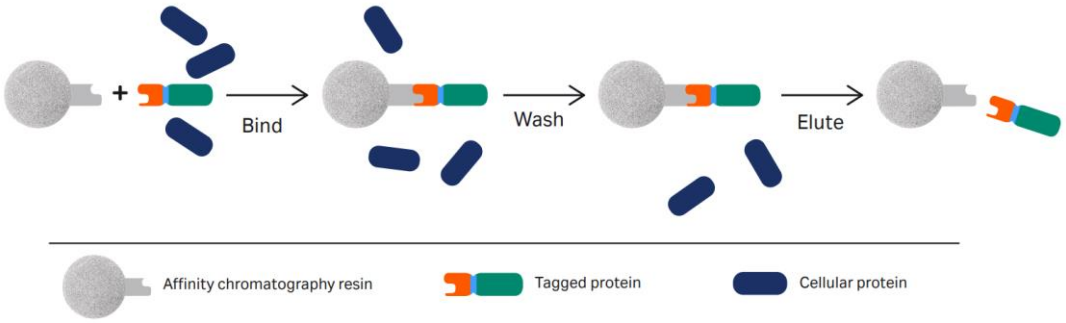

Figure 3.3. Affinity chromatography purification of tagged recombinant proteins.

General steps usually comprise: 1) Equilibration, affinity medium is equilibrated in binding buffer. 2) Sample application and wash, the sample is applied under conditions favouring specific binding of the tagged protein to the ligand. 3) Wash, unbound material is washed away. 4) Elution, conditions are changed to promote elution of the tagged protein, typically done using a competitive ligand. The eluted protein is usually in a purified and relatively concentrated form (Healthcare, 2017).

3.1.2.1 Purification of His-tagged recombinant proteins: PDI, roGFP2, PRDX4 and Ulp1

IMAC was performed using an AKTA FPLC System controlled through UNICORN software. This software allowed us to monitor the process in real-time and record several parameters like absorbance at 280 nm and the percentage of elution buffer injected (also system pressure, flow, and conductivity, among others).

Usually, a volume of 35 to 45 mL of protein sample was loaded into a pre-packed Ni-Sepharose High-Performance column (His-trap HP, GE Healthcare). Depending on expression yields, this volume could vary. Although not very common, some cellular proteins can contain two or more adjacent histidine residues, leading to a weak affinity for the Ni-Sepharose matrix. Therefore, these proteins may coelute with the target protein, causing considerable contamination of the final product (Schmitt et al., 1993). To avoid this weak binding of untagged proteins, we added 20 mM imidazole (final concentration) to the loading sample and biding buffer (Bornhorst & Falke, 2000).

The resultant IMAC chromatograms and SDS-Page confirmation for His-tag proteins are exemplified in Figure 3.4.

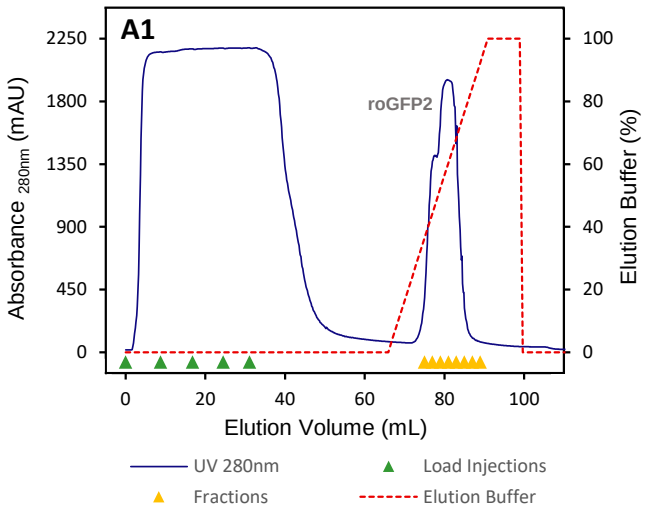
A1
roGFP2
Absorbance 280nm (mAU)
Elution Buffer (%)
Elution Volume (mL)
UV 280nm
Load Injections
Fractions
Elution Buffer

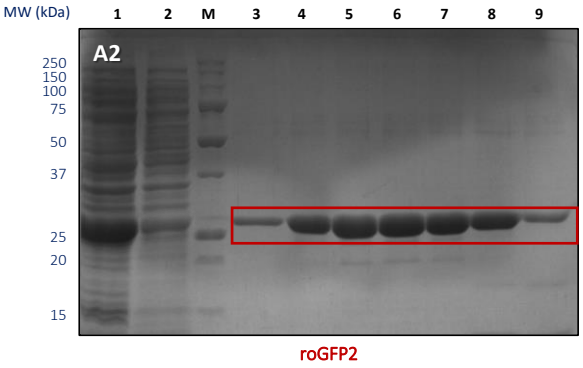
MW (kDa)
1 2 M 3 4 5 6 7 8 9
A2
250
150
100
75
50
37
25
20
15
roGFP2

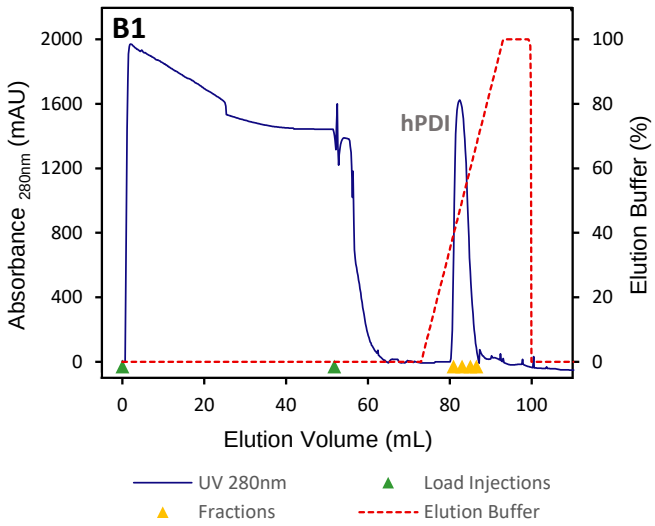
B1
hPDI
Absorbance 280nm (mAU)
Elution Buffer (%)
Elution Volume (mL)
UV 280nm
Load Injections
Fractions
Elution Buffer

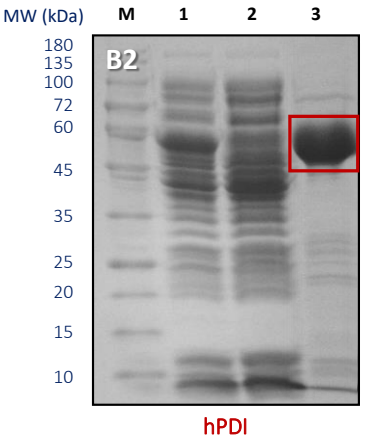
MW (kDa)
M 1 2 3
B2
180
135
100
72
60
45
35
25
20
15
10
hPDI

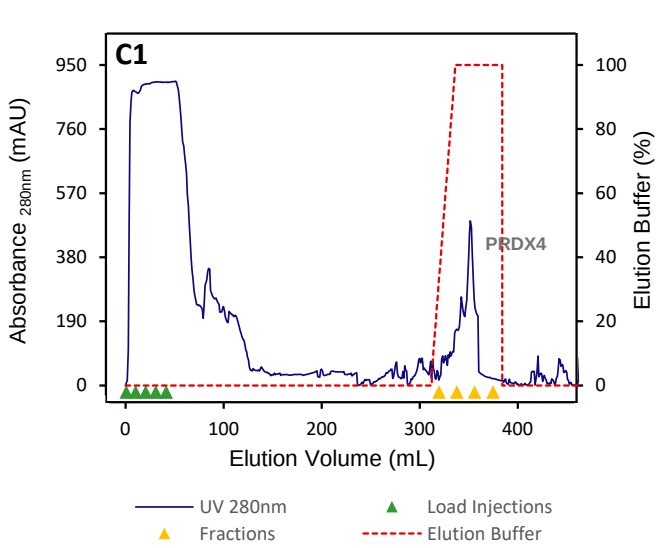
C1
PRDX4
Absorbance 280nm (mAU)
Elution Buffer (%)
Elution Volume (mL)
UV 280nm
Load Injections
Fractions
Elution Buffer

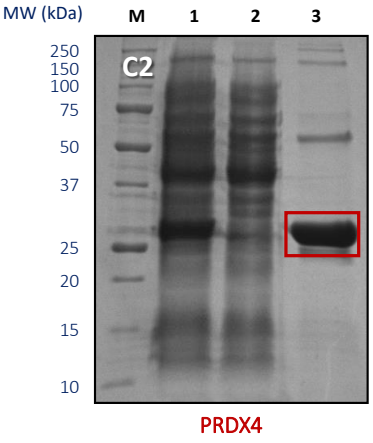
MW (kDa)
M 1 2 3
C2
250
150
100
75
50
37
25
20
15
10
PRDX4

(cont.)

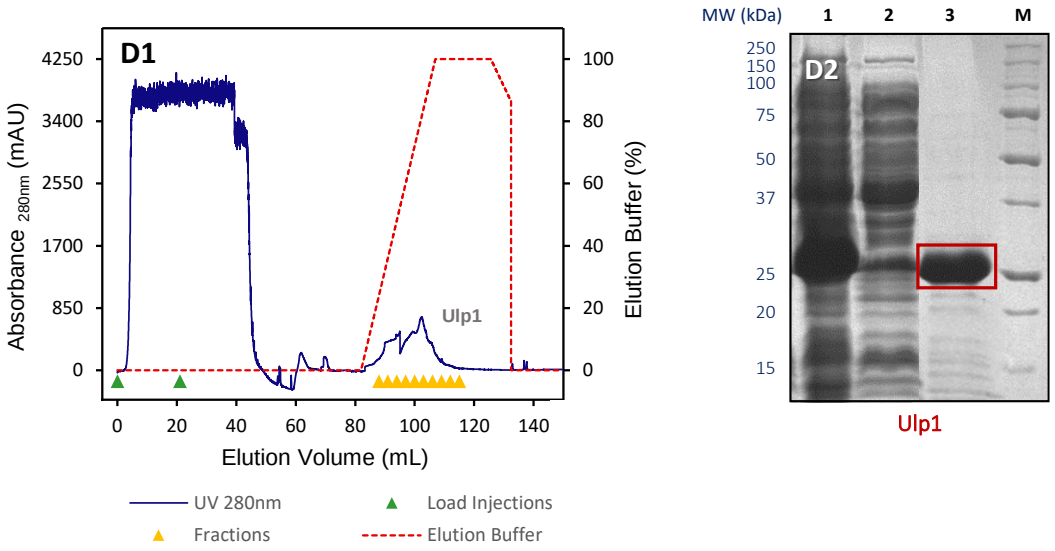

Figure 3.4. Characterization of the purification process of all His-tag recombinant proteins.

Proteins under analysis were roGFP2 (MW 29 kDa, panels A1 and A2), PDI (MW 56.8 kDa, panels B1 and B2), PRDX4 (MW 30.9 kDa, panels C1 and C2) and Ulp1 (MW 25.5 kDa, panels D1 and D2).
(Left column) IMAC purification chromatograms. In all panels is represented the sample load into a pre-packed Ni-Sepharose High-Performance column (His-trap HP, GE Healthcare, first high and broad peak) and elution of the target protein (second sharp peak) with a gradient of 500 mM imidazole.
(Right column) 12% SDS-Page gels used to validate the process and confirm protein purity. All panels show the sample loaded into the column (lane 1), the IMAC flow-through (lane 2), the eluted peak fractions of the target protein (lane 3 and upward) and the applied protein markers/ladders (Precision Plus Protein Unstained Standards from Bio-Rad and NZYBlue Protein Marker from NZYTech, lane M).

All His-tag proteins showed a similar purification profile when subject to IMAC (Figure 3.4, left panels). As the sample was injected into the system, a remarkable increase in absorbance was observed, corresponding to proteins that did not bind to the matrix (first high and broad peak). The recombinant protein containing the His-tag bound to the column's matrix (by selective immobilization due to its affinity to nickel coupled to the resin) and contaminant proteins were washed into the flow-through (FT) until a visible near-zero absorbance stabilization.

The competitive elution of the target protein was then performed with a linear gradient of imidazole (a histidine analogue) to preserve both protein structure and function (Healthcare, 2017), resulting in a defined second peak collected into fractions.

The analysis of Ulp1 purification chromatogram (Figure 3.4, panel D1) revealed a small broader peak during the elution phase compared to the other eluted proteins displaying sharper peaks (second peak, Figure 3.4, left panels A1 to C1). The SDS-PAGE gel (Figure 3.4, panel D2) of the flow-through (lane 2) revealed a small band of approx. 26 kDa, compatible with some Ulp1 that did not entirely bind to the matrix before elution, which may explain the eluted peak pattern, as some

previous protein loss might have occurred. Despite this, the gel of the purified protein sample (lane 3) revealed that very significant protein purification was achieved, with no other significant visible bands in the eluted fractions. There was no need to further purify the FT since Ulp1 expression and purification were very satisfactory, and the protein lost in the FT was irrelevant.

Evaluation of SDS-PAGE gels from IMAC purification for all His-tag proteins (Figure 3.4, right panels) clearly showed that the target protein, present in the sample loaded into the column (lane 1), was adequately retained in the matrix, and therefore was not traceable in the FT (lane 2), except for Ulp1 (as discussed above). It was also evident that the eluted fractions were efficiently purified, presenting a thick and prominent band at the expected molecular weight, with no contaminants for roGFP2 (panel A2, lane 3 and upward) and some minor visible bands for PDI, PRDX4 and Ulp1 (panels B2 to D2, lane 3).

3.1.2.2 Purification of GST-tagged recombinant protein: ERO1

GST-tagged ERO1 was subjected to batch Glutathione (GSH) affinity chromatography followed by GST tag cleavage with Ulp1 and subsequent Ulp1 removal through IMAC as described in the methodology (section 2.1).

Although there was no need to remove the His-tag from the previous proteins, the 26 kDa, GST tag is significantly larger than many other fusion protein affinity tags. Like GST complete amino acid sequence, tagged proteins with larger tags can also show tag enzymatic activity and eventually suffer dimerization (Healthcare, 2017). In this context, it was essential to proceed with the cleavage of ERO1 from the GST tag, avoiding such interference in the following oxidation assays.

Successful purification of this GST fusion protein required several strategic decisions and method optimization. It was verified that time played an essential factor in ERO1 purification. Extended processing (comprising more lengthy intermediary steps) resulted in a higher probability of protein degradation, leading to purification failure. It was also noted that contaminant proteins had some affinity to GSH in the matrix, compromising ERO1 purification yields. Moreover, prolonged incubation with Ulp1 might result in cleavage in nonspecific sites and ERO1 degradation as well. Alterations to the original methodology were focused on overcoming these problems. Both original and final optimized procedures are represented in Figure A.5 (Appendix III).

Modifying such procedures and using new or fully regenerated Glutathione Sepharose 4B improved the efficiency and consistency of ERO1 purification. Figure 3.5 shows the SDS-Page validation of all the novel ERO1 purification procedure (panel B), along with the resultant IMAC chromatogram for Ulp1 removal (panel A).

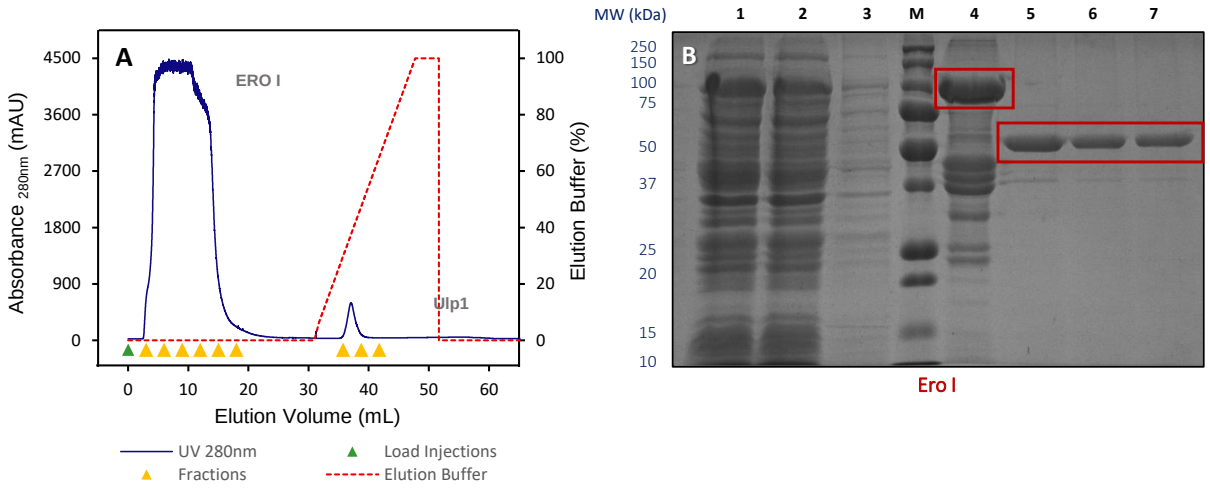

Figure 3.5. Characterization of the purification process of GST-tag recombinant protein ERO1.

(A) IMAC purification chromatogram of ERO1. The sample was injected (a blend of ERO1 and Ulp1) into a pre-packed Ni-Sepharose High-Performance column (His-trap HP, GE Healthcare) for Ulp1 removal and as Ulp1 binds to the resin through its His-tag, purified ERO1 was collected in the flow-through (first high and broad peak). The column was regenerated by eluting Ulp1 (second small sharp peak) with a linear gradient of 500 mM imidazole.
(B) 12% SDS-Page gel used to validate the purification process and confirm protein purity: cell lysate supernatant before binding to the GSH matrix (lane 1); 1st GSH matrix wash (lane 2 and 3); GSH matrix before incubation with Ulp1 (lane 4); the supernatant after Ulp1 cleavage loaded into the IMAC column (lane 5); ERO1 collected in the IMAC flow-through (lane 6); ERO1 after dialysis (lane 7) and the applied protein marker/ladder (Precision Plus Protein Unstained Standards from Bio-Rad, lane M). GST-ERO1 has an MW of 90 kDa and ERO1 51.6 kDa.

The SDS-PAGE gel for all steps of the purification process (Figure 3.5, panel B) clearly showed that GST-ERO1 fusion, which was present in the cell lysate supernatant (lane 1), bound to the glutathione-sepharose liquid matrix (a thick band of 90 kDa, lane 4), but part was presumably still traceable in the first wash supernatant (lane 2), suggesting some ERO1 loss.

It was also evident nonspecific binding of untagged contaminant proteins after the first wash (strong bands of proteins under 90 kDa on lane 4). With ERO1 still attached to the matrix, proceeding to Ulp1 cleavage of the GST tag proved effective as only ERO1 (MW 51.6 kDa) was released into the second matrix wash supernatant (along with Ulp1). The GST tag and contaminant proteins remained bound to the matrix, and ERO1 became very pure (even before IMAC, lane 5), justifying the original protocol improvement.

IMAC removal of Ulp1 resulted in a similar purification profile to that of His-tag proteins (Figure 3.4, left panels). In this case, as the sample (a blend of ERO1 and Ulp1) was injected into the system, a remarkable increase in absorbance was observed, corresponding to ERO1 not binding to the Ni-Sepharose matrix (first high and broad peak). Conversely, Ulp1 was retained by selective immobilization (due to the affinity of its His-tag to nickel coupled with the resin), and purified ERO1 was washed and collected in the flow-through (FT) until a visible near-zero absorbance stabilization.

The column was later regenerated by competitive elution of Ulp1 with a linear gradient of 500 mM imidazole, resulting in a defined second peak (a small peak due to the low concentration of Ulp1 present in the original sample).

A thick and prominent band at the predicted molecular weight (approx. 51.6 kDa) and no significant contaminant proteins were visible on the SDS-PAGE gel (Figure 3.5, panel B, lane 6), confirming that ERO1 was efficiently purified.

3.2 Fluorescence assays: *in vitro* oxidative folding of roGFP2

Several *in vitro* experiments were carried out to characterize the two oxidative protein folding pathways (PDI/ERO1 and PDI/PRDX4) operating in the endoplasmic reticulum, as well as their potential synergy. Reduced roGFP2 was used as substrate and, for each enzymatic pathway, its concentration was varied (from 0.1 to 10 μM) along with different catalysts concentrations (1, 3 and 5 μM).

As disulfide bonds were formed, the variation of the roGFP2 excitation spectrum was assessed through fluorescence spectroscopy by measuring the fluorescence emission intensity at 530 nm after sequential excitation from 380 to 520 nm. Excitation properties of roGFP2 are shown in Figure 3.6.

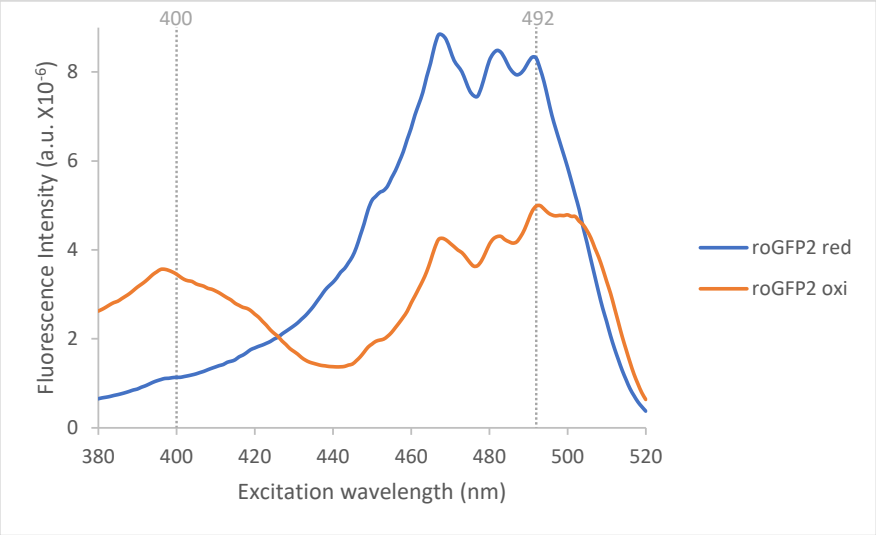

Figure 3.6. Excitation spectrum of roGFP2 in a fully oxidised and fully reduced state.

Emission was monitored at 530 nm. The maximum dynamic ranges (δ) were calculated from the 492/400 nm excitation ratios for fully reduced and fully oxidised probes. Vertical lines indicate both excitation wavelengths. Assay conditions: 0.1 µM roGFP2 in the presence of 20 mM DTT as a reducing agent (blue curve) and 20 µM H_2O_2 as an oxidizing agent (orange curve).

As shown in Figure 3.6, the excitation of the substrate protein roGFP2 reflects its oxidation state while disulfide bonds were being formed. The peak at 492 nm decreased in fluorescence with oxidation, whereas the peak at 400 nm increased. This change can be quantified by the variation in the fluorescence intensity ratio between both peaks, which was later used to calculate the initial reaction rates.

3.2.1 Main pathway: PDI / ERO1

This pathway was characterized throughout 35 experiments, each of which comprised one complete reaction (containing the substrate roGFP2 and the two enzymes) and five controls (including reduced and oxidised roGFP2 as standards), as outlined in the methodology (section 2.2.2). Figure 3.7 shows the time dependence of excitation spectra for a typical complete reaction (excitation wavelength vs. fluorescence intensity values, obtained directly from the raw data).

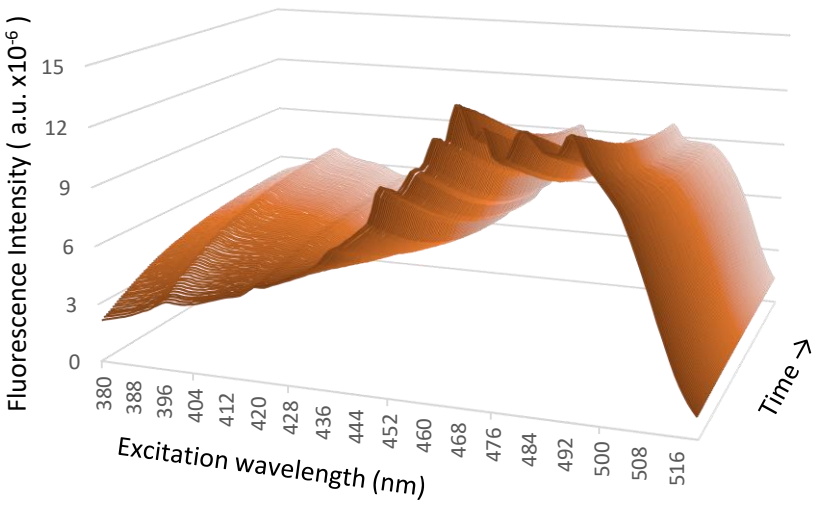

Figure 3.7. Original excitation spectrum of a PDI/ERO1 pathway assay.

Assay conditions: 5 µM reduced roGFP2 in the presence of 5 µM reduced PDI and 1 µM ERO1. The roGFP2 oxidation reaction was monitored in real-time over 100 scan cycles 14 s each with no delay between them. The fluorescence emission intensity at 530 nm after sequential excitation from 380 to 520 nm was measured using FluoroMax-4 (Horiba Scientific) controlled through FluorEssence software and paired with OriginPro for data management.

As expected, roGFP2's excitation peak at 492 nm decreased in fluorescence intensity over time, whereas the peak at 400 nm increased.

A representation of the fluorescence intensity ratio 492/400 nm for a typical assay, including the complete reaction and five controls, is shown in Figure 3.8.

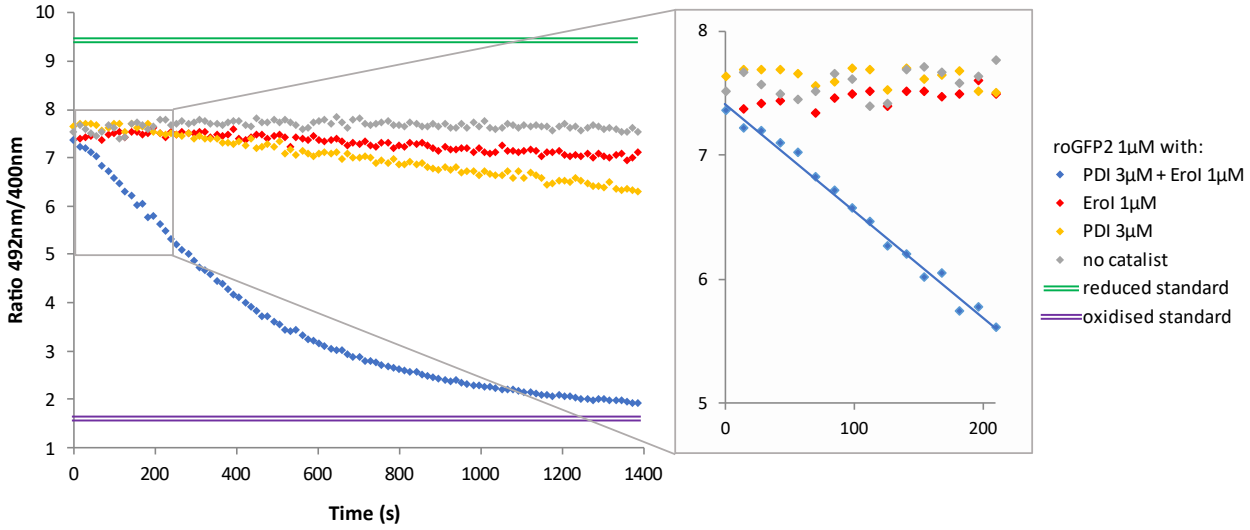

Figure 3.8. Representation of the fluorescence intensity ratio 492/400 nm variation over time obtained from the original excitation spectra of a PDI/ERO1 pathway assay.

Assay conditions: 1 µM reduced roGFP2 in the presence of 3 µM reduced PDI and 1 µM ERO1.
A zoom of the linear region considered for initial reaction rate calculation of roGFP2 oxidation is shown in the right panel. Initially, the ratio decreases rapidly with a slope of $1.48 \times 10^{-2}\,s^{-1}$ in the presence of both catalysts (reduced PDI and ERO1), as shown by the linear fit depicted as solid blue line. Control reactions did not show significant changes over time.

While the substrate protein was being oxidised in the presence of both enzymes, the ratio between both peaks (492 nm/400 nm) progressively decreased over time, until it reached a limit where roGFP2 was almost fully oxidised (1400 s). In each assay, this limit was reached more rapidly (or not) depending on the concentration of the enzymes catalysing the reaction and the substrate concentration itself. In contrast, control reactions did not reveal significant changes over time, as expected.

The apparent rate constants for roGFP2 oxidation were calculated from the linear fits of the fluorescence excitation ratio 492/400 nm (Table 3.1), considering the complete reaction in each experiment.

Table 3.1. Characterization of PDI/ERO1 pathway: Initial reaction rate constants (s^{-1}) of roGFP2 oxidation.

Substrate concentration was varied (from 0.1 to 10 µM) in the presence of different concentrations of PDI (reduced) and ERO1 (1, 3 and 5 µM).

	Initial reaction rate constants (x 10^3 / s)				
[roGFP$_2$] (µM)	**PDI 1µM ERO1 1µM**	**PDI 3µM ERO1 1µM**	**PDI 5µM ERO1 1µM**	**PDI 1µM ERO1 3µM**	**PDI 1µM ERO1 5µM**
0.1	1.62	11.6	19.5	4.17	3.98
0.5	2.43	17.1	21.6	4.91	5.17
1	8.65	14.8	17.3	6.27	5.35
3	4.05	10.2	10.1	2.55	2.94
5	2.28	11.6	5.22	3.25	3.67
7	2.63	10.1	8.73	2.45	2.55
10	1.17	2.85	6.41	1.51	3.86

A pattern emerged after observing the initial reaction rate constants for all conditions. When fixing catalysts concentrations but varying the substrate concentration (Table 3.1, columns), the oxidation rate increases at first and then progressively decreases for higher substrate concentrations, indicating that the substrate inhibits the reaction. These values, along with the corresponding fits, are presented in Figure 3.10.

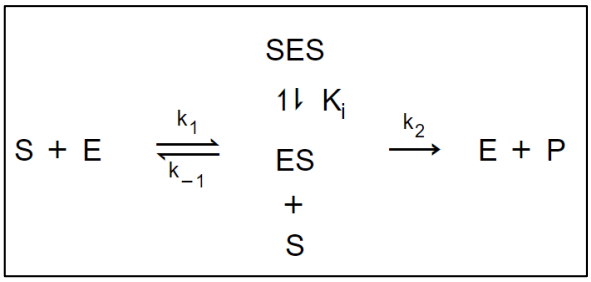

Figure 3.9. A reaction diagram for enzyme-substrate inhibition.

This model presumes that an enzyme **E** has two binding sites for its substrate **S**, a catalytic site that can produce the product **P**, and a non-catalytic (or allosteric) site. E.S denotes the substrate bound to the catalytic site, and two substrate molecules bound state by **S.E.S** (adapted from Reed et al., 2010)**.**

The data were fitted by nonlinear regression, applying the above substrate inhibition model (Figure 3.9), mathematically described by the following enzyme kinetics equation:

$$v = \frac{V_{max}.[S]}{K_m + [S] + \frac{[S]^2}{K_i}} \qquad (2)$$

Where,

$$V_{max} = k_2.[E] \quad , \quad K_m = \frac{k_{-1}+k_2}{k_1} \quad \text{and} \quad K_i = \frac{[ES].[S]}{[SES]} \; .$$

V_{max} is the maximum enzyme velocity if there is no substrate inhibition; Michaelis-Menten constant (**K_m**) is the dissociation constant of the enzyme-substrate complex (ES), and **K_i** is the dissociation equilibrium constant of the ternary complex (SES).

Using OriginPro, the following rationalized constraints were applied to fit the data:

$V_{max} < 0.05$ **$0.03 < K_m < 2$** **$2 < K_i < 10$** **$K_m < K_i$**

V_{max} was established based on the highest value of reaction rate obtained in the experiments. The constraint was imposed as around 2.5-fold the maximum reaction rate measured (approx. 0.02 s^{-1}).

The **K_m** and **K_i** constraints were set considering the maximum roGFP2 concentration tested (10 µM), and the rationale that **K_m** must be smaller than **K_i**, assumed that the catalytic-competent binding site should have a higher affinity for the substrate. Indeed, it is expected that the affinity for the first molecule of substrate, which is converted into product, should be greater than the affinity for the second molecule of substrate that prevents product formation.

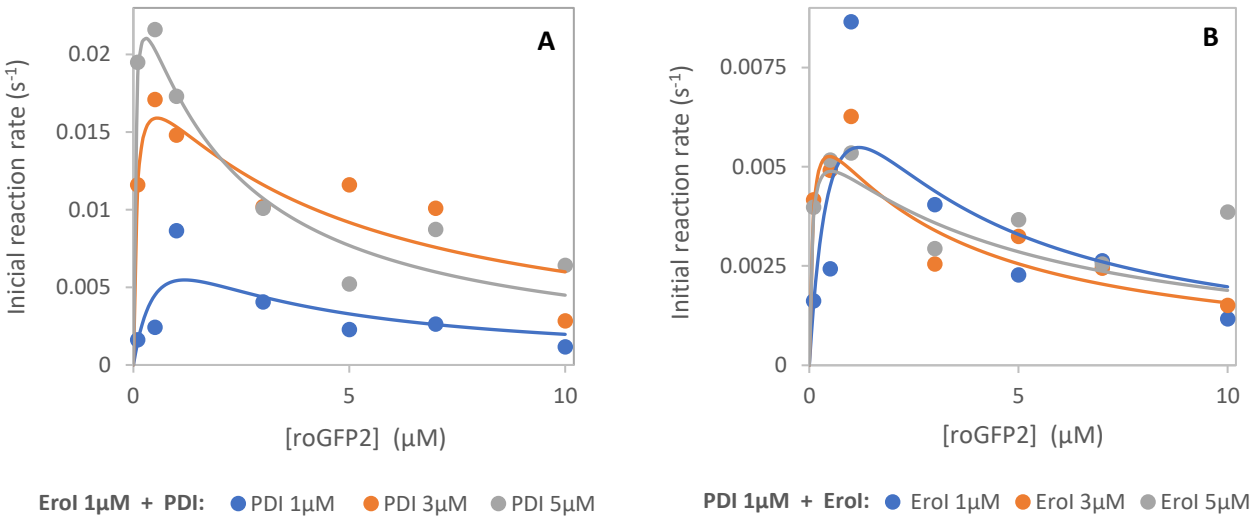

Figure 3.10. Representation of initial reaction rates of roGFP2 oxidation (dots) and the corresponding fits (solid lines) for PDI/ERO1 pathway, assuming substrate inhibition.

Substrate concentration was varied (from 0.1 to 10 µM) in the presence of different concentrations of reduced PDI (panel A) and ERO1 (panel B). The fits were obtained using equation (2) and OriginPro software.

Data in Figure 3.10 clearly shows the existence of substrate inhibition for all PDI/ERO1 concentration combinations. Reed and co-workers (2010) affirm that substrate inhibition is a biologically relevant regulatory mechanism. The authors also claim that substrate inhibition is sometimes misinterpreted as an artefact caused by employing artificially high substrate concentrations in *in vitro* settings. However, there are various physiological phenomena controlled by substrate inhibition, being an extremely widespread phenomenon in enzyme kinetics, and playing critical regulatory roles in several metabolic pathways (Kokkonen et al., 2021; Reed et al., 2010; Yoshino & Murakami, 2015).

When observing Figure 3.10, it is also evident that raising PDI concentration significantly impacts the reaction rate rather than increasing ERO1, implying that PDI-mediated oxidation of roGFP2 should be the reaction rate-limiting step. The reaction rate increases at low roGFP2 concentrations (up to 1 µM) as PDI concentration rises from 1 µM to 3 µM and then from 3 µM to 5 µM. For all roGFP2 concentrations, however, the reaction rate does not increase with ERO1 concentration.

The steady-state kinetic constants of roGFP2 oxidation were calculated, considering substrate inhibition fits (Table 3.2).

Table 3.2. Characterization of PDI/ERO1 pathway: Steady-state kinetic constants of roGFP2 oxidation, considering substrate inhibition.

	PDI 1µM ERO1 1µM	PDI 3µM ERO1 1µM	PDI 5µM ERO1 1µM	PDI 1µM ERO1 3µM	PDI 1µM ERO1 5µM
V_{max} (s^{-1})	0.012	0.020	0.027	0.007	0.006
K_m (µM)	0.705	0.071	0.040	0.080	0.060
Ki (µM)	2.0	4.3	2.0	2.9	4.6

The values in Table 3.2 show that the increase of ERO1 concentration leads to a decrease in the maximum reaction rate of roGFP2 oxidation. One possible explanation is that as ERO1 concentration rises, the PDI partition between roGFP2 and ERO1 binding shifts towards ERO1, and so more PDI is recruited for ERO1 binding, becoming less available to oxidise roGFP2.

As stated before, for substrate concentrations below enzyme inhibition (*i.e.*, for lower substrate concentrations), the reaction rate increases with the increase in PDI concentration, contrary to what happened with the rise in ERO1 concentration. This was already clear in Figure 3.10 and is also reflected in the $\mathbf{V_{max}}$ values in Table 3.2 (knowing that V_{max} is the maximum rate that would occur without substrate inhibition). Since the maximum rate increases as PDI concentration increases, we can confirm that roGFP2 oxidation by PDI is indeed the rate-limiting step of this pathway.

3.2.2 Alternative pathway: PDI / PRDX4

Experiments were carried out to characterize the PDI and PRDX4-mediated alternative pathway to protein oxidation (as described in the methodology, section 2.2.2), with H_2O_2 serving as a terminal electron acceptor for PRDX4. Introducing a large amount of H_2O_2 at the beginning of the reaction may oxidise sensitive amino acids in the enzymes, compromising their activity (Halliwell & Gutteridge, 1984). Therefore, the experimental approach was to generate H_2O_2 gradually through the presence of glucose and glucose oxidase (Panayiotidis et al., 1999), which would then be consumed by PRDX4 activity. Figure 3.11 shows the typical time course of roGFP2 excitation spectra for a complete reaction containing all the components required for protein disulfide bond formation.

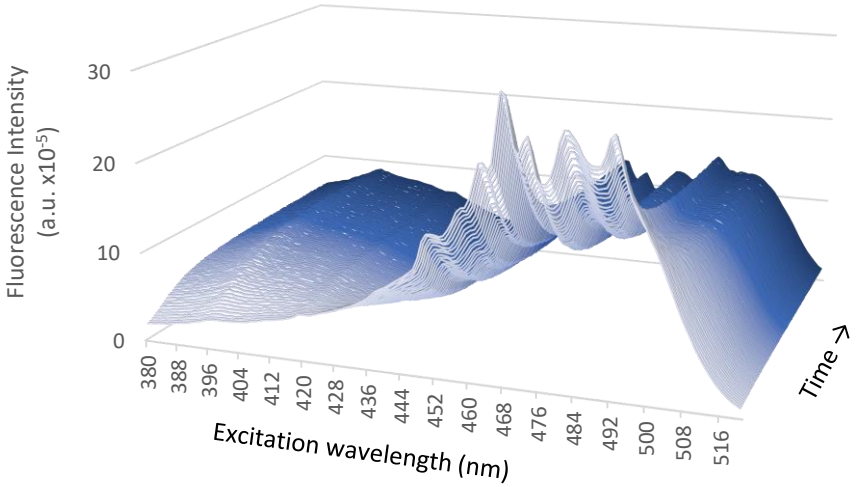

Figure 3.11. Original excitation spectrum of a PDI/PRDX4 pathway assay.

Assay conditions: 0.5 µM reduced roGFP2 in the presence of 3 µM reduced PDI and 1 µM PRDX4. The roGFP2 oxidation reaction was monitored in real-time over 100 scan cycles 14 s each with no delay between them. The fluorescence emission intensity at 530 nm after sequential excitation from 380 to 520 nm was measured using FluoroMax-4 (Horiba Scientific) controlled through FluorEssence software and paired with OriginPro for data management.

As previously observed in the PDI/ERO1 pathway, the fluorescence intensity of roGFP2 excited at 492 nm decreased as oxidation progressed, whereas the peak at 400 nm increased.

Figure 3.12 shows a representation of the fluorescence intensity ratio 492/400 nm for a typical assay, including the complete reaction triplicates and five controls. For clarity, only one reaction was presented for each negative control, as there was no relevant variation among the triplicates.

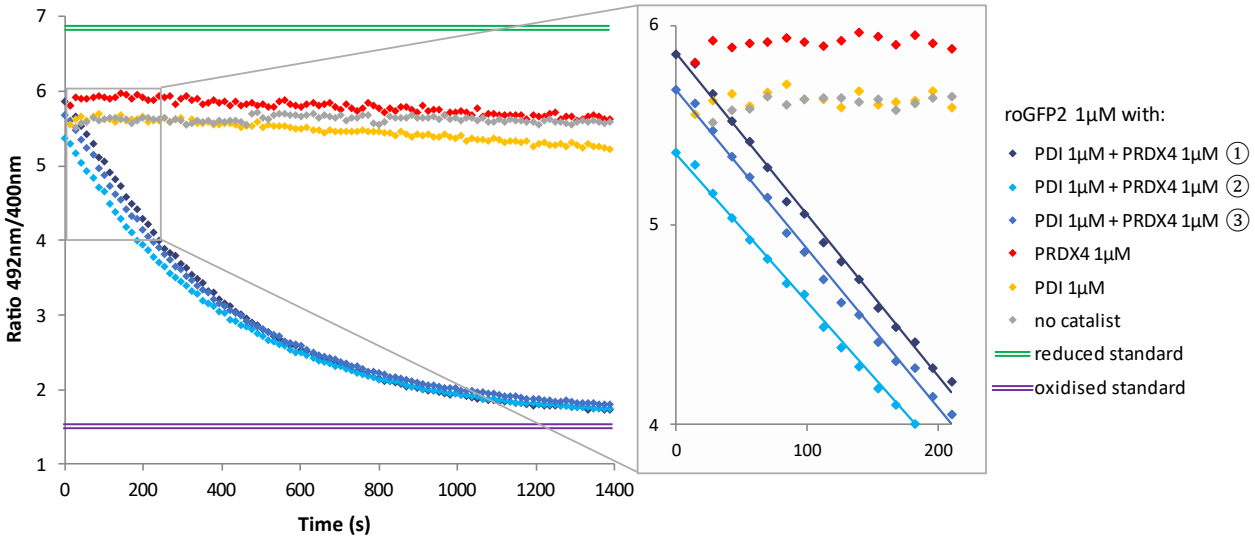

Figure 3.12. Representation of the fluorescence intensity ratio 492/400 nm variation over time, obtained from the original excitation spectra of a PDI/PRDX4 pathway assay.

Assay conditions: 3 µM reduced roGFP2 oxidised by 1 µM reduced PDI and 1 µM PRDX4, in the presence of glucose and glucose oxidase to generate H_2O_2 as a final electron acceptor for PRDX4.
A zoom of the linear region considered for calculating initial reaction rates of roGFP2 oxidation is shown in the right panel. Initially, the intensity ratio changes rapidly with slopes of $7.40 \times 10^{-3}\ s^{-1}$, $7.94 \times 10^{-3}\ s^{-1}$ and $8.08 \times 10^{-3}\ s^{-1}$ in the presence of both catalysts (reduced PDI and PRDX4), as shown by the linear fits depicted as solid blue lines. Control reactions were performed in the presence of glucose and glucose oxidase and did not show significant ratio variations over time.

In the presence of both enzymes, it is clear a decrease over time in the ratio between both peaks (492 nm/400 nm), while roGFP2 was being oxidised, reaching a limit where roGFP2 was almost fully oxidised (1400 s). As predicted, negative control reactions did not vary significantly over time.

Table 3.3 shows the apparent rate constants for roGFP2 oxidation, calculated as described above (section 3.2.1).

Table 3.3. Characterization of PDI/PRDX4 pathway: Initial reaction rate constants (s^{-1}) of roGFP2 oxidation.

Substrate concentration was changed (from 0.1 to 10 µM) in the presence of different concentrations of PDI (reduced) and PRDX4 (1, 3 and 5 µM).

[roGFP2] (µM)	Initial reaction rate mean ± SD[1] ($x10^3$ /s)				
	PDI 1µM PRDX4 1µM	PDI 3µM PRDX4 1µM	PDI 5µM PRDX4 1µM	PDI 1µM PRDX4 3µM	PDI 1µM PRDX4 5µM
0.1	14.0 ± 2.56	4.85 ± 0.74	5.19 ± 0.53	19.8 ± 2.44	18.2 ± 0.99
0.5	12.5 ± 1.76	28.0 ± 1.19	17.6 ± 1.01	21.9 ± 2.38	21.6 ± 2.19
1	9.43 ± 2.05	18.4 ± 0.15	15.0 ± 2.15	16.5 ± 1.27	20.8 ± 3.04
3	7.67 ± 0.38	12.8 ± 4.88	11.2 ± 3.54	9.36 ± 1.17	14.2 ± 0.61
5	7.94 ± 1.04	8.32 ± 0.36	8.60 ± 1.25	7.79 ± 1.78	ND[2]
7	3.04 ± 1.17	6.50 ± 0.87	9.97 ± 0.55	3.87 ± 0.34	16.0 ± 1.41
10	1.20 ± 0.29	4.44 ± 0.48	4.42 ± 0.16	3.31 ± 0.70	18.1 ± 0.14

[1] *Standard deviation*
[2] *Not determined*

Looking at the initial reaction rate constants, it was clear that all conditions followed the same pattern. When the enzyme concentrations are fixed but the substrate is varied (Table 3.3, columns), the oxidation rate initially increases and then gradually decreases for higher substrate concentrations, indicating that the substrate also inhibits this pathway.

The data were fitted by nonlinear regression, applying the substrate inhibition model described in equation (2) and the previously rationalized constraints (section 3.2.1). These values, along with the corresponding fits, are presented in Figure 3.13 (where it is clear the occurrence of substrate inhibition), and the steady-state kinetic constants for roGFP2 oxidation extracted from the fits are shown in Table 3.4.

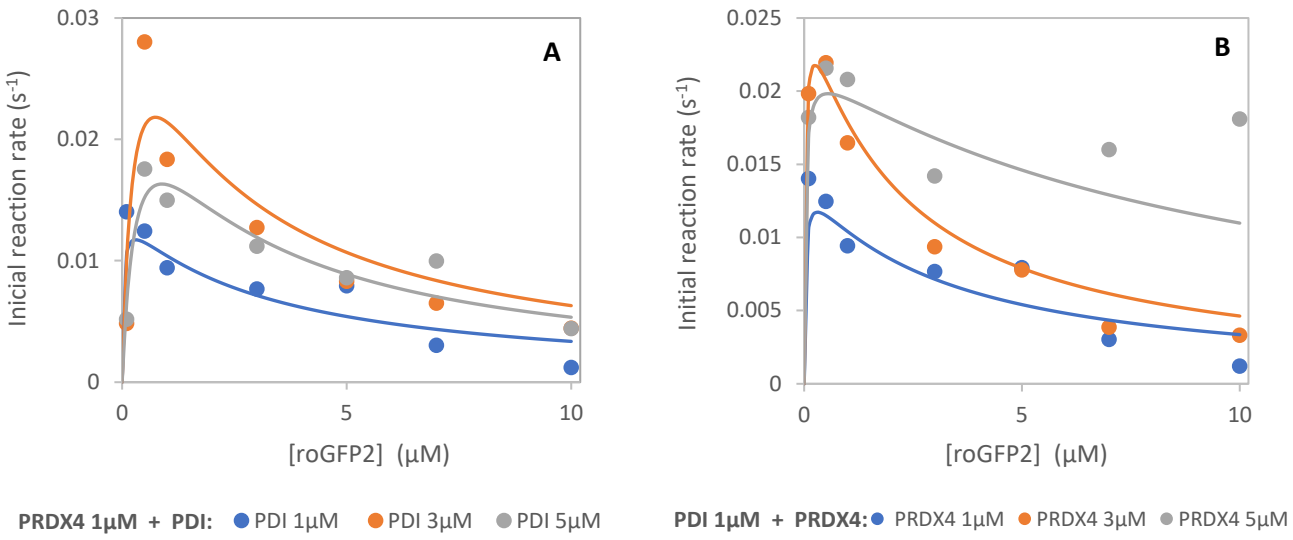

Figure 3.13. Representation of Initial reaction rates of roGFP2 oxidation (dots) and the corresponding fits (solid lines) for the PDI/PRDX4 pathway, assuming substrate inhibition.

Substrate concentration was varied (from 0.1 to 10 µM) in the presence of different concentrations of reduced PDI (panel A) and PRDX4 (panel B). The fits were obtained using equation (2) and OriginPro software.

Table 3.4. Characterization of PDI/PRDX4 pathway: Steady-state kinetic constants of roGFP2 oxidation, considering substrate inhibition.

	PDI 1µM PRDX4 1µM	PDI 3µM PRDX4 1µM	PDI 5µM PRDX4 1µM	PDI 1µM PRDX4 3µM	PDI 1µM PRDX4 5µM
V_{max} (s^{-1})	0.014	0.038	0.029	0.027	0.022
K_m (µM)	0.030	0.275	0.344	0.030	0.030
K_i (µM)	3.16	2.00	2.28	2.07	10.00

For the PDI/PRDX4 pathway, the maximum velocity increases with both PDI and PRDX4 concentration increase, up to a maximum of 3 µM. It is thought that substantially raising PRDX4 concentration (5 µM onwards) may result in some PDI interaction over PRDX4, having less PDI available to oxidise the substrate.

It was not possible to predict the reaction rate-limiting step for this pathway before substrate inhibition takes place.

3.2.3 Synergy between pathways: PDI / ERO1 / PRDX4

Two additional experiments combining the catalysts from PDI/ERO1 and PDI/PRDX4 were conducted to characterize the potential synergy between both pathways. In the first assay, as detailed in section 2.2.4, only roGFP2 and PDI were used in their reduced state (ERO1 and PRDX4 were initially oxidised). Conversely, the second assay started with all proteins reduced. Since the H_2O_2 produced by ERO1 is expected to be used by PRDX4, there was no glucose or glucose oxidase supplementation.

RoGFP2 fluorescence intensity ratio 492/400 nm for both assays is detailed in Figure 3.14 and Figure 3.15.

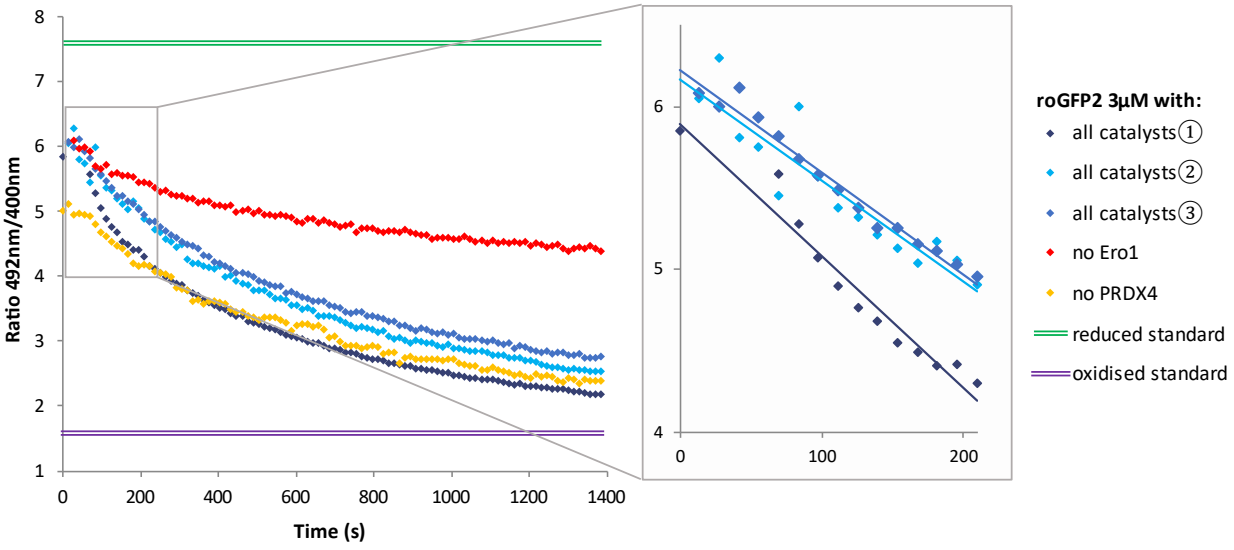

Figure 3.14. Representation of the fluorescence intensity ratio 492/400 nm variation over time, obtained from the original excitation spectra of the first synergy assay.

Assay conditions: 3 µM reduced roGFP2, 1 µM reduced PDI, 0.5 µM ERO1 and 0.5 µM PRDX4.
A zoom of the linear region considered for initial reaction rates calculations of roGFP2 oxidation is shown in the right panel. Initially, the rate changes rapidly with linear slope fits (solid blue lines) of $6.22 \times 10^{-3}\,s^{-1}$, $6.28 \times 10^{-3}\,s^{-1}$ and $8.07 \times 10^{-3}\,s^{-1}$ in the presence of the 3 catalysts (•,•,•). The control reaction without ERO1 (•) showed a minor ratio variation over time, while the control reaction without PRDX4 (•) showed a similar variation compared to the complete reaction.

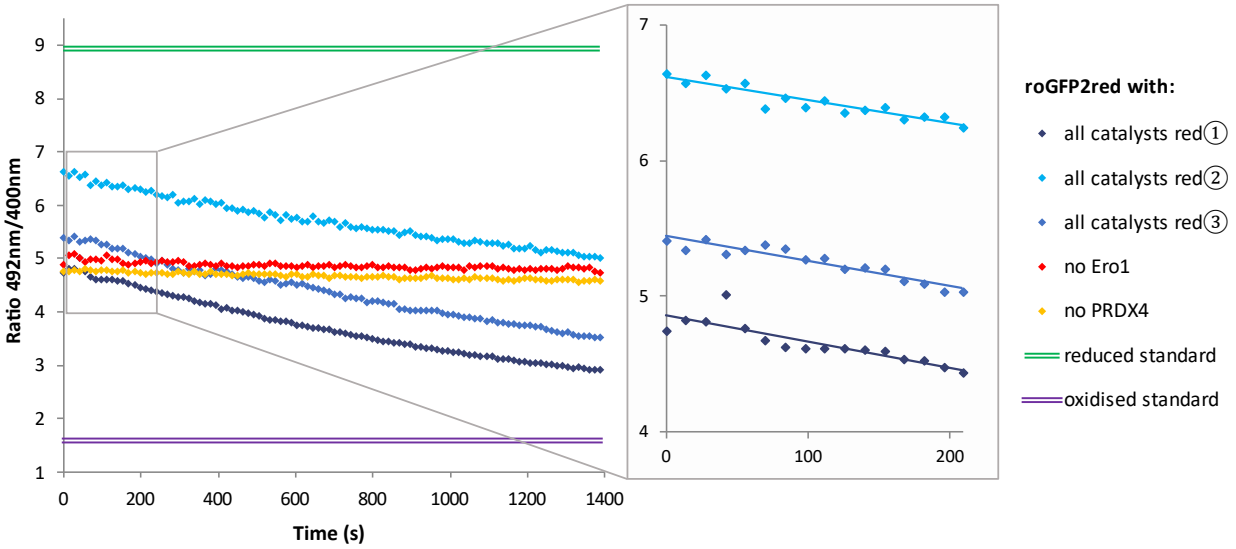

Figure 3.15. Representation of fluorescence intensity ratio 492/400 nm variation over time, obtained from the original excitation spectra of the second synergy assay.

Assay conditions: 3 µM roGFP2 in the presence of 1 µM PDI, 0.5 µM ERO1 and 0.5 µM PRDX4, all proteins reduced. A zoom of the linear region considered for initial reaction rates calculations of roGFP2 oxidation is shown in the right panel. Initially, the ratio changes rapidly with linear slope fits (solid blue lines) of $1.90 \times 10^{-3}\ s^{-1}$, $1.82 \times 10^{-3}\ s^{-1}$, $7.91 \times 10^{-3}\ s^{-1}$ and $1.71 \times 10^{-3}\ s^{-1}$ in the presence of the 3 catalysts (•,•,•,•). Control reactions without ERO1 or PRDX4 (•, • respectively) showed no significant ratio variation over time.

It is evident in Figure 3.14 that the control without PRDX4 yielded kinetics nearly identical to those observed for the complete reaction. This may be explained by the fact that oxidised ERO1 still acts over PDI, oxidizing it. However, in the absence of an H_2O_2 generating system, the control without ERO1 yielded low kinetics since PRDX4 can no longer oxidise PDI, and the reaction rate is negligible. Therefore, all roGFP2 oxidation results exclusively from the PDI/ERO1 pathway, *i.e.*, the presence of PRDX4 does not seem to affect the reaction rate.

In the first synergy assay (Figure 3.14), ERO1 was added in its oxidised state, acting similarly as in any assay of the main pathway (PDI/ERO1, Figure 3.8). Oxidised ERO1 automatically oxidises the reduced PDI. In turn, PDI oxidises the substrate (roGFP2) and only residually will be any PRDX4 reacting.

On the other hand, in the second synergy experiment (Figure 3.15), neither the majority of ERO1 nor PRDX4 oxidises the reduced PDI automatically. Firstly, the reduced ERO1 must be oxidised by residual oxygen in the buffer, producing H_2O_2, which will then oxidise PRDX4. Only after these initial oxidations will PRDX4 and ERO1 act over PDI, oxidizing it.

So it is expected that simultaneous pathways with oxidised ERO1 (first synergy assay, Figure 3.14) will work faster than simultaneous pathways with reduced ERO1 (second synergy assay, Figure 3.15). As predicted, when comparing the complete reactions of both synergy experiments, it was prominent that the second assay (all proteins reduced, Figure 3.15) yielded slower kinetics.

For the synergy experiments, the PDI/ERO1 path can always work on its own. In other words, observation of synergy is only possible if the PDI/ERO1 and PDI/PRDX4 negative controls have lower slopes than the complete PDI/ERO1/PRDX4 trial. Such only happens in the second assay because using reduced ERO1 (instead of the oxidised form) prevents the fast-starting of the PDI/ERO1 pathway. Initially, ERO1 must be oxidised by residual oxygen present in the buffer, generating H_2O_2, to act as the final electron acceptor to PRDX4 activity. Both pathways have a smooth start, becoming kinetically competitive on the oxidation of PDI. Oxidised PDI can then oxidise the substrate roGFP2 by establishing intramolecular disulfide bridges involving the oxidation of thiol groups in the cysteine residues.

This second simultaneous assay reinforced the results from previous studies where the authors established that PRDX4 further backs up thiol oxidation in higher eukaryotes (Zito et al., 2010) and showed that mammalian PRDX4 metabolises hydrogen peroxide produced by ERO1 (Tavender et al., 2010; Tavender & Bulleid, 2010).

The importance of such confirmation of both paths' interaction and synergy cannot be overstated. As stated before (Chapter 1), it is well-known that PDI's oxidation through the ERO1 secretory pathway generates reactive oxygen species as a by-product of disulfide bond formation while converting oxygen into hydrogen peroxide (Gross et al., 2006; Tu & Weissman, 2002). If not tightly regulated, this H_2O_2 production is expected to cause oxidative stress, eventually leading to cell death and apoptosis (Tavender et al., 2010). Conversely, PRDX4 can protect cells by further reducing the H_2O_2 into water, requiring a source of electrons for such activity, which it can obtain when oxidizing PDI (Tavender et al., 2010; Tavender & Bulleid, 2010; Zito et al., 2010). Although in an *in vitro* setting, our findings confirmed the possible synergy between ERO1 and PRDX4 pathways for oxidizing secretory proteins in the ER, with the latter being able to function not only independently (Konno et al., 2015; Zito et al., 2010), but also as an ERO1 co-dependent route. For now, the physiological significance of this backup mechanism remains unclear and should be further explored and investigated.

Chapter 4.
Conclusions and future perspectives

This work presents a set of new information that allows a better understanding of the catalytic efficiency of protein thiol oxidation by the main endoplasmic reticulum enzymatic pathway (PDI/ERO1) and its significant alternative (PDI/PRDX4) in an *in vitro* setting. This study resorted to several methodologies and approaches to reveal vital kinetic parameters of both pathways.

Recombinant protein expression in *E. coli* and subsequent purification by affinity chromatography of all the required enzymes (PDI, ERO1, PRDX4, roGFP2 and Ulp1) was successfully accomplished and proved to be a relatively straightforward and cost-effective way of obtaining these proteins for the ensuing *in vitro* assays. Although the protocols were previously established and optimised for most proteins, ERO1 purification has proven to be more complex, requiring more intermediary steps and several adjustments to the original process. Nevertheless, the implemented optimization improved the process's efficiency, resulting in a higher purified protein yield.

The catalytic efficiency of protein thiol oxidation by each enzymatic pathway was studied and evaluated throughout several *in vitro* assays where the fluorescent protein roGFP2 concentration was varied (from 0.1 to 10 µM) in the presence of different concentrations of the participating catalysts (1, 3 and 5 µM). Both pathways showed oxidative folding of roGFP2, although substrate inhibition was observed for higher substrate concentrations (above 1 µM or 0.5 µM in the primary and alternative pathways, respectively). The substrate acquired its native conformation by establishing intramolecular disulfide bridges involving the coupling of thiol groups from cysteine residues, previously reduced by DTT (a strong reduction agent).

It was showed that oxidation was substantially faster when catalysed by PDI/ERO1 and that PDI oxidation of roGFP2 was the rate-limiting step of this pathway, as roGFP2 oxidation rate was more dependent on PDI concentration than on ERO1, for substrate concentrations below enzyme inhibition. However, it was not possible to identify the reaction rate-limiting step for the alternative pathway (PDI/PRDX4) as the effect of substrate inhibition overshadowed it.

When testing together both pathways to evaluate a potential interaction, with PRDX4 using H_2O_2 produced by ERO1 as a final electron acceptor, it was verified that they could effectively coexist in synergy. ERO1, in its reduced form, was firstly oxidised by residual oxygen present in the buffer, generating H_2O_2, which may have acted as the final electron acceptor to PRDX4, oxidizing this protein. Once oxidised, both ERO1 and PRDX4 were able to act on PDI. When reduced ERO1 was used in the simultaneous assay, both pathways were found to initiate smoothly, becoming kinetically competitive in oxidizing PDI. Once oxidised, PDI could oxidise the substrate roGFP2.

PRDX4 is likely to cooperate with ERO1 to oxidise PDI and sustain oxidative folding of secretory proteins. However, the extent to which these two enzymes functionally overlap or complement each other in the cellular environment remains to be determined.

This was a comprehensive study involving extensive experimental work, and most of the proposed objectives have been successfully achieved. Nevertheless, some questions have emerged that may be addressed in the near future.

Regarding the alternative pathway (PDI/PRDX4), it would be interesting to explore, in further assays, a more detailed range of roGFP2 concentrations below substrate inhibition (*i.e.* below 0.5 µM) to allow a better characterization of this route and its reaction rate-limiting step. Future work could also focus on the biological implications of this substrate inhibition in both pathways and its significance, as this was beyond the original scope of this thesis and was not evaluated. This phenomenon appears to play a vital regulatory role in various metabolic processes (Reed et al., 2010) and further research on this topic may be helpful.

Finally, it would also be worthwhile to investigate additional synergy assays with a variety of enzyme concentrations to better understand the factors influencing the cooperation of both pathways towards the oxidative protein folding within the secretory compartment.

References

Abbasi, A., Corpeleijn, E., Postmus, D., Gansevoort, R. T., de Jong, P. E., Gans, R. O. B., Struck, J., Schulte, J., Hillege, H. L., van der Harst, P., Peelen, L. M., Beulens, J. W. J., Stolk, R. P., Navis, G., & Bakker, S. J. L. (2012). Peroxiredoxin 4, a novel circulating biomarker for oxidative stress and the risk of incident cardiovascular disease and all-cause mortality. *Journal of the American Heart Association*, *1*(5). https://doi.org/10.1161/JAHA.112.002956

Aller, I., Rouhier, N., & Meyer, A. J. (2013). Development of roGFP2-derived redox probes for measurement of the glutathione redox potential in the cytosol of severely glutathione-deficient rml1 seedlings. *Frontiers in Plant Science*, *4*(DEC), 506. https://doi.org/10.3389/fpls.2013.00506

Alvarez, A. F., & Georgellis, D. (2010). In Vitro and In Vivo Analysis of the ArcB/A Redox Signaling Pathway. In *Methods in Enzymology* (Vol. 471, pp. 205–228). Methods Enzymol. https://doi.org/10.1016/S0076-6879(10)71012-0

Andersen, C. L., Matthey-Dupraz, A., Missiakas, D., & Raina, S. (1997). A new Escherichia coli gene, dsbG, encodes a periplasmic protein involved in disulphide bond formation, required for recycling DsbA/DsbB and DsbC redox proteins. *Molecular Microbiology*, *26*(1), 121–132. https://doi.org/10.1046/j.1365-2958.1997.5581925.x

Anfinsen, C. B. (1973). Principles that Govern the Folding of Protein Chains. *Science*, *181*(4096), 223–230. https://doi.org/10.1126/SCIENCE.181.4096.223

Avezov, E., Cross, B. C. S. S., Schierle, G. S. K. K., Winters, M., Harding, H. P., Melo, E. P., Kaminski, C. F., & Ron, D. (2013). Lifetime imaging of a fluorescent protein sensor reveals surprising stability of ER thiol redox. *Journal of Cell Biology*, *201*(2), 337–349. https://doi.org/10.1083/jcb.201211155

Bartlett, A. I., & Radford, S. E. (2009). An expanding arsenal of experimental methods yields an explosion of insights into protein folding mechanisms. In *Nature Structural and Molecular Biology* (Vol. 16, Issue 6, pp. 582–588). https://doi.org/10.1038/nsmb.1592

Belousov, V. V., Fradkov, A. F., Lukyanov, K. A., Staroverov, D. B., Shakhbazov, K. S., Terskikh, A. V., & Lukyanov, S. (2006). Genetically encoded fluorescent indicator for intracellular hydrogen peroxide. *Nature Methods*, *3*(4), 281–286. https://doi.org/10.1038/nmeth866

Berg, J., Tymoczko, J., & Stryer, L. (2002). The Michaelis-Menten Model Accounts for the Kinetic Properties of Many Enzymes. In *Biochemistry* (5th ed., pp. 139–146). W H Freeman. https://www.ncbi.nlm.nih.gov/books/NBK22430/

Berkelman, T., Petersen, S., Sun, C., & Cater, S. (2010). Mini-PROTEAN® TGX™ precast gel for SDS-PAGE with improved stability: Comparison with standard Laemmli gels. *BioTechniques*, *48*(2), 156–157. https://doi.org/10.2144/000113372

Betz, S. F. (1993). Disulfide bonds and the stability of globular proteins. In *Protein Science* (Vol. 2, Issue 10, pp. 1551–1558). Protein Sci. https://doi.org/10.1002/pro.5560021002

Bizzarri, R., Serresi, M., Luin, S., & Beltram, F. (2009). Green fluorescent protein based pH indicators for in vivo use: A review. In *Analytical and Bioanalytical Chemistry* (Vol. 393, Issue 4, pp. 1107–1122). Anal Bioanal Chem. https://doi.org/10.1007/s00216-008-2515-9

Blais, J. D., Chin, K. T., Zito, E., Zhang, Y., Heldman, N., Harding, H. P., Fass, D., Thorpe, C., & Ron, D. (2010). A small molecule inhibitor of Endoplasmic Reticulum Oxidation 1 (ERO1) with selectively reversible thiol reactivity. *Journal of Biological Chemistry*, *285*(27), 20993–21003. https://doi.org/10.1074/jbc.M110.126599

Bornhorst, J. A., & Falke, J. J. (2000). Purification of proteins using polyhistidine affinity tags. In *Methods in Enzymology* (Vol. 326, pp. 245–254). Academic Press Inc. https://doi.org/10.1016/s0076-6879(00)26058-8

Brodsky, J. L., & Skach, W. R. (2011). Protein folding and quality control in the endoplasmic reticulum: Recent lessons from yeast and mammalian cell systems. In *Current Opinion in Cell Biology* (Vol. 23, Issue 4, pp. 464–475). Curr Opin Cell Biol. https://doi.org/10.1016/j.ceb.2011.05.004

Chang, R., & Ventura, S. (2011). Folding of Disulfide Proteins. In S. Ventura & R. Chang (Eds.), *Folding of Disulfide Proteins*. Springer New York. https://doi.org/10.1007/978-1-4419-7273-6

Chaplin, M., & Bucke, C. (1990). *Enzyme technology*. Cambridge University Press.

Chaudhuri, T. K., & Paul, S. (2006). Protein-misfolding diseases and chaperone-based therapeutic approaches. In *FEBS Journal* (Vol. 273, Issue 7, pp. 1331–1349). FEBS J. https://doi.org/10.1111/j.1742-4658.2006.05181.x

Chezeau, B., & Vial, C. (2019). Modeling and Simulation of the Biohydrogen Production Processes. In *Biohydrogen* (pp. 445–483). Elsevier. https://doi.org/10.1016/b978-0-444-64203-5.00019-8

Clark, D. P., & Pazdernik, N. J. (2009). Biotechnology Applying the Genetic Revolution. In *Science*. Academic Press/Elsevier.

Correia, C., Tavares, E., Lopes, C., Silva, J. G., Duarte, A., Geraldes, V., Rodrigues, M. A., & Melo, E. P. (2020). Stability of Protein Formulations at Subzero Temperatures by Isochoric Cooling. *Journal of Pharmaceutical Sciences*, *109*(1), 316–322. https://doi.org/10.1016/j.xphs.2019.06.017

Dalbey, R., & Heijne, G. von. (2002). Protein Targeting, Transport, and Translocation. In *Protein Targeting, Transport, and Translocation* (1st ed.). Academic Press.

Dobson, C. M. (2003). Protein folding and misfolding. In *Nature* (Vol. 426, Issue 6968, pp. 884–890). Nature. https://doi.org/10.1038/nature02261

Ellgaard, L., & Ruddock, L. W. (2005). The human protein disulphide isomerase family: Substrate interactions and functional properties. In *EMBO Reports* (Vol. 6, Issue 1, pp. 28–32). EMBO Rep. https://doi.org/10.1038/sj.embor.7400311

Esposito, S., Masala, A., Sanna, S., Rassu, M., Pimxayvong, V., Iaccarino, C., & Crosio, C. (2017). Redox-sensitive GFP to monitor oxidative stress in neurodegenerative diseases. *Reviews in the Neurosciences*, *28*(2), 133–144. https://doi.org/10.1515/revneuro-2016-0041

Feige, M. J., & Hendershot, L. M. (2011). Disulfide bonds in ER protein folding and homeostasis. In *Current Opinion in Cell Biology* (Vol. 23, Issue 2, pp. 167–175). https://doi.org/10.1016/j.ceb.2010.10.012

Frand, A. R., & Kaiser, C. A. (1999). Ero1p oxidizes protein disulfide isomerase in a pathway for disulfide bond formation in the endoplasmic reticulum. *Molecular Cell*, *4*(4), 469–477. https://doi.org/10.1016/S1097-2765(00)80198-7

Fu, J., Gao, J., Liang, Z., & Yang, D. (2021). PDI-regulated disulfide bond formation in protein folding and biomolecular assembly. In *Molecules* (Vol. 26, Issue 1, p. 171). NLM (Medline). https://doi.org/10.3390/MOLECULES26010171

Fujii, J., & Ikeda, Y. (2002). Advances in our understanding of peroxiredoxin, a multifunctional, mammalian redox protein. In *Redox Report* (Vol. 7, Issue 3, pp. 123–130). https://doi.org/10.1179/135100002125000352

Galligan, J. J., & Petersen, D. R. (2012). The human protein disulfide isomerase gene family. *Human Genomics*, *6*(1). https://doi.org/10.1186/1479-7364-6-6

Garg, B., Bisht, T., & Ling, Y. C. (2015). Graphene-based nanomaterials as efficient peroxidase mimetic catalysts for biosensing applications: An overview. In *Molecules* (Vol. 20, Issue 8, pp. 14155–14190). https://doi.org/10.3390/molecules200814155

Gomes, C. M., & Faísca, P. F. N. (2019). *Protein Folding: An Introduction* (pp. 1–63). https://doi.org/10.1007/978-3-319-00882-0_1

Gon, S., Faulkner, M. J., & Beckwith, J. (2006). In vivo requirement for glutaredoxins and thioredoxins in the reduction of the ribonucleotide reductases of Escherichia coli. *Antioxidants and Redox Signaling*, *8*(5–6), 735–742. https://doi.org/10.1089/ars.2006.8.735

Gross, E., Sevier, C. S., Heldman, N., Vitu, E., Bentzur, M., Kaiser, C. A., Thorpe, C., Fass, D., & Beckwith, J. (2006). Generating disulfides enzymatically: Reaction products and electron acceptors of the endoplasmic reticulum thiol oxidase Ero1p. *Proceedings of the National Academy of Sciences of the United States of America*, *103*(2), 299–304. https://doi.org/10.1073/pnas.0506448103

Halliwell, B., & Gutteridge, J. M. C. (1984). Oxygen toxicity, oxygen radicals, transition metals and disease. In *Biochemical Journal* (Vol. 219, Issue 1, pp. 1–14). https://doi.org/10.1042/bj2190001

Hanson, G. T., Aggeler, R., Oglesbee, D., Cannon, M., Capaldi, R. A., Tsien, R. Y., & Remington, S. J. (2004). Investigating Mitochondrial Redox Potential with Redox-sensitive Green Fluorescent Protein Indicators. *Journal of Biological Chemistry*, *279*(13), 13044–13053. https://doi.org/10.1074/jbc.M312846200

Hatahet, F., Ruddock, L. W., F, H., & LW, R. (2009). Protein Disulfide Isomerase : A Critical Evaluation of Its Function in Disulfide Bond Formation. *Antioxidants & Redox Signlaing*, *11*(11), 2807–2858. https://doi.org/10.1089/ars.2009.2466

Healthcare, G. (2017). Affinity Chromatography Vol. 2: Tagged Proteins. *Green Chemistry*, *19*(17), 4043–4047. www.gelifesciences.com

Hudson, D. A., Gannon, S. A., & Thorpe, C. (2015). Oxidative protein folding: From thiol-disulfide exchange reactions to the redox poise of the endoplasmic reticulum. *Free Radical Biology and Medicine*, *80*, 171–182. https://doi.org/10.1016/j.freeradbiomed.2014.07.037

Inaba, K. (2010). Structural basis of protein disulfide bond generation in the cell. In *Genes to Cells* (Vol. 15, Issue 9, pp. 935–943). Genes Cells. https://doi.org/10.1111/j.1365-2443.2010.01434.x

Inaba, K., Masui, S., Iida, H., Vavassori, S., Sitia, R., & Suzuki, M. (2010). Crystal structures of human Ero1α reveal the mechanisms of regulated and targeted oxidation of PDI. *EMBO Journal*, *29*(19), 3330–3343. https://doi.org/10.1038/emboj.2010.222

Jander, G., Martin, N. L., & Beckwith, J. (1994). Two cysteines in each periplasmic domain of the membrane protein DsbB are required for its function in protein disulfide bond formation. *EMBO Journal*, *13*(21), 5121–5127. https://doi.org/10.1002/j.1460-2075.1994.tb06841.x

Jeong, W., Bae, S. H., Toledano, M. B., & Rhee, S. G. (2012). Role of sulfiredoxin as a regulator of peroxiredoxin function and regulation of its expression. In *Free Radical Biology and Medicine* (Vol. 53, Issue 3, pp. 447–456). https://doi.org/10.1016/j.freeradbiomed.2012.05.020

Jia, W., Chen, P., & Cheng, Y. (2019). PRDX4 and Its Roles in Various Cancers. In *Technology in cancer research & treatment* (Vol. 18). NLM (Medline). https://doi.org/10.1177/1533033819864313

Kang, J. G., Paget, M. S., Seok, Y. J., Hahn, M. Y., Bae, J. B., Hahn, J. S., Kleanthous, C., Buttner, M. J., & Roe, J. H. (1999). RsrA, an anti-sigma factor regulated by redox change. *The EMBO Journal*, *18*(15), 4292. https://doi.org/10.1093/EMBOJ/18.15.4292

Karplus, P. A. (2015). A primer on peroxiredoxin biochemistry. *Free Radical Biology and Medicine*, *80*, 183–190. https://doi.org/10.1016/j.freeradbiomed.2014.10.009

Kokkonen, P., Beier, A., Mazurenko, S., Damborsky, J., Bednar, D., & Prokop, Z. (2021). Substrate inhibition by the blockage of product release and its control by tunnel engineering. *RSC Chemical Biology*, *2*(2), 645–655. https://doi.org/10.1039/d0cb00171f

Konno, T., Melo, E. P., Lopes, C., Mehmeti, I., Lenzen, S., Ron, D., & Avezov, E. (2015). ERO1-independent production of H2O2 within the endoplasmic reticulum fuels Prdx4-mediated oxidative protein folding. *Journal of Cell Biology*, *211*(2), 253–259. https://doi.org/10.1083/jcb.201506123

Lakowicz, J. R. (2006). Introduction to Fluorescence. In *Principles of Fluorescence Spectroscopy* (pp. 1–26). Springer US. https://doi.org/10.1007/978-0-387-46312-4_1

Landgraf, B. J., Ren, G., Masuch, T., Boyd, D., & Berkmen, M. (2017). From Biology to Biotechnology: Disulfide Bond Formation in Escherichia coli. In *Escherichia coli - Recent Advances on Physiology, Pathogenesis and Biotechnological Applications*. InTech. https://doi.org/10.5772/67393

Lee, C., Lee, S. M., Mukhopadhyay, P., Kim, S. J., Lee, S. C., Ahn, W. S., Yu, M. H., Storz, G., & Ryu, S. E. (2004). Redox regulation of OxyR requires specific disulfide bond formation involving a rapid kinetic reaction path. *Nature Structural and Molecular Biology*, *11*(12), 1179–1185. https://doi.org/10.1038/nsmb856

Leyens, G., Donnay, I., & Knoops, B. (2003). Cloning of bovine peroxiredoxins - Gene expression in bovine tissues and amino acid sequence comparison with rat, mouse and primate peroxiredoxins. *Comparative Biochemistry and Physiology - B Biochemistry and Molecular Biology*, *136*(4), 943–955. https://doi.org/10.1016/S1096-4959(03)00290-2

Malhotra, J. D., & Kaufman, R. J. (2007a). The endoplasmic reticulum and the unfolded protein response. In *Seminars in Cell and Developmental Biology* (Vol. 18, Issue 6, pp. 716–731). NIH Public Access. https://doi.org/10.1016/j.semcdb.2007.09.003

Malhotra, J. D., & Kaufman, R. J. (2007b). Endoplasmic reticulum stress and oxidative stress: A vicious cycle or a double-edged sword? In *Antioxidants and Redox Signaling* (Vol. 9, Issue 12, pp. 2277–2293). Mary Ann Liebert, Inc. 2 Madison Avenue Larchmont, NY 10538 USA. https://doi.org/10.1089/ars.2007.1782

Melo, E. P., Lopes, C., Gollwitzer, P., Lortz, S., Lenzen, S., Mehmeti, I., Kaminski, C. F., Ron, D., & Avezov, E.

(2017). TriPer, an optical probe tuned to the endoplasmic reticulum tracks changes in luminal H2O2. *BMC Biology*, *15*(1). https://doi.org/10.1186/s12915-017-0367-5

Metzger, M. B. (2009). *Protein Quality Control in the Endoplasmatic Reticulum and Cytosol*. Johns Hopkins University.

Mishra, M., Chawsheen, H., Wu, L., Jiang, H., & Wei, Q. (2013). PRDX4 (peroxiredoxin 4). *Atlas of Genetics and Cytogenetics in Oncology and Haematology*, *10*. https://doi.org/10.4267/2042/51538

Moroder, L., & Buchner, J. (Eds.). (2009). *Oxidative Folding of Peptides and Proteins* (1st editio). Royal Society of Chemistry. https://doi.org/10.1039/9781847559265

Morris, M. C. (2010). Fluorescent biosensors of intracellular targets from genetically encoded reporters to modular polypeptide probes. In *Cell Biochemistry and Biophysics* (Vol. 56, Issue 1, pp. 19–37). Cell Biochem Biophys. https://doi.org/10.1007/s12013-009-9070-7

Mullick, M., & Nayak, S. (2020). Comprehending the Unfolded Protein Response as a Conduit for Improved Mesenchymal Stem Cell-Based Therapeutics. *Regenerative Engineering and Translational Medicine*, *6*(2), 179–188. https://doi.org/10.1007/s40883-019-00143-0

NCBI. (2019). *National Center for Biotechnology Information*. PRDX4 Peroxiredoxin 4 [Homo Sapiens (Human)]. https://www.ncbi.nlm.nih.gov/gene/10549

Onuchic, J. N., & Wolynes, P. G. (2004). Theory of protein folding. In *Current Opinion in Structural Biology* (Vol. 14, Issue 1, pp. 70–75). Elsevier Ltd. https://doi.org/10.1016/j.sbi.2004.01.009

Østergaard, H., Henriksen, A., Hansen, F. G., & Winther, J. R. (2001). Shedding light on disulfide bond formation: Engineering a redox switch in green fluorescent protein. *EMBO Journal*, *20*(21), 5853–5862. https://doi.org/10.1093/emboj/20.21.5853

Panayiotidis, M., Tsolas, O., & Galaris, D. (1999). Glucose oxidase-produced H2O2 induces Ca2+-dependent DNA damage in human peripheral blood lymphocytes. *Free Radical Biology and Medicine*, *26*(5–6), 548–556. https://doi.org/10.1016/S0891-5849(98)00249-4

Powers, E. T., Morimoto, R. I., Dillin, A., Kelly, J. W., & Balch, W. E. (2009). Biological and chemical approaches to diseases of proteostasis deficiency. In *Annual Review of Biochemistry* (Vol. 78, pp. 959–991). Annu Rev Biochem. https://doi.org/10.1146/annurev.biochem.052308.114844

Qi, L., Tsai, B., & Arvan, P. (2017). New Insights into the Physiological Role of Endoplasmic Reticulum-Associated Degradation. In *Trends in Cell Biology* (Vol. 27, Issue 6, pp. 430–440). Elsevier Ltd. https://doi.org/10.1016/j.tcb.2016.12.002

Reed, M. C., Lieb, A., & Nijhout, H. F. (2010). The biological significance of substrate inhibition: A mechanism with diverse functions. In *BioEssays* (Vol. 32, Issue 5, pp. 422–429). John Wiley & Sons, Ltd. https://doi.org/10.1002/bies.200900167

Ren, G., & Bardwell, J. C. A. (2011). Engineered pathways for correct disulfide bond oxidation. *Antioxidants and Redox Signaling*, *14*(12), 2399–2412. https://doi.org/10.1089/ars.2010.3782

Reuter, W. H., Masuch, T., Ke, N., Lenon, M., Radzinski, M., Van Loi, V., Ren, G., Riggs, P., Antelmann, H., Reichmann, D., Leichert, L. I., & Berkmen, M. (2019). Utilizing redox-sensitive GFP fusions to detect in vivo redox changes in a genetically engineered prokaryote. *Redox Biology*, *26*, 101280.

Rhee, S. G., Kang, S. W., Chang, T. S., Jeong, W., & Kim, K. (2001). Peroxiredoxin, a novel family of peroxidases. *IUBMB Life*, *52*(1–2), 35–41. https://doi.org/10.1080/15216540252774748

Rhee, S. G., & Woo, H. A. (2011). Multiple functions of peroxiredoxins: Peroxidases, sensors and regulators of the intracellular messenger H2O2, and protein chaperones. *Antioxidants and Redox Signaling*, *15*(3), 781–794. https://doi.org/10.1089/ars.2010.3393

Robinson, P. J., & Bulleid, N. J. (2020). Mechanisms of Disulfide Bond Formation in Nascent Polypeptides Entering the Secretory Pathway. In *Cells* (Vol. 9, Issue 9). Multidisciplinary Digital Publishing Institute (MDPI). https://doi.org/10.3390/cells9091994

Sato, Y., & Inaba, K. (2012). Disulfide bond formation network in the three biological kingdoms, bacteria, fungi and mammals. *FEBS Journal*, *279*(13), 2262–2271. https://doi.org/10.1111/j.1742-4658.2012.08593.x

Schmitt, J., Hess, H., & Stunnenberg, H. G. (1993). Affinity purification of histidine-tagged proteins. *Molecular Biology Reports*, *18*(3), 223–230. https://doi.org/10.1007/BF01674434

Schulte, J. (2011). Peroxiredoxin 4: A multifunctional biomarker worthy of further exploration. In *BMC Medicine* (Vol. 9). https://doi.org/10.1186/1741-7015-9-137

Schwarzländer, M., Fricker, M. D., Müller, C., Marty, L., Brach, T., Novak, J., Sweetlove, L. J., Hell, R., & Meyer, A. J. (2008). Confocal imaging of glutathione redox potential in living plant cells. *Journal of Microscopy, 231*(2), 299–316. https://doi.org/10.1111/j.1365-2818.2008.02030.x

Selvakumari, T. (2018). Cell Structure and Function. In *Essentials of Anatomy for Dental Students* (Vol. 17, Issue 10, pp. 1–1). Jaypee Brothers Medical Publishers (P) Ltd. https://doi.org/10.5005/jp/books/14250_2

Sevier, C. S., & Kaiser, C. A. (2008). Ero1 and redox homeostasis in the endoplasmic reticulum. In *Biochimica et Biophysica Acta - Molecular Cell Research* (Vol. 1783, Issue 4, pp. 549–556). Elsevier. https://doi.org/10.1016/j.bbamcr.2007.12.011

Shergalis, A. G., Hu, S., Bankhead, A., & Neamati, N. (2020). Role of the ERO1-PDI interaction in oxidative protein folding and disease. In *Pharmacology and Therapeutics* (Vol. 210). Pharmacol Ther. https://doi.org/10.1016/j.pharmthera.2020.107525

Shergalis, A., & Neamati, N. (2016). Protein Disulfide Isomerase. In *Encyclopedia of Signaling Molecules* (pp. 1–12). Springer New York. https://doi.org/10.1007/978-1-4614-6438-9_101768-1

Slosky, L. M., BassiriRad, N. M., Symons, A. M., Thompson, M., Doyle, T., Forte, B. L., Staatz, W. D., Bui, L., Neumann, W. L., Mantyh, P. W., Salvemini, D., Largent-Milnes, T. M., & Vanderah, T. W. (2016). The cystine/glutamate antiporter system xc- drives breast tumor cell glutamate release and cancer-induced bone pain. *Pain, 157*(11), 2605–2616. https://doi.org/10.1097/j.pain.0000000000000681

Tavender, T. J., & Bulleid, N. J. (2010). Peroxiredoxin IV protects cells from oxidative stress by removing H 2O2 produced during disulphide formation. *Journal of Cell Science, 123*(15), 2672–2679. https://doi.org/10.1242/jcs.067843

Tavender, T. J., Springate, J. J., & Bulleid, N. J. (2010). Recycling of peroxiredoxin IV provides a novel pathway for disulphide formation in the endoplasmic reticulum. *EMBO Journal, 29*(24), 4185–4197. https://doi.org/10.1038/emboj.2010.273

Thomasson, W. (F. of A. S. for E. B.). (1997). *Unraveling the Mystery of Protein Folding.* http://pratclif.com/biologie-moleculaire/Unraveling the Mystery of Protein Folding.htm

Tompa, P. (2009). Structure and function of intrinsically disordered proteins. In *Structure and Function of Intrinsically Disordered Proteins*. Chapman and Hall/CRC. https://doi.org/10.1201/9781420078930

Tu, B. P., & Weissman, J. S. (2002). The FAD- and O(2)-dependent reaction cycle of Ero1-mediated oxidative protein folding in the endoplasmic reticulum. *Molecular Cell, 10*(5), 983–994. https://doi.org/10.1016/s1097-2765(02)00696-2

Tu, B. P., & Weissman, J. S. (2004). Oxidative protein folding in eukaryotes: Mechanisms and consequences. *Journal of Cell Biology, 164*(3), 341–346. https://doi.org/10.1083/jcb.200311055

Van Anken, E., & Braakman, I. (2005). Versatility of the endoplasmic reticulum protein folding factory. In *Critical Reviews in Biochemistry and Molecular Biology* (Vol. 40, Issue 4, pp. 191–228). Taylor & Francis. https://doi.org/10.1080/10409230591008161

Walker, K. W., & Gilbert, H. F. (1994). Effect of redox environment on the in vitro and in vivo folding of RTEM-1 β-lactamase and Escherichia coli alkaline phosphatase. *Journal of Biological Chemistry, 269*(45), 28487–28493. https://doi.org/10.1016/s0021-9258(18)46953-0

Wang, C., Chen, S., Wang, X., Wang, L., Wallis, A. K., Freedman, R. B., & Wang, C. C. (2010). Plasticity of human protein disulfide isomerase: Evidence for mobility around the x-linker region and its functional significance. *Journal of Biological Chemistry, 285*(35), 26788–26797. https://doi.org/10.1074/jbc.M110.107839

Wang, S., & Kaufman, R. J. (2012). The impact of the unfolded protein response on human disease. In *Journal of Cell Biology* (Vol. 197, Issue 7, pp. 857–867). The Rockefeller University Press. https://doi.org/10.1083/jcb.201110131

Wierer, S., Elgass, K., Bieker, S., Zentgraf, U., Meixner, A. J., & Schleifenbaum, F. (2011). Determination of the in vivo redox potential using roGFP and fluorescence spectra obtained from one-wavelength excitation. *Imaging, Manipulation, and Analysis of Biomolecules, Cells, and Tissues IX, 7902*, 790211. https://doi.org/10.1117/12.873753

Yoshino, M., & Murakami, K. (2015). Analysis of the substrate inhibition of complete and partial types. *SpringerPlus*, *4*(1). https://doi.org/10.1186/s40064-015-1082-8

Zavada, S. R., Battsengel, T., & Scott, T. F. (2016). Radical-mediated enzymatic polymerizations. *International Journal of Molecular Sciences*, *17*(2), 195. https://doi.org/10.3390/ijms17020195

Zinn, K. M., & Leopold, I. H. (1973). Molecular biology of the cell. In *International Ophthalmology Clinics* (6th ed, Vol. 13, Issue 3, pp. 53–81). W. W. Norton & Co. https://doi.org/10.1097/00004397-197301330-00007

Zito, E., Hansen, H. G., Yeo, G. S. H., Fujii, J., & Ron, D. (2012). Endoplasmic Reticulum Thiol Oxidase Deficiency Leads to Ascorbic Acid Depletion and Noncanonical Scurvy in Mice. *Molecular Cell*, *48*(1), 39–51. https://doi.org/10.1016/j.molcel.2012.08.010

Zito, E., Melo, E. P., Yang, Y., Wahlander, Å., Neubert, T. A., & Ron, D. (2010). Oxidative protein folding by an endoplasmic reticulum-localized peroxiredoxin. *Molecular Cell*, *40*(5), 787–797. https://doi.org/10.1016/j.molcel.2010.11.010

Appendices

Appendix I SDS-PAGE

The underlying principles of SDS-PAGE were described by Berkelman and colleagues (2010) as:

« SDS-PAGE relies on a discontinuous buffer system. Two ions differing in electrophoretic mobility (glycinate and chloride) form a moving boundary when voltage is applied. Proteins have an intermediate mobility that causes them to concentrate, or stack, into a narrow zone at the beginning of electrophoresis. As that zone moves through the gel, the sieving effect of the polyacrylamide gel matrix causes proteins of different molecular weights to move at different rates. This stacking effect is responsible for the high resolving power of SDS-PAGE: the sample is loaded in a relatively broad zone, and the moving boundary concentrates the proteins into sharp bands prior to separation. Protein samples for SDS-PAGE are prepared using SDS and a thiol reducing agent, usually β-mercaptoethanol or dithiothreitol (DTT). SDS forms complexes with proteins, giving them a rodlike shape and similar mass-to-charge ratio. The reducing agent disrupts disulfide bonds between and within proteins, allowing complete denaturation and dissociation. Heat treatment in the presence of SDS and reducing agent effectively eliminates the effects of native charge and higher order structure on electrophoretic mobility, so the migration distance depends primarily on molecular weight. Molecular weight is estimated by comparison to standards of known molecular weight. »

Appendix II Plasmids restriction maps

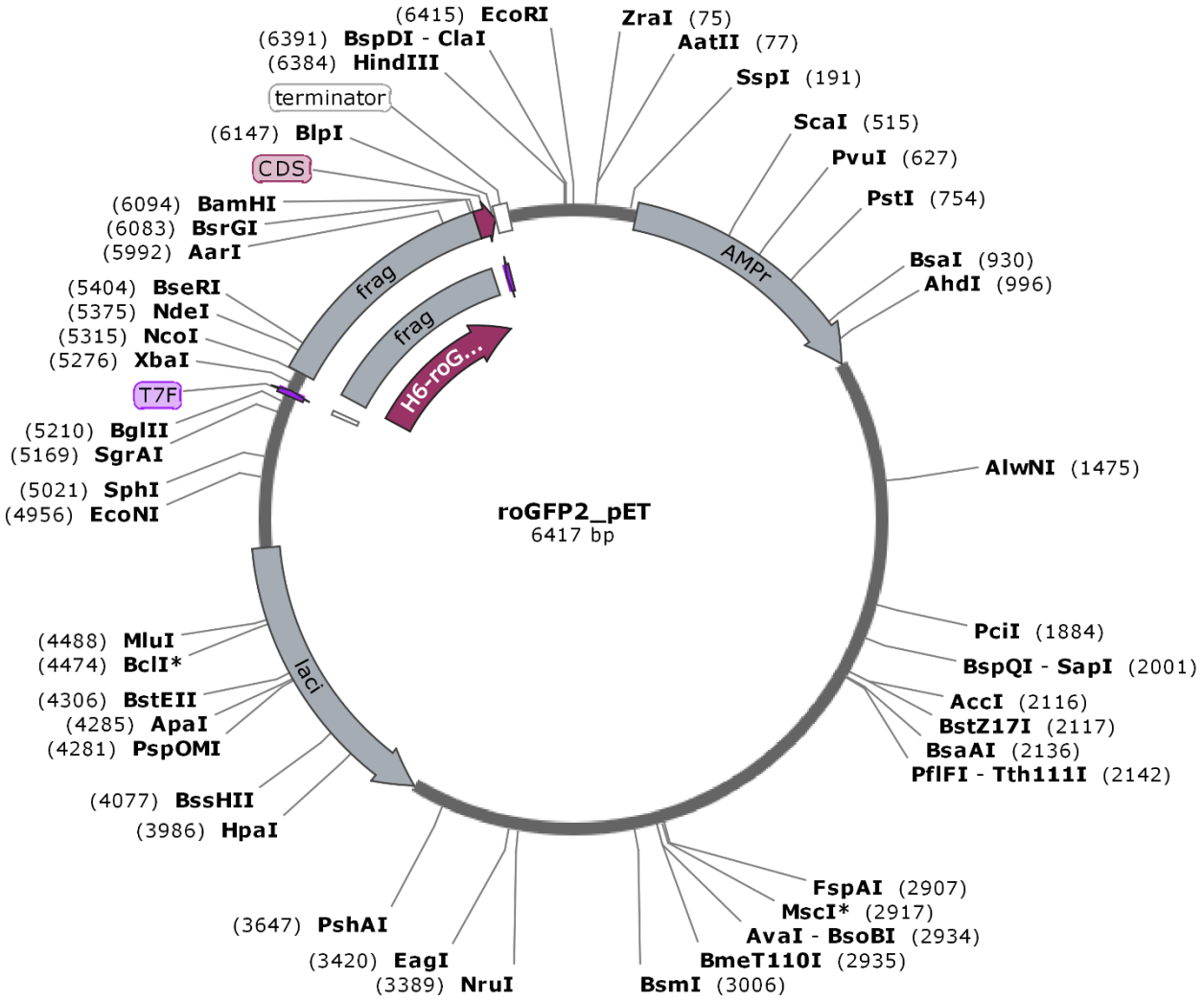

Figure A.1. Restriction maps of recombinant plasmid used to express roGFP2.

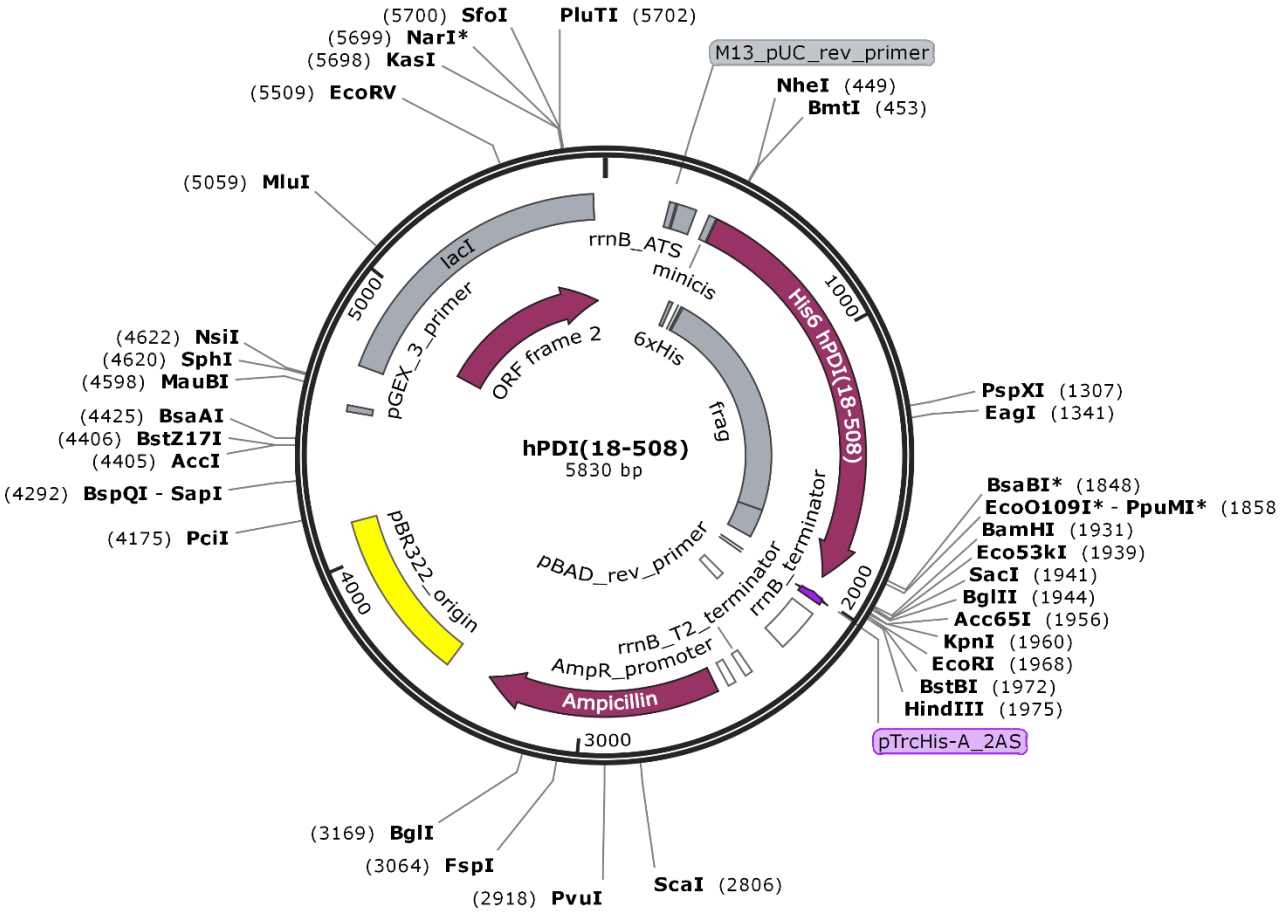

Figure A.2. Restriction maps of recombinant plasmid used to express PDI.

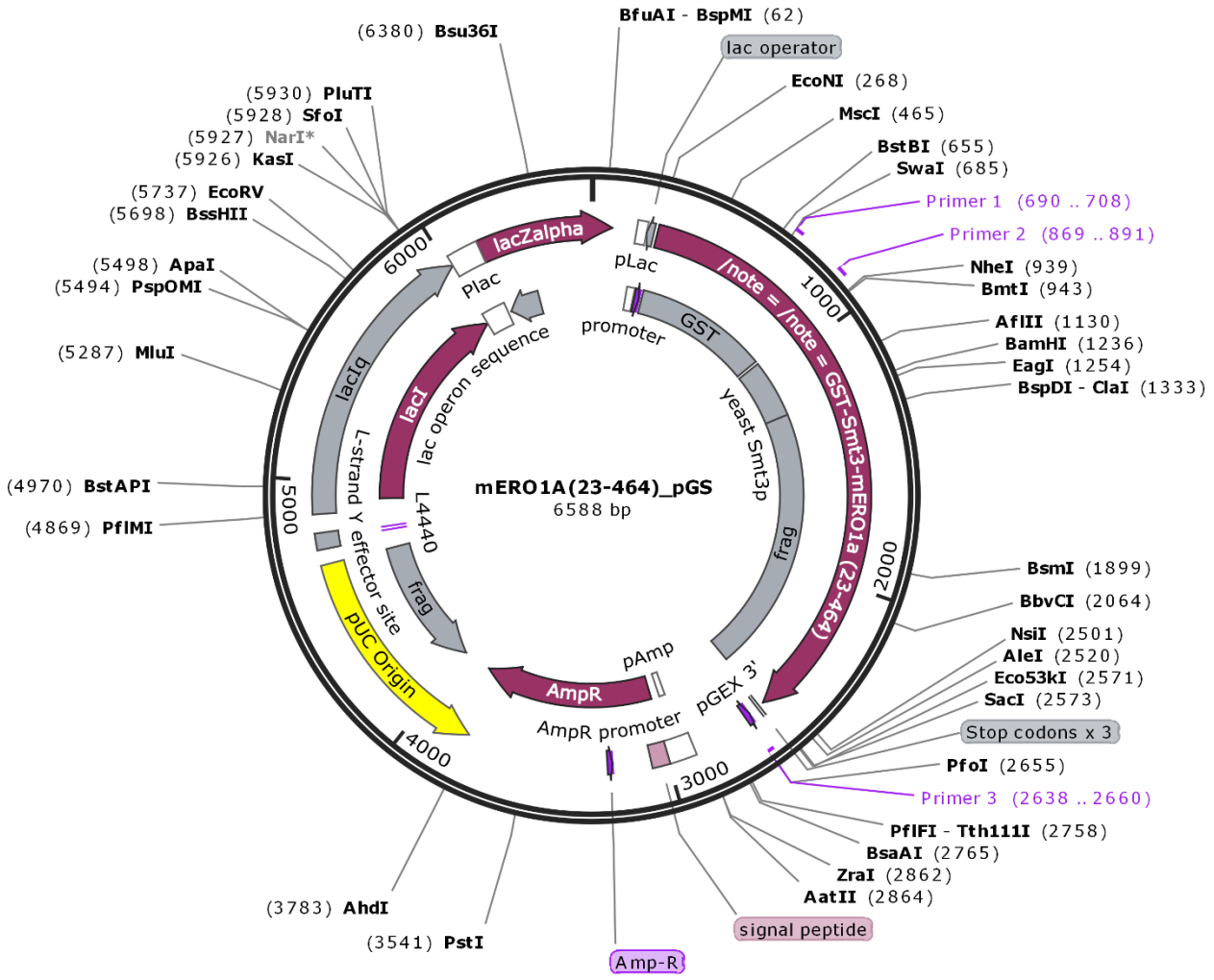

Figure A.3. Restriction maps of recombinant plasmid used to express ERO1.

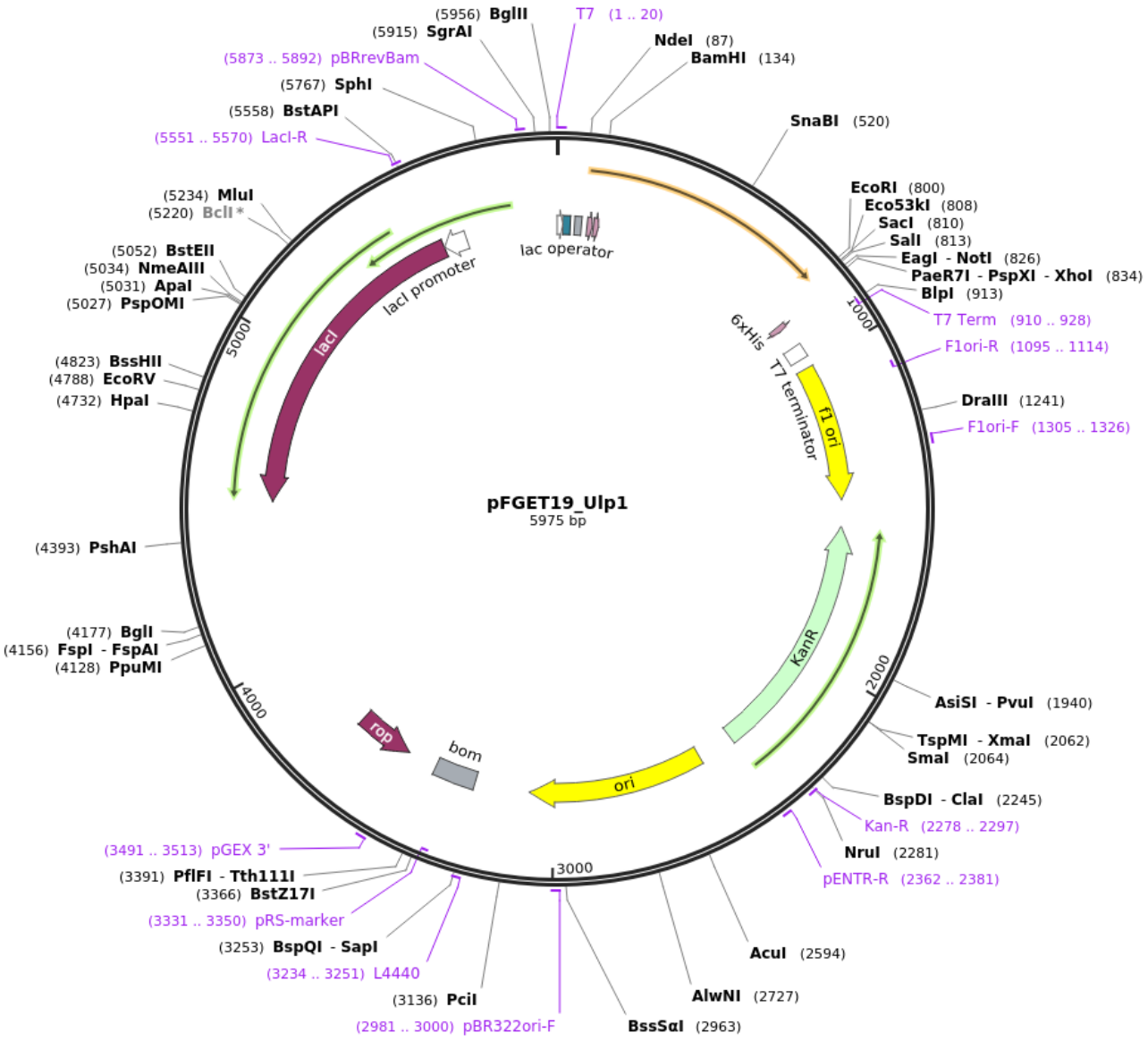

Figure A.4. Restriction maps of recombinant plasmid used to express ULP1.

Appendix III ERO1 purification diagram

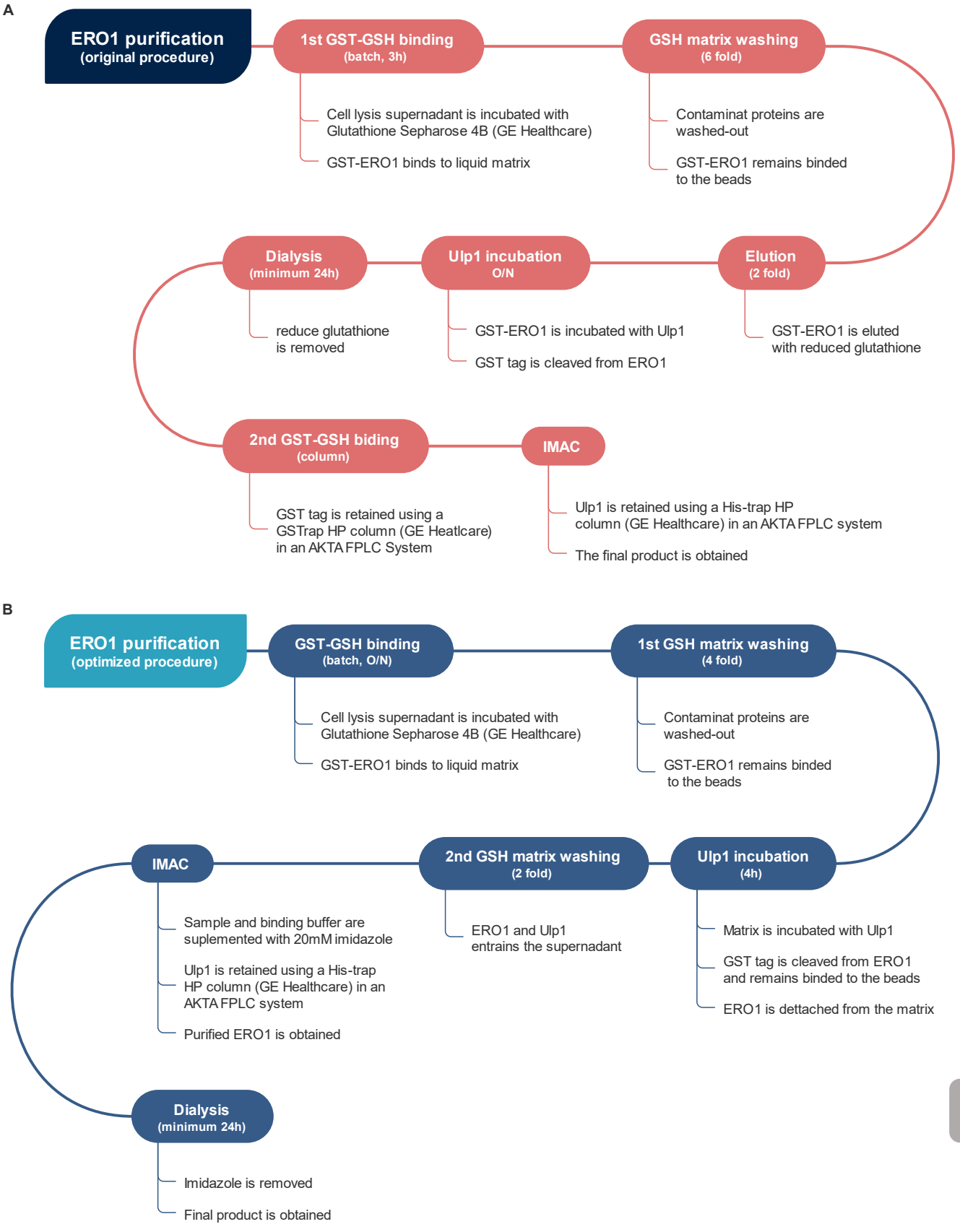

Figure A.5. Diagram illustrating sequential steps in ERO1 purification: original (A) and optimized procedure (B).